Master's thesis

NTNU
Norwegian University of Science and Technology
Faculty of Natural Sciences
Department of Chemistry

Erlend Gammelsæter

Examining Oxidized Mn and Fe as Adsorbents of Hg and Pb in Seawater

An Incubation Experiment

Master's thesis in Environmental Toxicology and Chemistry
Supervisor: Murat Van Ardelan
August 2023

NTNU
Norwegian University of
Science and Technology

Erlend Gammelsæter

Examining Oxidized Mn and Fe as Adsorbents of Hg and Pb in Seawater

An Incubation Experiment

Master's thesis in Environmental Toxicology and Chemistry
Supervisor: Murat Van Ardelan
August 2023

Norwegian University of Science and Technology
Faculty of Natural Sciences
Department of Chemistry

NTNU
Norwegian University of
Science and Technology

Abstract

The marine cycle of Hg and Pb are of importance due to their toxic effect on marine life. Biogeochemical cycles of redox sensitive Fe and Mn are coupled with the cycles of Hg and Pb. Oxidized species of Fe and Mn form colloids and particles that can adsorb toxic elements. Therefore, this study aimed to investigate Hg and Pb adsorption onto *in situ* oxidized Fe and Mn (*in situ* Fe, Mn, or MnFe) to reflect natural processes.

This study had an experimental approach. The matrix was seawater collected at 80-meter depth in Trondheim Fjord, Norway, spiked with 0.005 pM Hg and 2.0 pM Pb. Three treatments were tested, i.e., Mn, Fe, and MnFe combined (1:1 ratio). For each treatment, 10, 25, 50, and 100 nM Fe(II) and/or Mn(II) were added to the experiment.

Adsorption of studied elements onto the walls of polyethylene bottles showed to be an important artifact for Pb, Fe, and Mn. Wall adsorption explained by most of the dPb measurements were below limit of detection between 2 and 16 hours in the incubation period. The wall desorption test indicated that the Fe and Mn treatments between 25 and 50 nM adsorbed Pb. A mass balance was calculated implying that not all of Pb, Fe, and Mn was recovered from the wall by the wall desorption method applied. Hg, Pb, Mn, and Fe did not show any overall trend of contamination. A second order polynomial function is proposed for polyethylene wall adsorption of TPb in seawater matrixes. However, more data are needed to investigate this further. A particle dynamic model is proposed to illustrate the major chemical and physical processes occurring in bottles stored with seawater. Lastly, an assessment of the experiment with suggestions for improvements are given.

Sammendrag

Kunnskap om hvordan Hg og Pb sirkulerer i det marine miljøet er viktig fordi de er toksiske for marint liv. Forskning tyder på at redokssensitive elementer som Mn og Fe tar en viktig del i disse syklusene. Mn og Fe danner kolloider og partikler i de øvre vannmassene som kan adsorbere Hg og Pb. Målet med denne studien var å undersøke adsorpsjon av Hg og Pb av Fe og Mn som har blitt oksidert *in situ* (*in situ* Fe, Mn eller MnFe) for å forstå de naturlige prosessene i sjøvann.

Denne studien hadde en eksperimentell tilnærming. Sjøvann ble innhentet fra 80 meter dybde i Trondheimsfjorden og tilsatt 0.005 pM Hg og 2.0 pM Pb. I eksperimentet ble tre ulike behandlinger testet: Mn, Fe og kombinasjonen av de (1:1 forhold). For hver behandling ble 10, 25, 50 og 100 nM Fe(II) og/eller Mn(II) tilsatt.

Pb, Fe og Mn adsorberte signifikant på veggene i flaskene. Derfor var de fleste målinger av dPb under deteksjonsgrensen mellom 2 og 16 timer. En desopsjonstest indikerte at behandlingene med Fe og Mn mellom 25 og 10 nM adsorberte Pb. Basert på en beregning av massebalanse ble det antatt at ikke alt Pb, Fe og Mn ble desorbert av veggene. Hg, Pb, Mn og Fe viste ingen generell trend av å ha blitt kontaminert. En annengradsfunksjon er foreslått for veggadsorpsjon av TPb på polyetylenflaskene i sjøvann. Mer data er nødvendig for å undersøke dette videre. En modell er foreslått for å illustrere kjemiske og fysiske prosesser når sjøvann er lagret på flasker. Til slutt er det gjennomført en vurdering av eksperimentet med forslag til forbedringer.

Acknowledgement

I would like to express the gratitude to the people that have helped and supported me during the last year.

First of all, I am especially grateful to my supervisor, Murat Van Ardelan, for his help, guidance, and support during the past year. It has been inspiring and motivative to work under his supervision. I have always felt more motivated after a talk in his office.

A special thanks to Nicolas Sanchez and Stephen Gustav Kohler for their constructive feedback on the master's thesis, their supervision in the laboratory work, and educational discussions. I would like to thank Nicolas for training me with the seaFAST, and Stephen for training me on the Hg analysis.

I would like to thank Mathew Kuttivadakkethil Avarachen for his help in planning the study design, and for helping with the practical preparations to the experiment. I am also grateful for the assistance at the start of the experiment.

Kyyas Seyitmuhammedov and Anica Simic have been carrying out the ICP-MS analysis of which I am very grateful.

I had the pleasure of working with Minda Nielsen and Olav Bjørnberg with the preparation of the experiment as well as during the sampling period. I am grateful for their assistance.

During the Hg analysis, I had the pleasure to work with Maurice Sifrin. I would like to thank him for guiding me when I was new to the instrument. I am also thankful for that he shared the calibration curve from the seaFAST with me.

Håkon Røe has helped me with the visual presentation of the particle dynamic model. I am very happy with the result and thankful for his help.

I would like to thank Anders Lervik for the discussions concerning the statistical analysis of the results.

I would like to thank Hannes Bräuer for motivational talks.

Lastly, I would like to thank family and friends for the support during the thesis. In particular, my girlfriend Melis Terzi for the support and for keeping the spirit high during the process. Thanks to the students in Demokrit and the students at the ENVITOX program that have made this a memorable journey.

Table of Contents

List of Figures

List of Tables

List of Abbreviations

ANOVA	Analysis of variance
Control 1	Seawater
Control 2	Seawater + Hg, Pb, As, Cr spike
CVAFS	Cold Vapor Atomic Fluorescence Spectrometry
DI	Deionized
dTe	Dissolved trace element (colloids smaller than 0.2 µm)
EDTriA	ethylenediaminetriacetate
Experimental bottles	1 L polyethylene bottles used during the incubation period.
Fe oxide	All oxidized species of Fe
HMO	Hydrous manganese oxide
ICP-MS	Inductively Coupled Plasma Mass Spectrometry
IDA	iminodiacetate
In situ Mn, Fe, or MnFe	Mn(II) and/or Fe(II) added as an experimental treatment and that subsequently oxidizes *in situ*
LOD	Limit of detection
mbsl	Meter below sea level
Mn oxide	All oxidized species of Mn
m/z	Mass-to-charge ratio
MQW	Milli-Q water
PE	Polyethylene
rps	Revolutions per minute
RSD	Relative standard deviation
std	Standard deviation
SW	Seawater
Te	Trace elements
TTe	Total acid leachable trace elements
UP	Ultra-pure

1 Introduction

Anthropogenic activities have substantially altered the natural Hg and Pb cycle. Hg and Pb are released from anthropogenic activities through mining activities, smelting, as well as combustion of biomass, coal, and fossil fuel combustion (Bridgestock et al., 2016). The anthropogenic emissions have led to approximately 450 % increase in atmospheric Hg (AMAP, 2021) and a 10-fold increase in reactive Pb flux in the terrestrial and marine environment since pre-industrial times (Pacyna & Pacyna, 2001). Natural emission sources of Hg and Pb include volcanic eruptions, geogenic events, wildfires, vegetation, and soil derived dust (AMAP, 2021; Nriagu, 1989).

In seawater, Hg and Pb are in trace concentrations in nanomolar and picomolar range. Regardless of their low concentration, these elements are toxic and therefore exhibit an adverse effect to marine life (Ross et al., 2017). Knowledge about the cycle of toxic trace elements is highlighted by United Nations Sustainable Development Goal number 14 which concerns the marine environment. In particular, Goal 14 a) aims to increase the scientific knowledge with regards to the marine environment (United Nations n.d.).

Marine trace elements are important to study. Human activities such as fossil fuel combustion leads to warming of the oceans, with resulting lower oxygen content. Moreover, the increase in atmospheric carbon dioxide (CO_2) leads to ocean acidification due to the change in the carbonate equilibria (AMAP, 2018; Gruber et al., 2021). These factors ultimately affect the marine biogeochemistry of trace elements. When there is less oxygen in the waters, redox sensitive elements such as Fe and Mn are affected (Tebo, 1991). The increased temperature at surface results in stratified water columns and less mixing of oxygen between the surface and deeper waters. The stratification results in an increase in the suboxic and anoxic zones (Gruber et al., 2021) which also affect the Fe and Mn species. With lower pH in the benthic seawater, sedimented elements can become mobilized and diffuse into the water column. As an example, Pb becomes more mobile at lower pH (Wang et al., 2019).

1.1.1 Literature

Various marine particles have been extensively researched for their adsorption capacities of trace elements. For instance, Yang et al. (2013) measured Pb adsorption onto six different particles and saw that MnO_2 and Fe_2O_3 adsorbed more Pb than SiO_2, $CaCO_3$, Al_2O_3, and Kaolinite. Koschinsky et al. (2003) measured adsorption of various trace elements onto resuspended deep-sea sediments. Their findings indicates that cations, i.e., hydrated cations, e.g., Mn^{2+}, and cationic chloro-complexes, e.g., $PbCl^{+}$, are predominantly adsorbed onto negatively charged Mn oxides. In contrast, oxyanions, e.g., $HAsO_4^{2-}$, and neutrally charged species, e.g., $PbCO_3^{0}$, are adsorbed onto Fe oxide particles. Andreae (1979) measured a depletion of arsenate in interstitial seawater, hypothesizing co-scavenging with Fe and Mn oxides. Concerning Hg, Liang et al. (2013) saw that Hg adsorbed stronger to Fe than Mn. On the contrary Kohler, Kull, et al. (2022) saw a correlation between Hg and Mn in sediments whereas Fe was not correlated with Hg. In overall, there is a common consensus that Mn and Fe particles are important scavengers for toxic trace elements such as Hg, Pb, Cr, and As. However, it is ambiguous whether Fe, Mn, or the combination of them has the better adsorption capacity for toxic trace elements.

An overview of experimental incubation studies that researched Hg and Pb adsorption onto Fe and Mn oxides is presented in Table 1.1. Their main findings, their relevance, limitation, and justification why the paper was selected is explained for each article in the table. Common for these studies is that they have investigated adsorption of Hg, Pb, Cr, and As onto particulate Fe and Mn and/or at higher concentrations than what is found in proximity to anoxic intrinsic waters. It remains unclear how efficient initially oxidized Fe and Mn adsorb Hg, Pb, As, and Cr in seawater.

Table 1.1: Experimental studies conducted on Hg and Pb adsorption onto Fe and Mn particles. HMO = hydrous manganese oxide.

Article	Main Findings	Relevance	Limitations	Why
(Lockwood & Chen, 1973)	- Hg adsorption onto MnO_2 was repressed due to Cl complexation. - $Hg(OH)_2$ adsorbed more rapidly than $Hg(Cl)_2$.	- Investigated Hg removal by HMO at a wide range of environmental conditions.	- Used single electrolytes (NaCl and $NaClO_4$) to mimic seawater conditions. - Studied aged Mn oxides. - Experiment fixed at 25 degrees. - Studied high mercury concentrations.	- One of the first experimental studies that investigated toxic element adsorption onto Mn oxides in natural waters.
(Liang et al., 2013)	- Cl complexation of Hg inhibited adsorption onto Mn and Fe oxides. - Cl complexation inhibited adsorption onto amorphous more than crystalline structures. - Humic acid increased Hg adsorption in seawater	- Investigated Hg adsorption onto amorphous Mn and Fe hydroxides at simulated seawater conditions. - XRD analysis to determine structure and properties of Fe and Mn hydroxides. - Compared Hg adsorption of amorphous and crystalline structures.	- Investigated aged species of Fe and Mn. - Used high concentrations (>0,5 µM) of Hg.	- In the present study, unfiltrated seawater was used. Therefore, there was of interest to know the sorption capacity of amorphous relative to crystalline structures. - The properties of Mn and Fe oxides are important to understand why they are good adsorbents.
(Lu et al., 2014)	- *In situ* formed MnFe had high affinity for Hg. - Oxides flocculated and scavenged Hg. - MnO_2 or MnOOH and FeOOH were dominating species.	- Incubation experiment of *in situ* formation of MnFe. - XPS analysis to reveal structure of oxides. - Provide mechanisms for flocculation.	- Freshwater conditions. - Incubation at 25 °C. - Fe(II) added to pre-oxidized MnO_4^-. - High concentration in µg/L scale.	- The structure of initially formed Mn and Fe oxides is important to understand why they are good adsorbents.
(Koschinsky et al., 2003)	- Resuspended particulate Fe and Mn adsorbed the most dTe. - Pb was particle reactive to a wide range of particles. - Mn adsorb cations.	- Incubation experiment on natural particles and their element adsorption. - Seawater conditions.	- They investigated sedimented particles. - High particulate concentration.	- Their findings indicate which adsorbent that can be expected to adsorb which adsorbate. - Measured Pb adsorption onto

	- Fe adsorb anions and neutrally charges species.			various Fe and Mn particles.
(Wang et al., 2019)	- Pb was more particle reactive at pH 6-8 more than at pH below 5 - Pb adsorption onto MnO_2 and Fe_2O_3 was highly influenced by particle size. - Natural MnO_2 adsorbed better than hematite.	- Investigated sorption of Pb onto 12 marine particles at different pH, salinities, and time scales.	- Used hematite as natural Fe oxide. - Only measured adsorption as a function of time onto illite. - Suspended particulate matter concentration relevant for estuarine waters.	- Their findings indicate which adsorbent that can be expected to adsorb which adsorbate. - Measured Pb adsorption onto various Fe and Mn particles.
(Swallow et al., 1980)	- Pb^{2+} adsorption decreased because of Cl complexation at higher ionic strength. - Higher adsorption capacity was suggested for permeable oxide structures.	- Laboratory experiment of Pb sorption onto hydrous ferric oxide in the range from no ionic strength to simulated seawater. - Tested different Pb to Fe ratios.	- Used hydrous ferric oxide only. - High Pb and Fe concentration.	- Adsorbate to adsorbent ratio have an important influence on adsorption.

1.1.2 Research Questions

This study sought to fill the knowledge gap in which the adsorption capacity of initially oxidized Fe and Mn were investigated. Three research questions were aimed to be answered in this study:

- Which of the Fe and Mn oxides are the more important adsorbent for Hg and Pb in seawater?
- Which oxide concentration has the most profound effect on Hg and Pb adsorption?
- How long time does it take for the adsorption of Hg and Pb to adsorb onto initially formed Fe and Mn oxides to approach equilibrium?

1.1.3 Objective

Fe and Mn are redox sensitive elements cycling in the ocean. In anoxic intrinsic waters, they form soluble reduced species that can diffuse upwards the water column. When they reach oxic layers, they oxidize and precipitates as colloids and particles that can adsorb toxic elements. The objective of this study is to investigate how efficient Hg and Pb are adsorbed onto *in situ* oxidized Mn, Fe and MnFe (*in situ* Mn, Fe, or MnFe) in seawater. To approach this objective, an incubation experiment will be conducted to simulate the process in which reduced Fe and Mn becomes oxidized and adsorb Hg and Pb.

To answer the research questions, the most effective adsorbent of the oxidized Fe, Mn, and the combination of MnFe (1:1 ratio) will be evaluated in separate treatments. Furthermore, the most effective adsorbent concentration will be investigated by adding 10, 25, 50, and 100 nM Mn and/or Fe. The incubation period will be 14 days to study the time frame until equilibrium is reached between the adsorbent and adsorbate.

The incubation experiment is kept environmentally relevant by using coastal seawater, collected at 80 meters depth, as matrix. The experiment is to be carried out at similar

temperatures as found at this depth, approximately 10 °C (Azad et al., 2019). Furthermore, by sampling dissolved and total trace elements, information on the size distribution is gathered.

Alongside the main experiment, it is of interest to compare centrifugation with filtration to investigate the success of separating particulates (>0.2 µm) from the suspension. Additionally, another test is to be performed on adsorption of toxic elements onto the polyethylene walls in the bottles.

The analysis of the trace elements is approached in two ways. Hg samples is analyzed with MERX® autosampler coupled with Brooks Rand Model III Cold Vapor Atomic Fluorescence Spectrometer (CVAFS). Due to the low concentration of Pb, the samples will be preconcentrated onto NOBIAS Chelate-PA1 resin with seaFAST operated in offline mode prior to Inductively Coupled Plasm Mass Spectrometry (ICP-MS) analysis.

2 Theory

2.1 Hg in the Marine Environment

2.1.1 Sources

Elemental gaseous mercury is transported over longer distances in the atmosphere compared to Hg^{2+} that is more reactive and soluble in aerosols. Gas phase mercury can further undergo oxidation steps in the atmosphere to divalent mercury (AMAP, 2021). Mercury is considered to be reactive when it is deposited as Hg^{2+} in the ocean because it is a charged species with no ligands that readily takes part in biogeochemical reactions (Cossa et al., 1996). For these reasons, atmospheric deposition is a dominant source of reactive mercury to the remote marine environment (AMAP, 2021; Batrakova et al., 2014).

A considerable amount of atmospheric mercury deposited on land can be transported to the coast with river systems (AMAP, 2021). However, as much as 90 % of total mercury transported by rivers are bound to particles and can be considered as non-reactive. It will not take part in any reaction but sink down to sediments with the particles (Cossa et al., 1996).

A third source of mercury is coming from the ocean itself. Ocean currents transports mercury between the oceans. Upwelling brings mercury from deep zones in the ocean to the surface. Upwelling is a physical mechanism when deep water is brought to the surface because the current is directed towards land. Another is advection when the temperature and the salinity is conservative throughout the water column, mixing can bring mercury to the surface (AMAP, 2021).

2.1.2 Speciation

Mercury forms complexes with chloride in seawater in which $HgCl_4^{2-}$, $HgCl_3^-$, $HgCl_2^-$, and $HgBrCl^-$ is dominating species (Grassi & Netti, 2000). The complex stability between mercury and chloride can be explained by the classification of mercury as a class B metal. Class B-type metal cations are recognized with features such as low electronegativity and high polarizability and prefer to bind anions with similar behavior with respect to kinetics and equilibrium (Stumm & Morgan, 1996, pp. 283-287). For this reason, mercury forms complexes with chloride over hydroxide ions (Lockwood & Chen, 1973; Stumm & Morgan, 1996, p. 665). Furthermore, the chloride complexes stabilize mercury in the solution which leads to decreased Hg adsorption onto particles (Turner, 1987) (Liang, 2013).

2.1.3 Cycle

Divalent mercury in the marine environment can undergo three dominating processes, i.e., reduction of Hg(II) to Hg(0) that can escape from the water column through evasion, adsorption to particles with resulting scavenging through the water column, and methylation (Lamborg et al., 2014).

Hg(II) can be reduced to Hg(0) through photoreduction and dark reduction. Photo-mediated mercury reduction is many times faster than dark reduction. Especially, mercury bound to ligands with chromophores as functional group, e.g., dissolved organic matter, have increased reduction rates due to electron transfer from ligand to metal. However, this

has been found to be more relevant in coastal regions where these ligands are more abundant (Batrakova et al., 2014). The light energy is an efficient catalyst and there has been shown that surface waters can be supersaturated in dissolved gaseous mercury during daytime in temperate climate regions (Castelle et al., 2009). In opposite to photochemical reduction, dark reduction occurs in absence of light below the light penetrating depth or under the sea ice. Dark reduction is driven by bacteria and algae that utilizes Hg^{2+} as electron acceptor (Batrakova et al., 2014). Even though dark reduction is much slower than photochemical reduction, gaseous elemental mercury can accumulate over time, e.g., when sea-ice hinders the evasion of gaseous mercury (AMAP, 2021).

Hg(II) is a scavenging element that can be removed from the surface waters driven by adsorption onto particles that settles through gravitational force. To determine the distribution of an element between dissolved or particulate phase, the Kd value are a fundamental parameter. That is, particulate concentration divided by dissolved concentration (Batrakova et al., 2014). The Kd value of Hg can be significantly different between oceans, influenced by changes in environmental conditions. For instance, the extent of Hg adsorption depends on the geochemical composition of the particle, particle concentrations, and planktonic organisms (Cui et al., 2021). Cui et al. (2021) found that MnO_2 and $Fe(OH)_3$ particles had a highly strong affinity for Hg compared to other marine particles. This was in accordance with another study that hypothesized that Mn oxides are important scavengers for Hg in Arctic seas in the little-known winter-time mercury cycle (Kohler, Heimbürger-Boavida, et al., 2022). However, Kd of Hg in marine waters is complex, and the findings from Cui et al. (2021) indicates that MnO_2, and $Fe(OH)_3$ particulates have a negligible effect on Hg in oceanic surface waters because of their low concentrations. In a previous study, the same authors hypothesized that organic matter offer a more important surface for Hg adsorption in surface waters due the higher concentrations of phytoplankton (Lamborg et al., 2014). Overall, studies of particulate interaction with Hg are important to better understand the Hg cycle in seawater.

When mercury reaches suboxic and anoxic zones in the water, bacteria can cause methylation and dimethylation in which one and two CH_3 groups attaches to the mercury ion, respectively. However, methylation can occur in the whole water column if there is high biological activity. Compared to biotic methylation, abiotic methylation is considered less important as the main source is from hydrothermal vents (Batrakova et al., 2014).

2.2 Pb in the Marine Environment

2.2.1 Sources

Pb is geochemically behaving like mercury and is transported to the ocean through atmospheric and continental runoff pathways. Although, Pb has a lower volatility than mercury, Pb can be released to the atmosphere from smelting industry and fossil fuel combustion. Pb is only stable in gas phase at high temperature so when it cools down in the atmosphere, Pb either react or adsorbs to aerosols (Boyle et al., 2014). The reactivity results in a short atmospheric residence time as short as days as it gets washed out through wet deposition. There has also been found that dry deposition of North-African mineral dust is a significant contribution to the total Pb deposition in the Atlantic ocean (Bridgestock et al., 2016). Pb can enter the marine environment from mining sites, smelting industry, and coal burning. Long range transportation can also be a source of Pb to rural oceanic waters (Boyle et al., 2014).

2.2.2 Speciation

Pb(II) is considered as an intermediate type metal cation between class A and class B metals. However, it has more common properties with class B metals (Stumm & Morgan, 1996, p. 287). Therefore, Pb is found in association with both chloride (Cl^-) and carbonate (CO_3^{2-}) anions, as shown in the speciation diagram in Figure 2.1. The pH in seawater is approximately 8.2. At this pH in the speciation diagram, Pb is 50.2 % associated with carbonate ions and 23.8 % associated with chloride. The mixed-ligand species $PbCO_3Cl^-$ is the second most important species making up a proportion of 16.1 % (Powell et al., 2009). However, the authors empathize the uncertainties in the stability constant of $PbCO_3$ and $PbCl_4^{2-}$.

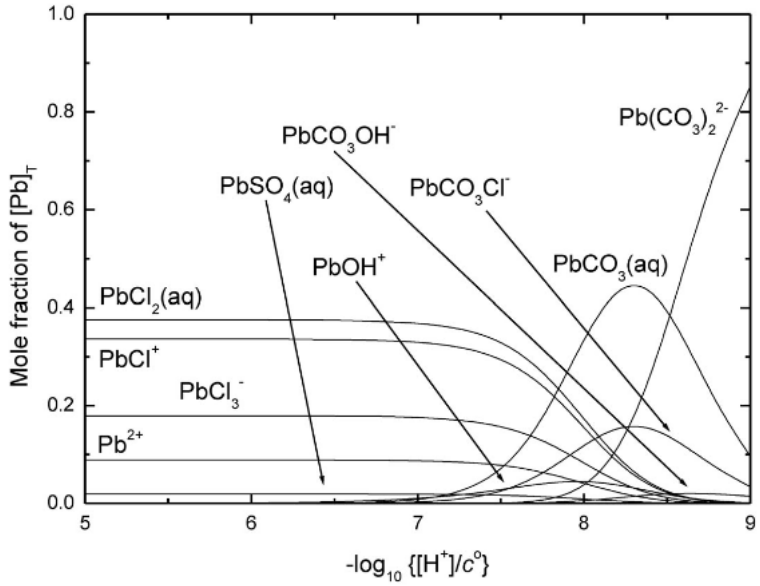

Figure 2.1: Speciation diagram of Pb in a simulated seawater system. At equilibrium with atmosphere at 25°C. [Pb^{2+}] = 1 mol/dm³, I_C = 0.67 mol/dm³. Reproduced from Powell et al. (2009).

2.2.3 Cycle

Pb is a scavenging element and its distribution in the marine environment is to a large extent controlled by particle adsorption or complexation and resulting scavenging through the water column. The scavenging distribution of Pb in the water column is shown in Figure 2.2. The particle reactivity of Pb results in a residence time shorter than two years in surface waters. That means that the Pb concentration in surface waters is in equilibrium with the atmospherically input flux (Boyle et al., 2014). Similar to the Kd values of Hg, Bam et al. (2020) measured that the Kd value of Pb is influenced by the geochemical composition and concentration of the particles. They measured changes in Kd values in different oceans. The authors postulate that the higher Kd values of Pb was explained by somewhat higher Mn concentrations even though the low abundance of this mineral in surface water. Accordingly, two experimental studies demonstrated that Pb exhibits a stronger adsorption affinity for MnO_2 compared to other marine particles (Wang et al., 2019; Yang et al., 2013). In another study, Tang et al. (2017) investigated Pb in the North Atlantic, and they measured that Pb had a higher affinity for inorganic particles over particulate organic matter. Overall, even though the distribution of Pb between dissolved and particulate phases are dependent on the particulate, the element is efficiently scavenged through the water column.

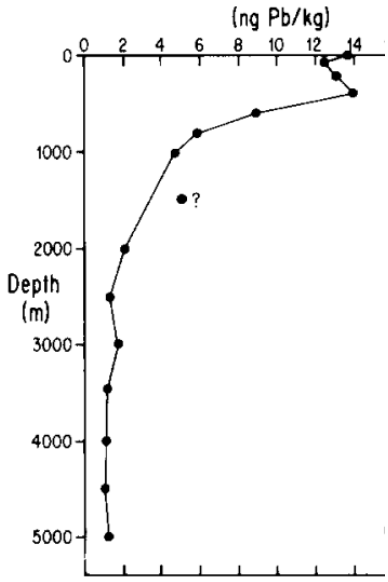

Figure 2.2: Pb distribution in the water column in the central northeast Pacific Ocean. Reproduced from Schaule and Patterson (1981).

Ultimately particulate Pb settles in the sediments. However, the benthic biogeochemical control factors of Pb are poorly known (Vieira et al., 2019). Two general processes are hypothesized, i.e., it can be buried in the sediments with the scavenging particle (Schaule & Patterson, 1981) or mobilized to the surroundings (Vieira et al., 2019). With ocean acidification, new research postulates that Pb might become mobilized from the sediments as the pH decreases (Gao et al., 2023). Another release mechanism is related to Fe and Mn oxide particles. Pb can be released to the ambient water when the Fe and Mn oxides become reduced and dissolved in the anoxic environment (Vieira et al., 2019).

2.3 Fe and Mn in the Marine Environment

2.3.1 Sources

Fe and Mn are two of the most abundant trace elements in the terrestrial environment and on the earth's crust. On the contrary, their concentrations rapidly decrease in distance to the coastal areas because of the formation of oxide particles. River discharge and land erosion are major sources to the coastal environment, whilst atmospheric deposition through dust events and volcanic eruptions are major sources to the rural ocean (Breitbarth et al., 2010). Hydrothermal vents can introduce Fe and Mn from the deep sea (Cui et al., 2021).

2.3.2 Speciation

Fe and Mn can be considered as a polymorph element in seawater since it is present as a myriad of different crystallographic structures. For simplicity, the term oxide is used as an analogue to all oxidized species of Fe and Mn in the rest of the thesis.

2.3.2.1 Size Classes in Seawater

Marine geochemistry comprises a complex variety of size fractions which is commonly divided into three size ranges, i.e., particulates, colloids, and dissolved phases. There is no clear size distinction between particles and dissolved phases in a solution. As defined by Everett (1972), colloids are a suspension of molecules between particulate and dissolved phases with at least one dimension between 1 nm and 1 µm. In order to approach this

definition in applied marine geochemistry, elements that passes filters with 0.45 µm pores (Berger et al., 2008) or 0.2 µm pores (Berger et al., 2008; Kanna et al., 2020; Krisch et al., 2021) are referred to as dissolved. Conversely, particulates are solid phases in a suspension with a diameter above these pore sizes.

2.3.2.2 Redox Reactions of Fe and Mn

Reduction oxidation reactions are defined as exchange of electrons between one electron donor and one electron acceptor (Stumm & Morgan, 1996, p. 426). In nature, Fe and Mn have a short range of stable oxidation states. Fe species exist in oxidation states (II) and (III) whereas Mn is predominantly in oxidation states (II) and (IV). The benthic waters in proximity to the sediments is known for its reducing environments. Here, the dissolved oxygen concentration is low (suboxic) or absent (anoxic), and Fe and Mn exist in their reduced oxidation state (II). Conversely, surface waters are generally rich in dissolved oxygen that can react with Fe(II) and Mn(II). The process is an oxidation reaction in which oxygen is the electron acceptor, whereas the metals are the electron donors. The oxidation reaction of Fe and Mn are noted in equation (1) (van de Velde et al., 2021) and (2) (Jones et al., 2011), respectively.

$$4Fe^{2+} + O_2 + 4H^+ \rightarrow 4Fe^{3+} + 2H_2O \quad \textbf{(1)}$$

$$2Mn^{2+} + O_2 + 2H_2O \rightarrow 2MnO_2 + 4H^+ \quad \textbf{(2)}$$

Upon Fe oxidation, colloids are formed from Fe precipitation. In normal seawater conditions at pH 8.0, insoluble $Fe(OH)_3$ is the dominating specie, making up 92 % of the total species (Millero et al., 1995). The reaction with water is shown below.

$$Fe^{3+}{}_{(aq)} + 3H_2O \rightarrow Fe(OH)_{3\,(s)} + 3H^+ \quad \textbf{(3)}$$

Even though both Fe and Mn can be oxidized by oxygen, their reaction kinetics differ substantially. The different reaction kinetics between Fe and Mn can be explained by Figure 2.3. In the figure, the redox potentials of selected Fe and Mn oxides are presented together with other redox couples. The high redox potential of Fe^{3+}/Fe^{2+} can be ignored because it is only relevant in acidic conditions when Fe does not form precipitates. The other redox couples between Fe^{2+} and its various species have a redox potential below 0. This signifies that Fe^{2+} becomes easily oxidized in natural waters. Conversely, the different oxides of Mn are found within a narrow positive range in redox potential. Therefore, Mn particles can oxidize other proximate species in seawater, whereas the oxidation of Mn(II) itself is slow (Liu et al., 2022).

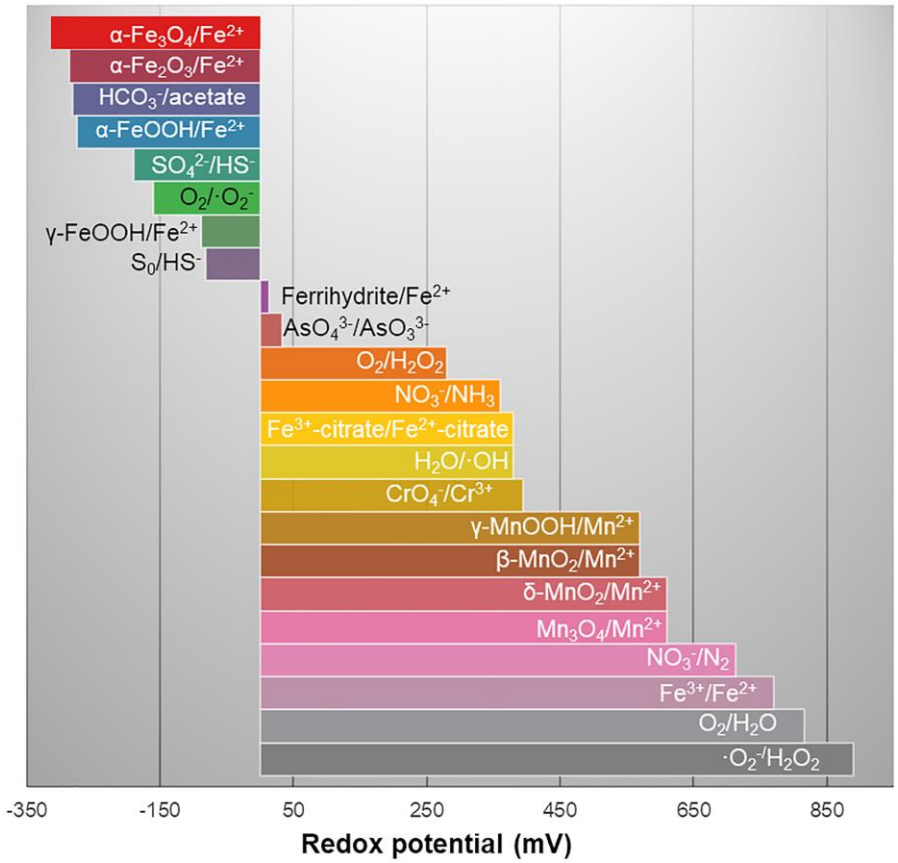

Figure 2.3: Redox potentials of Fe and Mn species. The illustration is reproduced from Liu et al. (2022).

The oxidation rates of Fe and Mn can be calculated from equation (4) (Raiswell & Canfield, 2012, p. 92) and **(5**) (Tebo, 1991), respectively. As noted, the reaction kinetics of both Fe and Mn are dependent on the oxygen and hydroxide concentration in the ambient water. Although, the pH has a greater influence than oxygen on the reaction due to the second order $[OH^-]$ term in both reactions. Because of the strong oxidation potential of MnO_2, reaction **(5**) suggests an autocatalytic oxidation of Mn in heterogenous waters. Thus, the more suspended Mn particles, the faster will Mn(II) become oxidized (Liu et al., 2022).

$$-\frac{d[Fe(II)]}{dt} = k[Fe(II)][O_2][OH^-]^2 \quad \textbf{(4)}$$

$$-\frac{d[Mn(II)]}{dt} = k[Mn(II)][MnO_2][O_2][OH^-]^2 \quad \textbf{(5)}$$

2.3.2.3 Aging

Once formed, $Fe(OH)_3$ are thermodynamically stable and compose a precursor for more refractory Fe species. These colloids form stable complexes that attract each other to form clusters of amorphous nanoparticulate $Fe(O,OH,OH_2)_6$ that further aggregates to colloids (Raiswell & Canfield, 2012, p. 15). These initial amorphous hydroxides are commonly referred to hydrous ferric oxide. Similarly, amorphous Mn is referred to as hydrous manganese oxides. When Fe oxides age, they lose water and develop a crystalline structure (Turner & Hunter, 2001, p. 345). The crystal that forms depend on the precise

environmental conditions that forms the oxide. Ferrihydrite is a crystal species found in many coastal waters. This mineral is poorly structured and does not become more crystalline with aging. However, ferrihydrite is an important precursor to other minerals such as the more thermodynamically stable minerals goethite and hematite (Cornell & Schwertmann, 2003, pp. 23-24). Schwertmann et al. (2004) did an experimental study where they showed that the conversion from ferryhidrite to the more crystalline structures goethite and hematite is slow at environmentally relevant conditions. At 10 degrees, the half-life of the ferrihydrite conversion was found to be approximately 400 days.

Initially formed oxides of Fe and Mn have an amorphous structure with high porosity. They form minuscale particles resulting in high specific surface area, often more than 100 m^2/g (Cornell & Schwertmann, 2003, p. 3). With aging, the porosity decreases (Liang et al., 2013). For instance the more refractory goethite has a lower specific surface area than its precursor ferrihydrite (Turner & Hunter, 2001, p. 330).

2.3.3 Adsorption Properties of Fe and Mn Oxides

A quality of Fe and Mn oxides is their high affinity for trace elements owing to the surface charge properties, surface active sites, and the porous structure (Trivedi & Axe, 2001). Although, the inorganic complexation of Fe is important, Fe in oxygenated seawater is predominantly associated with organic ligands (Cullen et al., 2006). The affinity Fe has for organic ligands can be explained by its high hydrolysis constant. The stability of elements by organic ligands is proposed by scholars to be increasing with the hydrolysis constant of the metal ion. (Turner & Hunter, 2001, p. 206). Humic substances transported to coastal areas by land erosion can also adsorb onto Mn colloids (Oldham et al., 2017). Additional sources of organic ligands originate from primary producers, which release these compounds to facilitate the uptake of Fe (Leventhal et al., 2019). In overall, organic ligands generally results in an increased colloidal fraction of the oxide (Leventhal et al., 2019; Oldham et al., 2017).

2.3.3.1 Surface Charge Characteristics

Point of zero charge is an important parameter to account the surface charge properties of a complex. The point of zero charge describes when the overall electrical charge of a complex is zero. The complex has a positive charge when the pH is below the point of zero charge. Oppositely, the surface charge is positive when the pH is above the point of zero charge (Liang et al., 2013). The point of zero charge is 7-9 for Fe (Kosmulski, 2002; Trivedi & Axe, 2001) and 2-3 for Mn (Kosmulski, 2002). In seawater, Fe is neutral, and Mn has a negatively charge (Koschinsky et al., 2003; Stumm & Morgan, 1996, p. 539).

Because of charge - charge attraction, anions and oxyanions have a preference for Fe, whereas cations have a preference for Mn (Koschinsky et al., 2003; Krauskopf, 1956). $HAsO_4^{2-}$ and $PbCO_3^0$ is associated with Fe. Hydrated cations, e.g., Mn^{2+}, and cations weakly associated with chloro- complexes, e.g., $MnCl^+$, $PbCl^+$, are adsorbed on the negative surfaces (Koschinsky et al., 2003).

2.3.3.2 Surface Active Sites

The surface-active sites of Fe and Mn precipitates are hydroxyls and oxygen groups (Lu et al., 2014). Trace elements may adsorb onto the oxygen-carrying groups (Tiffreau et al., 1995). Proposed adsorption mechanisms are given below. Equation (6) and (7) is supported by Koschinsky et al. (2003), and equation (8) is taken from Turner and Hunter

(2001, p. 329) and Stumm and Morgan (1996, p. 572). The equal sign (=) represents the surface of the adsorbent.

$$2 \equiv MnO_2H^+ + Me^{2+} \rightleftharpoons 2 \equiv MnO_2\text{-}Me^{2+} + 2\ H^+ \quad \textbf{(6)}$$

$$\equiv FeO\text{-}OH + HAsO_4^{2-} \rightleftharpoons \equiv FeO\text{-}O\text{-}AsO_3H^- + OH^- \quad \textbf{(7)}$$

$$\equiv FeOH + Me^{2+} \rightleftharpoons \equiv FeOM^+ + H^+ \quad \textbf{(8)}$$

Fe and Mn may behave as a Lewis acid and base depending on the adsorbate. As seen in the equations above, the adsorption of divalent cations leads to the release of a hydrogen ion whereas the adsorption of an anion leads to release of a hydroxide ion.

2.3.3.3 Seawater Influence on Adsorption Rates

The ionic strength in seawater has implications on the adsorption rates. The reaction rates are lowered for species with opposite charge whereas the reaction rates increase for species with similar charge. For uncharged species, the ionic strength has little effect (Stumm & Morgan, 1996, p. 75).

2.3.4 Cycle

Fe and Mn are controlled by redox gradients in seawater, and thus their cycle in the environment is to a large extent controlled by this feature. When rivers and atmospheric inputs are the sources of Fe and Mn, they enter the surface waters as oxide particles. In this form, they are thermodynamically and kinetically stable as Fe(III) and Mn(IV). Gravitational settling results in concentration distribution that decreases with depth. When they enter the anoxic environment at depth and in sediments, they become reduced to soluble Mn(II) and Fe(II). Upon the reduction reaction, they can slowly diffuse upwards the water column (Nealson & Saffarini, 1994). Wintertime overturning, resuspension events, and upwelling may enhance the upward transportation of Fe and Mn to the oxic surface waters (Vieira et al., 2019). Lastly, they become oxidized in the presence of oxygen and scavenge back to the sediments (Nealson & Saffarini, 1994).

The theoretical electrochemical information presented above can be seen in nature. Fe is rapidly oxidized in oxygenated seawater, and within orders of minutes, Fe(II) is completely removed (Raiswell & Canfield, 2012, p. 92), whereas the oxidation of Mn is slower (Stumm & Morgan, 1996, pp. 684-686). For this reason, Fe has a shorter cycle around the suboxic zones compared to Mn, as presented in Figure 2.4. The slow Mn oxidation allow the element to migrate further up into oxidized waters before it forms colloids and particles. Conversely, below the suboxic zone, Mn becomes more rapidly reduced than Fe. This allows Mn to solubilize earlier and diffuse upwards again. Fe particles are more resistant to dissolution reduction and reach further down in the water column. Overall, the difference in redox potentials between Fe and Mn leads to fractionation in water systems (Liu et al., 2022).

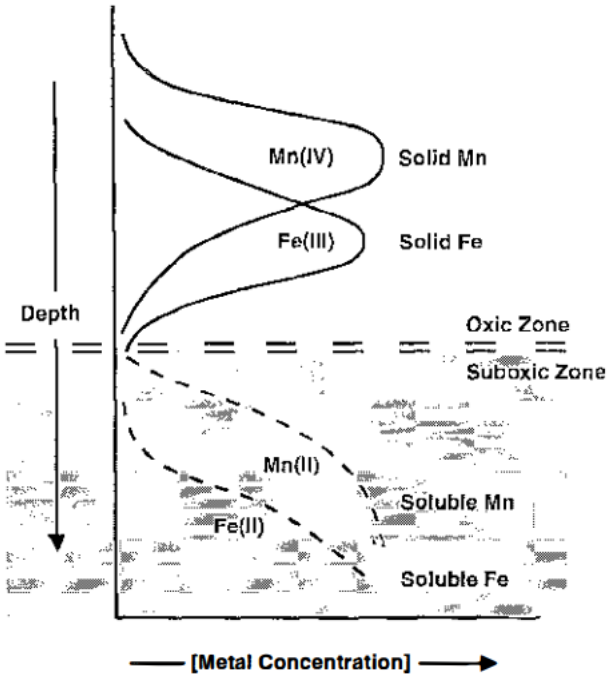

Figure 2.4: Illustration of the vertical distribution of Fe and Mn in the water column. Reproduced from Nealson and Saffarini (1994).

The table below presents a summary of trace element concentrations that are found in the marine environment. The table is categorized into the upper 50 meters and the water masses between 50 and 300 meters. As mentioned, Fe and Mn are transported to the marine environment from land erosion and atmospheric deposition which could explain the variability in their concentrations in different studies. THg concentrations are approximately 1 pM, and TPb concentrations are in the sub nanomolar range.

Table 2.1: Concentrations of trace elements at different depths. mbsl = meter below sea level. Note the different unit size of THg. The sign "~" signify approximate values. *Values are given in nmol kg^{-1}.

mbsl	TFe (nM)	TMn (nM)	THg (pM)	TPb (nM)
0 - 50m	~45-90[a] 20.7 – 707[d] ~10[h]	7.23 – 123[d] 4.2 – 18.1[f] ~14 - 18.2[a]	1.6 – 3.2[c] 0.14 – 0.45[b] 0.5 – 2.5[e]	0.013 – 0.516[d] 0.045 – 0.107*[g] ~0.056*[g]
50 – 300m	~45 – 180[a] ~80[h]	~18.2 – 137[a] 9.2 – 473.3[f]	0.10 - 1.55[b]	~0.24 – 2.4[a] ~0.026*[g]

[a] (Bruvold et al., 2023) Førde Fjord, Fjord
[b] (Azad et al., 2019) Hardangerfjord, Norway
[c] (Coquery & Cossa, 1995) North Sea
[d] (Vieira et al., 2019) Chukci Sea
[e](Charette et al., 2020) Central Arctic Ocean
[f] (Oldham et al., 2017) Saguenay Fjord Canada
[g] (Seo et al., 2021) Japan Sea
[h] (Hurst et al., 2010) Southeastern Bering Sea

3 Materials and Methods

3.1 Study Design

3.1.1 Parameters in the Experiment

Fe(II) and Mn(II) was prepared from the salts iron(II) sulphate heptahydrate and manganese(II) carbonate, respectively. These salts were applied because of their low toxicity and their ease of solubilization. Furthermore, 10, 25, 50, and 100 nM concentrations of Fe and/or Mn were applied in the experiment as this is considered to reflect natural processes. See section 3.2.3.1 for the preparation of *in situ* oxidized Fe and Mn (*in situ* Fe, Mn, or MnFe).

The concentration of toxic trace elements in coastal seawater are normally in sub nanomolar (TPb) and sub picomolar (THg) range, as shown in Table 3.2. Therefore, these toxic elements were spiked in the experiment to be able to observe any effect of the treatments. The spikes were intended to reflect the natural concentrations and processes of toxic element adsorption. The spike preparation can be found in section 3.2.3.2.

Cr and As were included in the experiment because other research hypothesize that Fe and Mn have affinity for those elements (Andreae, 1979; Koschinsky et al., 2003).

Unfiltered seawater was collected from the Trondheim Fjord at 80 meters depth. This ensured an environmentally relevant matrix. The seawater collection is further elaborated in section 3.2.2.

3.1.2 Experimental Set-Up

The incubation experiment included three compartments, i.e., seawater control, spiked seawater control and the Fe and Mn treatments. The seawater control contained only seawater, and the purpose of this control was to measure the background chemical composition of the seawater including the processes in the system over time. Moreover, seawater control was incorporated instead of blanks as it was used to correct the treatments. The spiked seawater control contained seawater spiked with the toxic elements Hg, Pb, Cr, and As. The purpose of the spiked seawater control was to obtain information on the response of the spiked toxic elements in seawater. Furthermore, the spiked seawater control was used to correct the treatments for background adsorption process. That is, other adsorption processes than what could be explained by the treatments. Lastly, three treatments with Mn, Fe, and MnFe (1:1 ratio) contained the spiked seawater with 10, 25, 50, and 100 nM *in situ* Fe(II) and/or Mn(II). In the thesis, the treatments are abbreviated with treatment and concentration, e.g., Mn treatment with 10 nM concentration is written Mn10.

Figure 3.1 show an illustration of the set-up for each sampling time. There were two duplicates of each control. Regarding the treatments, there were four different concentrations of each of the three treatments. The preparation of the experiment is described in detail in section 3.2.

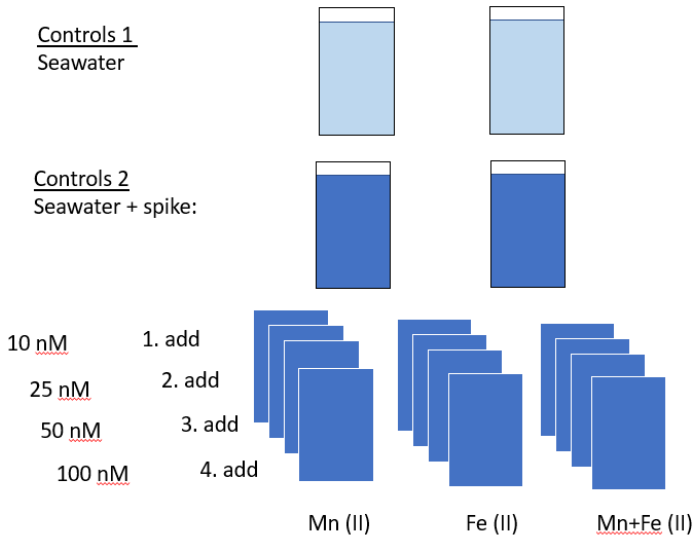

Figure 3.1: Illustration of the experimental set-up at each sampling time.

Polyethylene bottles were used as storage material in the incubation period. These bottles are hereafter referred to as experimental bottles. Each bottle was opened and sampled once. Therefore, every experimental bottle was discarded after it had been sampled. At each sampling time, there were 16 experimental bottles, and there were 8 sampling times in the incubation period. Hence, a total number of 128 1 L bottles were used in the experiment, as shown by the experimental set-up in the photograph below. The cleaning procedure of the experimental bottles are given in detail in Box 3.1.

Figure 3.2: Experimental set-up in laboratory. The following color code were used during the experiment: Mn (red), Control 2 (blank), Control 1 (blank), MnFe (yellow and black stripes), Fe (black). Time zero had been sampled when photo was taken.

The decision to monitor the changes in trace element concentration over 14 days was due to the uncertainty concerning the time required for the systems to approach equilibrium. The sampling was carried out with more frequency at the beginning of the incubation period with longer time intervals later in the experiment. The reason was that there were expected to occur most chemical changes at the beginning of the experiment which stabilized over time as the system approached equilibrium. Table 3.1 gives an overview of the sampling times during the experiment.

Total Hg (THg), dissolved trace elements (dTe) and total acid leachable trace elements (TTe) were also sampled. dTe was defined as the colloids and solutes that passed the 0.2 µm filter. TTe is elements weakly bound to the solid phase that can be freed into the acid preservative solution during storage by hydrogen substitution (Joksič et al., 2005). pH was measured at 64 hours, 6 days, 10 days, and 14 days. Two wall desorption tests were carried out 16 and 19 weeks after the experiment was started to investigate the influence of the walls as adsorption surface of the elements. In addition to the main sampling, the centrifugation test was carried out 10 days and 14 days into the experiment. The test was carried out to investigate whether centrifugation would be as efficient as filtration in separating the Fe and Mn colloids by their size.

Table 3.1: Overview of sampling times during the experiment.

Time from the Start of the Experiment	Sample Collected
2 hours	THg, dTe, TTe
16 hours	THg, dTe, TTe
40 hours	THg, dTe, TTe
64 hours	THg, dTe, TTe + pH
144 hours	THg, dTe, TTe + pH
192 hours	THg, dTe, TTe
240 hours	THg, dTe, TTe + pH + centrifugation
336 hours	THg, dTe, TTe + pH + centrifugation
16 weeks	Wall desorption test Pb, Mn, Fe
19 weeks	Wall desorption test Hg

3.1.3 Laboratory Working Practices

When working with trace elements in nanomolar and picomolar ranges in natural seawater, good working practices are important to mitigate contamination of the samples. Numerous sources of contamination may arise from sampling to analysis. Marine biogeochemists have realized in the last three decades that historic measurements of trace element concentration may be elevated inaccurate due to an element contribution related to sample treatment. Especially Fe and Mn are abundant elements in the environment where samples are handled or processed, i.e., boats and conventional laboratories, posing high risk of contamination (USEPA, 1995).

Sources to contamination include dust and aerosols, unclean laboratory equipment, dirt on gloves, metal surfaces, unclean workbench reagents, and cross-contamination by mixing caps between tubes. Therefore, effective measures include trace metal free sampling tubes, acid washed materials, clean workbench, and immediately change of gloves if they are suspected to be contaminated. Additionally, cross-contamination of samples during

analysis, i.e., carryover, may occur when a sample with high concentration is placed immediately before a sample with low concentration (USEPA, 1995, 2002). Even though there are many possible causes of contamination, the two most important measures are knowledge regarding contamination and to follow this strictly in the job (USEPA, 2002).

To facilitate a cleanroom working environment, several actions were made during the experimental period. The experiment was carried through in an assigned laboratory surrounded by plastic to ensure clean working environment, see photos in Figure 3.2 and Figure 3.3. The floor at the entrance was covered by a cleanroom sticky mat and the entrance was physically separated from the laboratory. Electrolux Plasmawave (with HEPA filter) air cleaner was functioning while the laboratory work was carried through. Additionally, cleanroom clothing was worn while working in the cleanroom i.e., shoe covers, bouffant hat, cleanroom lab coat, and goggles as well as nitrile gloves when sampling. The temperature was approximately 10 °C. In addition, the lights were the only source of light, and they were switched off outside the experimental working time. This limited the impact of light on the chemistry in the bottles.

Figure 3.3: Entrance to the laboratory. The laboratory is separated from the surroundings with plastic. The blue sticky mat can be seen at the entrance.

3.2 Preparations of the Experiment

3.2.1 Cleaning of Experimental Bottles

The experimental bottles were cleaned and preconditioned according to the acid washing protocol written in Box 3.1.

Box 3.1: Acid Washing Protocol of Experimental Bottles

Equipment's and reagents:

- 128 1 L PE bottles
- 2 plastic jerrycans
- MQW
- 1 M HNO_3
  Dilution from 14 M HNO_3: Fill jerrycan with 13 L MQW and 1 L 14 M HNO_3.
- 0,1M UP HNO_3
  Dilution from 14 M UP HNO_3: Fill PE bottles with MQW and add 8 mL 14 M UP HNO_3
- Peristaltic pump

Working practices to minimize contamination:

- Work in a fume hood to minimize risk of contamination from ambient air when the experimental bottles are filled and emptied,
- Clean and cover fume hood with plastic film when filling bottles with acid.
- Always wear nitric gloves when handling the experimental bottles

Methodology:

1. Rinse the bottles in MQW.
   Rinse the bottles inside 2-3 times, rinse the caps, and outside the bottles.

2. Clean the bottles with 1M HNO_3.
   Fill the bottles 0,5 to 1 cm from top. Cap the bottle and turn it one time so that acid touches the inside of the cap. Store the bottles for 3 days in fume hood.

3. Empty the bottles for acid and rinse 3 times with MQW
   I. Add 50 mL of MQ water to the bottle. Cap the bottle and carefully turn it so that the water touches all the bottle surface. Empty.
   II. Repeat previous step with 100 mL MQW and empty the bottle.
   III. Repeat one more time by filling approximately 2 dL MQW to the bottles. Empty the bottles.

4. Look for impurities outside of the bottle. If visible, wipe with MQW and single-use wipes.

5. Clean the bottles with 0,1M UP HNO_3.
   Fill the bottles with MQW 0,5 to 1 cm from top. Add 8 mL 14 M UP HNO_3. Cap the bottle, turn it to mix the acid. Store the bottles for 5 days in fume hood.

Box 3.1 Continued

6. Empty the bottles for acid and rinse 3 times with MQW
   Follow procedure as in step 3.

7. Preconditioning with seawater
   Three times: Fill approximately 1 dL SW to each bottle using a peristaltic pump. Turn the bottle so that SW touches all the inner surface of the bottle. Leave the bottle for approximately 5 min before emptying.

Abbreviations: PE: polyethylene, MQW: Milli-Q water, UP: ultra-pure, SW: seawater

3.2.2 Collection of Seawater Used as Matrix

The seawater used in the experiment was collected from the Trondheim Fjord at 80-meter depth by a continuous pump that belongs to Trondheim Biological Station. Two 100 L barrels were filled three times before unfiltered seawater was collected. The seawater was collected between 8 and 9 o'clock on November 7th, i.e., 30 hours prior to the start of the experiment. The seawater was stored at room temperature until the beginning of the experiment.

3.2.3 Preparation of Chemical Stock Solutions

All chemicals used in the experiment were of analytical reagent grade.

3.2.3.1 *In situ* Fe and Mn Preparation

The preparation of Fe and Mn solutions were done at the same day as the start of the experiment. Exactly 0,0556 g iron (II) sulphate heptahydrate (278 Mwt) and 0.0238 g manganese (II) carbonate (114.95 Mwt) was weighted on a Mettler Toledo AG204 DeltaRange scale with 0.1 mg readability. The metal crystals were transferred to each 125 mL plastic bottle and dissolved in 124 mL Milli-Q water acidified with 1 mL UP HNO_3 to pH ~0.93. The solutions contained 207 µM Mn(II) and 200 µM Fe(II). The acidification and dark storage prior to the experiment was to avoid oxidation of the compounds. Any oxidation of these ions would be visible as these complexes emit colors when oxidized.

3.2.3.2 Hg, Pb, Cr, and As Spike Preparation

The intended concentrations of the spikes were 5.0 pM Hg, 2.0 nM Pb, 5.1 nM Cr, and 25 nM As. However, upon the incubation period, it was realized that there was a mistake in the calculation in the spike preparation by a factor of 1 000. Hence, all spike concentrations were 1 000 times lower than intended. The next paragraph explains the spike preparation with updated numbers.

The subsequent steps in the spike preparation are shown in Table 3.2. The spikes were prepared in the following way. Four stock solutions containing respectively 1 000 ppm Hg, Pb, Cr, and As were used for the spike preparation. In the first dilution step, 0.1 mL Hg, and 1 mL of the respective Pb, Cr, and As spikes were added to each separate 1 L volumetric flask. In the next step, 0.1 mL Hg, 10.5 mL Pb, 10.5 mL Cr, and 10 mL As were added separately to new 1 L volumetric flasks. Between every dilution step, the spike solutions were added to unfilled volumetric flasks containing Milli-Q water acidified with UP HNO_3. Upon spike addition, the volumetric flasks were filled with Milli-Q water to reach 1

L. The pH was then below 1,8. Additionally, the flasks were turned to homogenize the solutions in every dilution step.

Table 3.2: Concentrations in the subsequent dilution steps during the preparation of spike. Note the different units in the columns.

Element	Stock solution (ppm)	Stock solution (mM)	First dilution (µM)	Second dilution (nM)
Hg	1000	5.0	0.50	0.050
Pb	1000	4.8	4.8	51
Cr	1000	19.6	19.6	206
As	1000	13.3	13.3	133

3.2.4 The Start of the Experiment

The experiment was prepared in following steps. A peristaltic pump was applied to transfer the seawater from the barrel to the experimental bottles. The transfer hose was rinsed with 0.5 M UP HNO_3 prior to use. The hose was conditioned with seawater as it was used to pre-condition the experimental bottles. One of the two barrels containing seawater was used to precondition the experimental bottles, as described in the acid washing protocol. The seawater in this barrel was continued to be used for the seawater control. First, only 2 bottles were filled with seawater. They were assigned to be duplicates of the time zero seawater control. The samples were collected immediately from the bottle. Thereafter, the other 14 seawater control bottles were filled.

The seawater on the other, untapped barrel was used as matrix for the seawater spike controls and the treatments. The barrel was added 10 mL Hg, 4 mL Pb, 2.5 mL Cr, and 19 mL As with a repetitive pipette (Eppendorf multipipette) plus to reach an accurate element concentration of 5.0×10^{-3} pM Hg, 2.0 pM Pb, 5.1 pM Cr, and 25 pM As. The seawater in the barrel was then homogenised by pumping the seawater back to the barrel for few minutes. Similar to the seawater controls, 2 experimental bottles were assigned to be duplicates of the time zero spiked seawater control. The samples from these bottles were collected immediately. Thereafter, the other 14 spiked seawater control bottles were filled.

Lastly, the treatment bottles were prepared. 96 experimental bottles were filled with the spiked seawater in the barrel. After the bottles were filled, they were ordered into groups. 32 bottles were assigned each treatment, i.e., Mn, Fe, and MnFe. Within each treatment, they were grouped into four. One for each concentration of *in situ* Mn and/or Fe, i.e., 10, 25, 50, and 100 nM. To accomplish the accurate concentration of Fe and Mn, a repetitive pipette plus was used. 0.05 mL were added to achieve 10 nM. Similarly, 0.125 mL for 25 nM, 0.25 mL for 50 nM and 0.5 mL for 100 nM. The bottles were then turned upside down several times upon addition to homogenize the seawater. However, due to the higher Mn (207 nM) concentration relative to Fe (200 nM) concentration, the final concentrations in the bottles were different. Accurate Mn concentration was 10, 26, 52, and 104 nM. For simplicity, the Mn concentrations will be further referred to as the same concentration as Fe.

The starting time of each compartment is defined as follows. Seawater control, and spiked seawater control are defined as the moment when the first sample was taken. For the treatments, the starting time was the moment when Fe and Mn was added to the bottles.

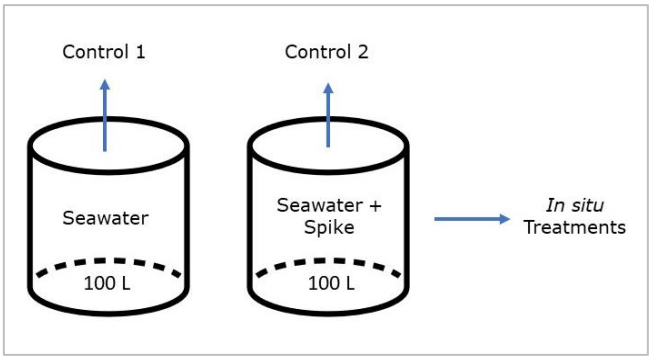

Figure 3.4: Illustration of which barrel with seawater that was used to fill the experimental bottles: seawater control (Control 1), spiked seawater control (Control 2), and the treatments.

3.3 Sampling

The sampling time is recorded as the moment of acidification of the samples. The time window between the collection of each subsample and the acidification was about 10 minutes. This time frame was not thought to be critical.

3.3.1 Trace Element Sampling

All the work related to Pb, As, Cr, Fe, and Mn sampling was carried through in a laminar air flow chamber (AirClean 600 PCR workstation). First, dTe were sampled, i.e., everything smaller than 0.2 µm. It was sampled from undisturbed seawater containers to minimize the particle concentration on filter. The seawater was poured into syringe barrels connected to a 0.2 µm Acropak 200 Capsule with supor membrane. 50 mL VWR conical centrifuge tubes, metal free, clear sterile (falcon tubes) were placed underneath the filter holder. Between 45- and 50- mL seawater was sampled. The filtration was driven by atmospheric pressure, although, it was necessary to use a plunger the very first time to allow the seawater to flow across the membrane. The filters were re-used over the sampling period. Therefore, the seawater control, spiked seawater control, and the Fe/Mn treatments 10, 25, 50, and 100 nM had one assigned filter to avoid particle interferences across the concentration gradient. The filtration process can be seen on the photograph below.

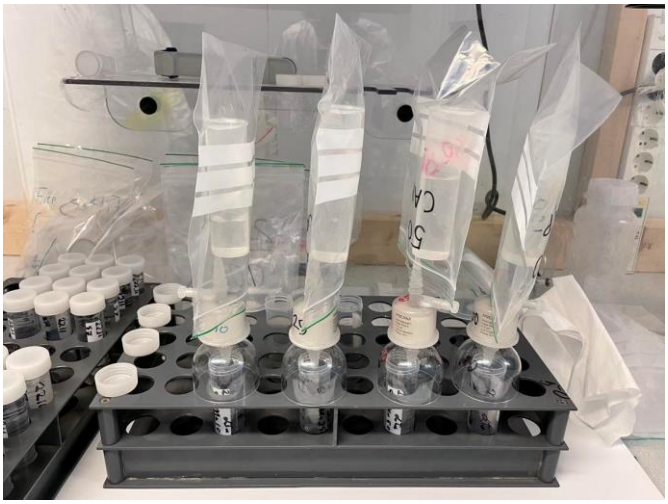

Figure 3.5: Filtration step for dTe sampling. Filtration of *in situ* Mn/Fe concentration from left to right: 10, 25, 50, and 100 nM.

Upon the dTe sampling, TTe were collected. Prior to the TTe sampling, the experimental bottles were turned to resuspend any sedimented colloids or particulates. Thereafter, total trace elements were sampled by pouring 45 - 50 mL seawater into the falcon tubes.

Dissolved and total trace element samples were then acidified with 3 droplets (1 drop = 0.04 mL) 14.7 M UP HNO_3 to pH < 1.8. The samples were stored at ~ 9 °C until analysis.

3.3.2 Total Hg Sampling

Amber glass vials were dried 8 hours in heat oven at 50 °C. Prior to usage, the vials were capped and stored dark in plastic bag.

The Hg samples were collected by pouring the seawater from undisturbed experimental bottles into the glass vials. The vials were filled to the top so there were no headspaces in the vials. Then, the vials were capped tightly, placed in individual zip-lock polyethylene bags, and stored dark at ~ 4 °C until analysis.

3.3.3 pH Measurements

pH was measured directly in the experimental bottles. Therefore, it was measured after all the samples were taken to avoid any contamination from the probe or the ambient air. The pH meter (Thermo Fischer Orion Star portable pH meter) was calibration checked with a standard (pH 4.01) prior to usage at every sampling time. The probe was stirred few times in the water to create a minor turbulence and then hold still in the centre of the bottle. Equilibrium was defined as when 30 seconds passed or when the pH – value did not change in 10 seconds. Since H^+ activity is dependent on temperature, both pH and temperature were recorded.

3.3.4 Centrifugation

3.3.4.1 Theory

Calculation of the centrifugation time can be computed by Stokes law, equation (9). The formula gives the terminal velocity of the particle, previously explained by Antonopoulou et al. (2018). As they write in the paper, the particle in the suspension is assumed to be a hard sphere.

$$uT = \frac{d^2(\rho_d - \rho_c)a}{18\mu_c} \quad \textbf{(9)}$$

Where:

d: particle diameter

ρ_d: density of particulate

ρ_c: density of medium

μ_c: viscosity of medium

a: centrifugal acceleration given by equation (10)

$$a = (2\pi n)^2 r \quad \textbf{(10)}$$

Where:

n: number of centrifuge revolutions per second

r: distance from axis of rotation to the suspension surface

When placing the tubes in the racks in the centrifuge, several factors must be taken into consideration. The weight of the tubes must be evenly distributed between the holders to avoid any damage on the centrifuge. The tubes should never be exposed to g-forces higher than what is advised by manufacturer. If the tubes have a conical bottom, the selected rack must be fit accordingly to minimize the gap between the tube and the supporting wall. If there is lack of support from the rack, the tubes may break or buckle during centrifugation. Additionally, the tubes should be filled at least 75 % to avoid any extra stress on the plastic material in the tube (Carter et al., n.d).

3.3.4.2 Method

At day 10, samples from experimental bottle MnFe100 were centrifugation. At day 14, samples from both MnFe50 and MnFe100, were centrifugated. From each experimental bottle, 8 falcon tubes were filled with 45 mL seawater. The samples from each experimental bottle were centrifugated separately.

The tubes were centrifugated with Eppendorf Centrifuge 5810 at 3000 rpm for 27 min. The centrifugation settings were calculated from Stokes law in equation (9). Upon each centrifugation, 4 mL supernatant was evenly pipetted from the 8 centrifugation tubes. First, supernatant samples for Hg analysis were collected on two amber glass vials filled to the top. Next, two falcon tubes were filled with 45 mL supernatant for dissolved trace element analysis. Lastly, two precipitate samples were collected by discarding supernatant until 15 mL remained in the centrifugated tubes. The trace element samples were acidified as the other trace element samples. The pipetting work was carried through in an open fume hood with the surface covered in plastic film to avoid contamination and turbulent air flow into the chamber.

Upon four months storage, the precipitate samples were further filtrated with a 0.2 µm polycarbonate filter. The reason behind the filtration was to exclude any particles that could introduce particles to the delicate seaFAST system, see section 3.4.1.

The filter had previously been used to filter the seawater controls. Therefore, the membrane was rinsed by flowing 50 mL 0.5 M UP HNO_3 solution through it, followed by 50 mL Milli-Q water. Between every sample, the filter was rinsed with 15 mL MQ-water to prevent cross-contamination between the samples. The Milli-Q water stopped dripping before next sample was filtered to avoid dilution effect of the samples. The first sample collected was a blank sample containing only Milli-Q water. The purpose was to account for the possible leaching of trace elements from the filter.

The parameters used for the calculation of centrifugation time are given in Table 3.4. Values for seawater density and absolute viscosity at 10 °C were retrieved from (ToolBox, 2005).

Table 3.3: Values used to calculate the settings for centrifugation. rps = revolutions per minute.

Parameter	Value
Particle diameter (d)	2×10^{-5} cm
Density of particle (ρ_d)	5 g/cm^3
Density of medium (ρ_c)	1.027 g/cm^3
Viscosity of medium (μ_c)	0.0141 g/cms
Number of revolutions per second (n)	50 rps
Distance from axis of rotation to the suspension surface (r)	9 cm

3.3.5 Wall Desorption Test

3.3.5.1 Trace Elements

One experimental bottle from each control and treatment were taken for the test, i.e., 16 bottles in total. The bottles were emptied and rinsed twice with approximately 15 mL Milli-Q water. Next, approximately 15 mL 0.1 M UP HNO_3 was added to the bottle. The bottles were turned so that the solution touched all the surface. Thereafter, the solution was poured into pre-weighted falcon tubes. This was done twice for each bottle, i.e., 30 - 35 mL sample volume was collected. Additionally, one blank sample containing only Milli-Q water and 0.1 M UP HNO_3 was collected. The falcon tubes were weighted after sampling, and the exact sample weight was calculated. Lastly, the samples were stored dark at 10 °C until analysis.

3.3.5.2 Hg

One experimental bottle from each control and treatment were taken for the test, i.e., 16 bottles in total. The experimental bottles were emptied and rinsed twice with 15 mL Milli-Q water. Next, 15 mL water was added to the bottle before 0.1 % BrCl was added with pipette. The experimental bottles were turned so that the liquid touched the inside of the container. Thereafter, the solution was sampled twice onto 40 mL pre-weighted glass vials. The vails were weighted after sampling and the exact weight was recorded. The samples were stored dark at 4 °C until analysis. After a while, the yellow color vanished, indicating the depletion of BrCl. Therefore, additionally 30 µL BrCl was pipetted to the samples to reach 0.1 v/v % concentration.

3.4 Analysis and Instrumentation

3.4.1 Preconcentration with seaFAST

3.4.1.1 Theory

The chemical analysis of trace elements in seawater is challenging because of the complex matrix. The salt in the seawater can precipitate in the ICP-MS and the major ions can interfere with the trace elements during analysis. The extremely low trace element to major ion concentration poses another difficulty. Other issues are related to different elemental behavior during sample extraction (Biller & Bruland, 2012; Wuttig et al., 2019). Therefore, scientists apply purification and extraction methodologies during sample preparation to overcome these challenges. Solid phase extraction has shown to be a superior method because of the efficiency and the very low blanks. The seawater matrix is quickly removed and the preconcentration of trace elements results in very low detection limits. Another

advantage is the possibility for automatization that allows multiple samples to be analyzed with minimized risk of sample contamination (Ge et al., 2022).

seaFAST is an automated instrument that utilizes solid phase extraction to preconcentrate trace elements in seawater and it has several modes of operation. It can be operated in inline mode when it is connected directly to an inductively coupled plasma mass spectrometer (ICP-MS). Preconcentration mode can be applied in both offline and inline mode. The analytes in the sample are retained on a preconcentration column. The eluted samples can then be brought to further analysis in ICP-MS (Elemental Scientific-2, n.d.). Figure 3.6 provides an overview over which elements that can be targeted by different modes in seaFAST.

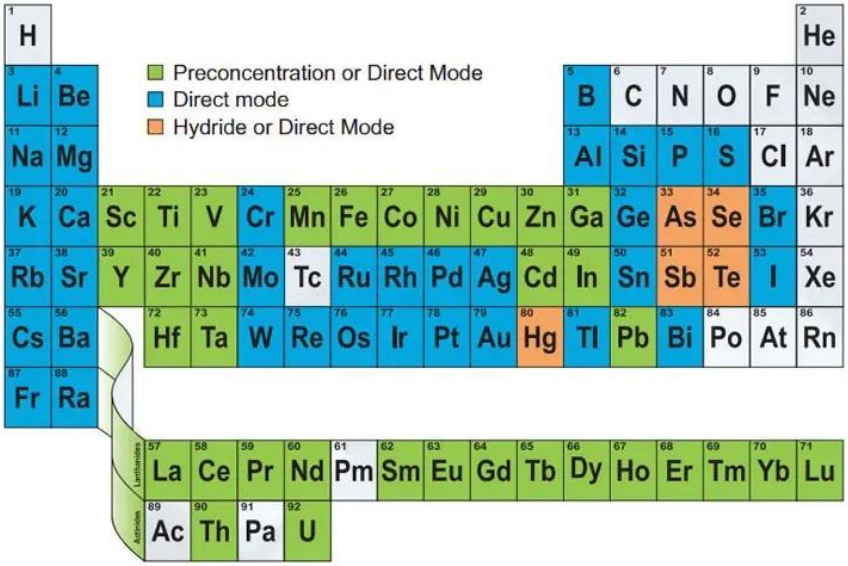

Figure 3.6: Overview over which elements that can be analyzed in different modes in seaFAST. Reproduced from Elemental Scientific-2 (n.d)

Figure 3.7 gives a schematic overview of the system assembly lines in seaFAST. The sequence is initiated by a vacuum pump aspirating a preselected volume of seawater into a perfluoroalkoxy alkane sample loop. There are two columns used in the sequence. In the first column, ammonia acetate becomes rinsed for any trace element it may contain before it gets mixed with the sample in a 4 mL sample loop. The buffer is prepared from supra pure reagents. The sample and the buffer are then passing over the second column which is for preconcentration of the sample, Figure 3.8 1). The seawater matrix passes freely while the trace elements are retained onto the column. The extent of preconcentration is determined by the number of load cycles. To make sure there is no matrix left on the resin, the column is rinsed with Milli-Q water (0.055 µS/cm), Figure 3.8 2). At the same time, the sampling probe is rinsed with 1 M UP HNO_3. Finally, 1 M UP HNO_3 is loaded on the preconcentration column and the chelated trace elements elute though the sampling probe into clean sampling vials, Figure 3.8 3). In the end, the system is cleaned. Both the buffer column and the precondition column are rinsed by the remaining elution acid and 1 M UP HNO_3. Thereafter, the preconcentration column is preconditioned with ammonia acetate buffer and 18 MΩ. The probe on the autosampler is rinsed in 1 M HNO_3. The system is then ready for the next sample (Ge et al., 2022; Rapp et al., 2017).

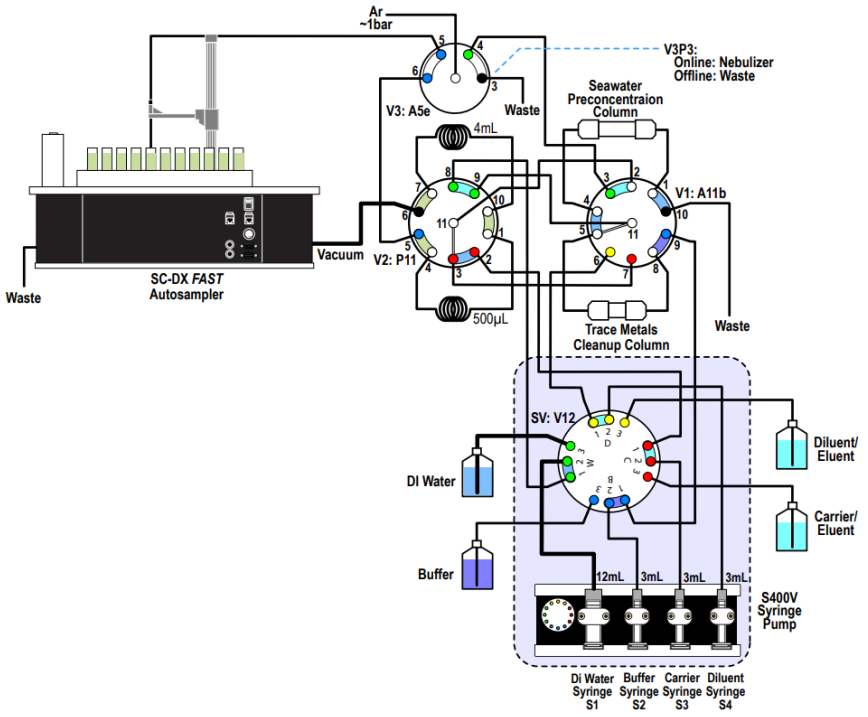

Figure 3.7: Schematic overview of the seaFAST system assembly lines. Reproduced from Elemental Scientific (n.d.).

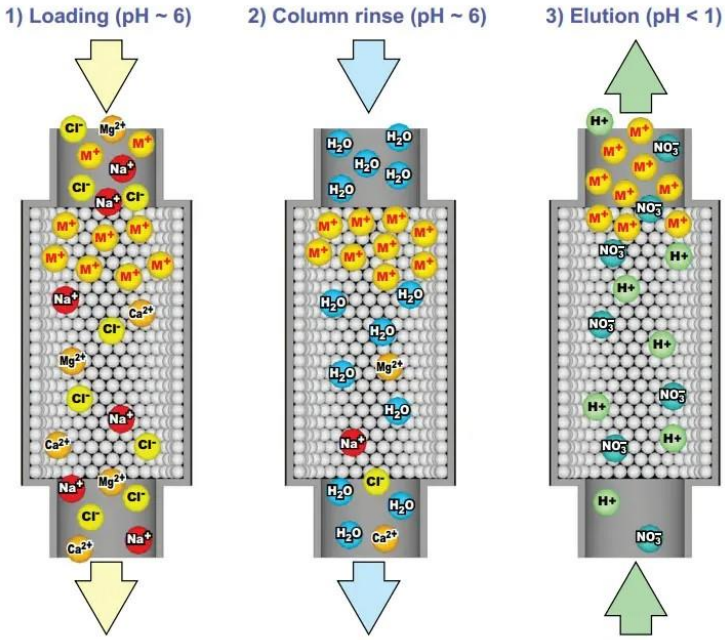

Figure 3.8: Visual presentation of the preconcentration steps on the column. Reproduced from Elemental Scientific-2 (n.d).

Several resins containing different functional groups are developed to retain trace elements. One commercially available chelating resin is the onto NOBIAS Chelate-PA1 resin -chelate PA1 which has a high metal affinity due to the two functional groups iminodiacetic acid (IDA) and ethylenediaminetriacetic acid (EDTriA), illustrated in Figure 3.9. The two functional groups are immobilized on a hydrophilic methacrylate resin (Wuttig et al., 2019).

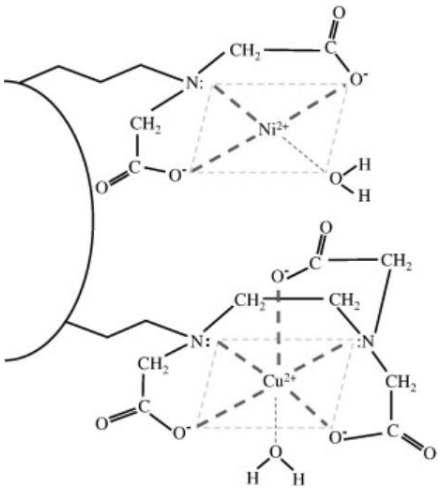

Figure 3.9: Complexation of elements onto NOBIAS Chelate-PA1. In the figure, Ni^{2+} and Cu^{2+} is bounded by the IDA and EDTriA functional groups, respectvely. Reproduced from Biller and Bruland (2012).

NOBIAS chelate-PA1 is a powerful resin since it can retain multiple elements with high recovery at optimum pH. Since it is the functional groups that binds to the trace elements, the retention and recovery of the elements is a function of pH. Because elements have slightly different affinity for the functional groups, they are released from the chelate at different pH values. Therefore, the acidified samples must be buffered to a pH where the recovery is optimum for the analyte of interest. If there are more analytes, a pH that gives best average recovery should be used (Rapp et al., 2017). Previous works have used pH 6.20 ± 0.02 for preconcentration of Cd, Co, Cu, Fe, Ga, Mn, Ni, Pb, Ti, and Zn (Wuttig et al., 2019) and pH 6.2 ± 0.3 (Biller & Bruland, 2012) and pH 6.0 ± 0.2 (Samanta et al., 2021) for the same elements except Ga and Ti.

3.4.1.2 Sample Run

12 selected samples were pre-analyzed on the ICP-MS to investigate whether the elemental concentrations were high enough for direct analysis. In the ICP-MS analysis, each sample were measured five times. The relative standard deviation was higher than 5 % for Pb, As, and Cr explained by their low concentration. Therefore, the samples were decided to be preconcentrated with seaFAST. However, the seaFAST at Norwegian University of Science and Technology could only be operated in offline preconcentration mode. As shown in Figure 3.6, seaFAST has low recovery of Cr and Mn when its operated offline. Therefore, As and Cr were not considered any further. See Appendix A, Table 0.1 for the preliminary results.

Prior to analysis of Pb, Fe, and Mn with ICP-MS, the samples were preconcentrated with seaFAST from Elemental Scientific Incorporative operated in offline mode. The method followed (Elemental Scientific n.d.). The seaFAST preconcentration was performed in a positively pressured laboratory to avoid contamination from dust particles.

First, dTe and supernatant from the centrifugation test were run with a preconcentration factor of 10 times. The samples were aligned in increasing concentration order to avoid any possible carryover. The set-up of the batches started with seawater control samples followed by spiked seawater control samples and thereafter increasing concentration of Mn, Fe, and MnFe samples. The capacity of the seaFAST was 21 samples per batch including blanks and standard. There were 7 batches and each batch started with one method blank sample. The method blanks were 50 mL falcon tubes filled with Milli-Q water

and 3 drops UP HNO_3. The UP HNO_3 was the same acid that was used for sample preservation. In batch one, three, and seven, the blank sample was followed by NASS-7 seawater certified reference material purchased from National Research Council of Canada. Upon preconcentration of each batch, the sample vials were capped immediately to avoid any further up-concentration due to sample evaporation.

TTe samples collected at 2 hours, 16 hours, 64 hours, and 14 days were preconcentrated and analyzed. Since TTe samples may have contained particles, the samples were placed in the seaFAST rack at least 5 hours prior to the run to let the particles precipitate in the falcon tube. The sampling probe was adjusted to highest possible height so that particulates would not be injected to the instrument while ensuring that air would not be aspirated.

Precipitate samples from the centrifugation test contained 15 mL sample volume. For this reason, only a single 10 mL sample injection was proceeded with a 5 times preconcentration factor. The instrumental settings for wall adsorption samples were kept unchanged from dissolved samples.

To control the accuracy and consistency of the elution volume, 35 of the first 145 samples were randomly selected and weighted on Mettler Toledo AG204 DeltaRange scale upon the seaFAST operation. Pre-weighted tubes were statistically compared with tubes after the elution. A two-tailed T-test proved that the elution volume was 2 mL at a 5 % significance level, see Appendix F, Table 0.6. There was not seen any drift in elution volume neither, see Appendix F, Figure 0.10.

Table 3.4 presents a summary of the parameters used to operate the seaFAST. The eluent consisted of 1 M UP HNO_3 spiked with two internal standards, Lutetium and Gallium; For each liter eluent, 18.0 µg/L Lutetium solution was prepared by pipetting 1800 µL from a 1:10 000 ppm stock solution. 6.97 µg/L Gallium was prepared by pipetting 700 µL from a 1:10 000 ppm stock solution. The buffer comprised of 280 mL suprapur glacial acetic acid, 280 mL 25 % suprapur ammonium hydroxide, and 440 mL Milli-Q water. Due to the exothermic reaction, the buffer was prepared one day in advance. The pH was measured (Thermo Scientific Orion Dual Star pH meter) and adjusted to reach a target pH between 6.0 and 6.2. For a comprehensive method description of the seaFAST operation, see the seaFAST protocol in Appendix B.

Table 3.4: seaFAST preconcentration parameters.

Parameter	**Setting**
Mode of Analysis	Offline preconcentration
Gas and flow rate	Argon, 1 bar ± 0.1
Column resin	NOBIAS Chelate-PA1
Carrier	Milli-Q water 18 Ω
Rinse solution	0.6 M UP HNO_3
Buffer	Ammonia acetate buffer, pH 6.0 – 6.2
Eluent	1 mol/L UP HNO_3
Sample pH	1
Preconcentration factor	10, 5 for precipitate sample
Initial volume of sample	45 - 50 mL (dTe, TTe, supernatant), 30 – 35 mL (wall desorption test), and 15 mL (precipitate sample)
Final elution volume	2 mL
Sample throughput	32 min/ sample. 25 min for precipitate samples

3.4.1.3 Quality Control

The result of the blank samples is summarized in Table 3.5. The limit of detection (LOD) was determined as three times the standard deviation of analysis blanks. Three analysis blanks associated with total trace element samples were suspected to have a contamination introduction and were therefore excluded, this is shown in Table 0.2 in Appendix A.

Table 3.5: Analysis blanks and detection limits in nmol L^{-1} ± 1 std. n=number of blanks. All values are corrected for the preconcentration factor. Detection limit = 3 x std of the blanks.

Element	Analysis blanks (nmol L^{-1}) n=5	Detection limit (nmol L^{-1}) (LOD = 3 x std)
Fe	0.804 ± 0.279	0.873
Mn	0.047 ± 0.013	0.039
Pb	0.011 ± 0.0070	0.021

Table 3.6 compares the elemental concentrations in the certified reference material with the analyzed concentration in this study. The precision is given as the relative standard deviation (RSD) of the analyzed reference material. The RSD was 8.3 % for Fe and 7.1 % for Mn. The accuracy was calculated as percentage of the measured concentration to the concentration in NASS-7. The accuracy of Fe and Mn was 83.1 % and 92.2 % respectively. Pb was below the detection limit. One Pb measurement was excluded due to contamination and is shown in Table 0.3 in Appendix A.

Table 3.6: Analyzed certified reference material and available consensus values in nmol L^{-1} ± 1 standard deviation. n=number of measurements. All values are corrected for blanks and the preconcentration factor. <LOD = below detection limit. *n = 4.

Element	NASS-7 consensus value (nmol L^{-1})	This study n = 5 (nmol L^{-1})	Accuracy (%)	Precision (%)
Fe	6.29 ± 0.47	0.29 ± 0.024	83.1	8.3
Mn	14 ± 1	0.69 ± 0.049	92.2	7.1
Pb	0.013 ± 0.004	< LOD*	na	na

Internal spikes were used to control any drift related to the elution of analytes. The recovery of Lu and Ga is presented in Figure 3.10. The most important information obtained was that the ratio between them remained constant (Middag et al., 2015). The recovery of lutetium and gallium were 88.5 ± 7.0 % and 62.0 ± 5.3 %, respectively.

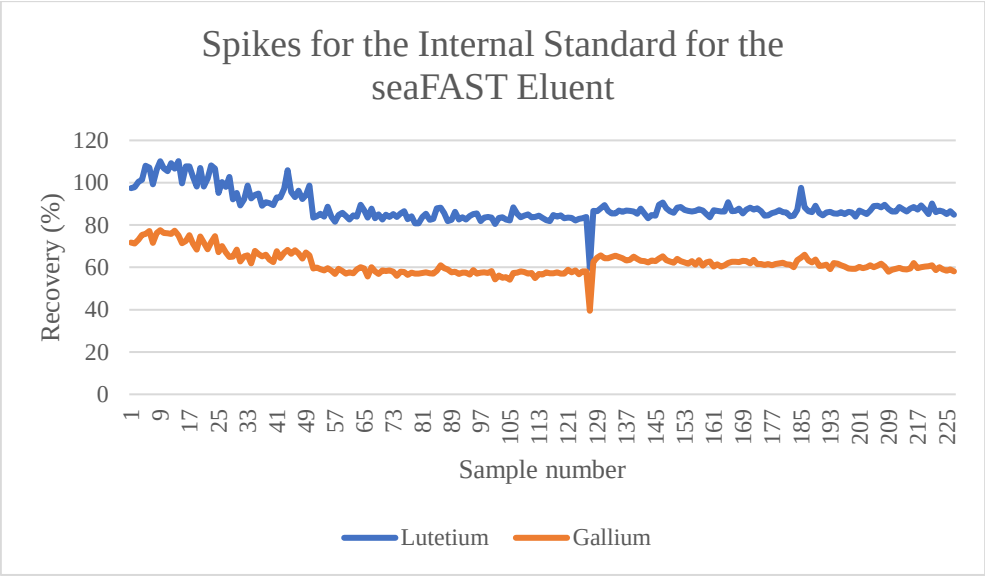

Figure 3.10: Recovery of the Lu and Ga spikes for the internal standard for the seaFAST eluent.

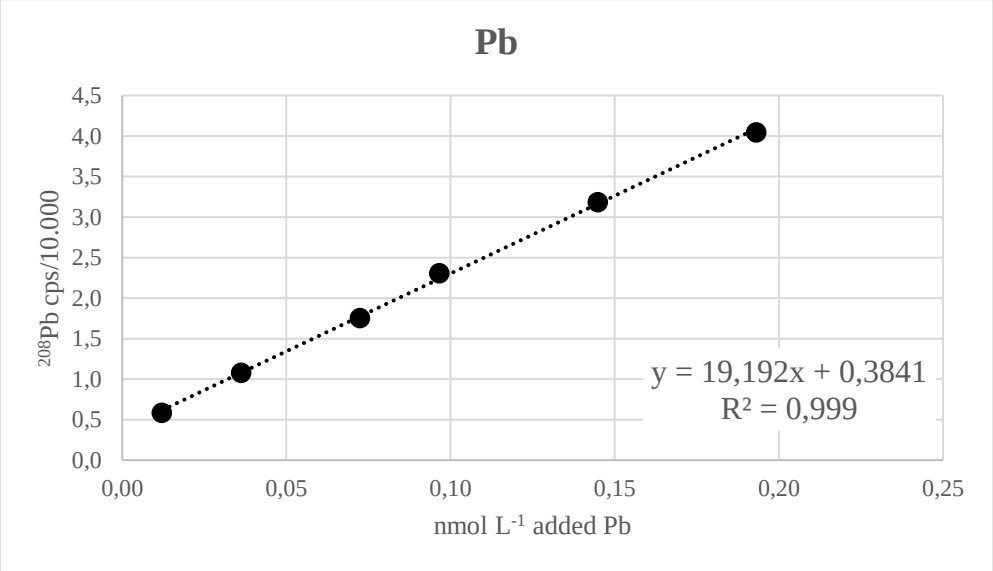

Figure 3.11: Linear regression of the 6- point calibration curve of Pb.

Figure 3.11 shows a six-point calibration curve of Pb. The calibration curve shows how the resin in the seaFAST behaves at different analyte concentrations. The calibration curve of Pb had a R^2 value of 0.999 in the range 0.01 to 0.19 nM. The calibration curve was run by other laboratory technicians after the samples in the present study had been run. The calibration curve was considered to reflect the recovery of Pb in this study because it was run within the same period. Only seawater with similar concentration range had been run in between. Thus, no contamination of the system had occurred between the sample processing of samples in this study and the calibration curve.

3.4.2 Detection Methods

3.4.2.1 Inductively Coupled Plasma Mass Spectrometry (ICP-MS)

Inductively coupled plasma mass spectrometry (ICP-MS) is an analytical instrument that is used in inorganic chemistry to analyze elements in a sample. It is commonly used because of the low matrix effects and the high sensitivity (< 0.01 ppb). Although sample preparation such as acid digestion and filtration is often a necessity since particles above 20 µm may clog the nebulizer. The ICP-MS can be coupled with separation techniques, such as gas chromatography, to analyze volatile metals, metalloids, and organometals. However, it is most used alone to measure total concentrations of analytes in which it is not specific to elemental speciation (Gianguzza et al., 2000, p. 273). It can also be paired with seaFAST to directly analyze elements in seawater in ultra-trace samples.

The ICP-MS consists of two parts; an ionizing plasma that ionizes the analytes before they get separated based on mass to charge ratio (m/z) in the mass spectrometer. First, the sample is injected into a concentric glass nebulizer that transforms the liquid sample into fine aerosols. Larger droplets drain out whilst the finest aerosols are introduced to the plasm that consists of hot, partly ionized argon gas (West et al., 2014, pp. 778-779). In the plasma, the elements are subject to different processes that occurs in orders of milliseconds. First, the elements in the aerosols are released due to the evaporation of the liquid matrix on each aerosol. The elements then vaporize from solid to liquid state and thereby becomes atomized. Next, the atomized elements become ionized by the excess of electrons in the plasma before it is focused by two interface cones and an ion lens and transported to the mass spectrometer (Beauchemin, 2000, p. 5). A quadrupole can be used to separate the different masses prior to detection. The mass analyzer consists of four parallel rods. The electrical field between them is alternating and is tuned to allow a certain mass to charge ratio to pass. All other m/z ratios will be excluded. A rapid change in the electrical current allows the mass analyzer to have a high throughput of multiple elements (West et al., 2014, p. 806).

Trace Element Analysis

The samples were analyzed for elemental composition using NexION 5000 Multi-Quadrupole (Perkin Elmer, USA) inductive coupled plasma mass spectrometry (ICP-MS) system equipped with prepFAST M5 autosamplers (ESI, USA). Accuracy of the analysis were determined using certified reference material NASS-7, given in Table 3.6. System parameters during analysis is listed in Table 3.7. Every sample was analyzed five times. The results are reported with the average value. The relative standard deviation of the analytes was used as an internal control of each analyte measurements. The analysis was carried out by external laboratory technicians at Institute for Chemistry at Norwegian University of Science and Technology.

Table 3.7: NexION 5000 ICP-MS parameters.

General Parameters	
RF Power	1500 W
Nebulizer gas flow	0.95 L/min
Ion guide mode	Focusing
Hyperskimmer voltage	2
Skimmer cone	5
NH_3 Mode	
NH_3 gas flow	0.6 mL/min
O_2 Mode	
O_2 gas flow	0.9 mL/min

3.4.2.2 Cold Vapor Atomic Fluorescence Spectrometer (CVAFS)

In this study, the MERX® autosampler coupled with Brooks Rand Model III Cold Vapor Atomic Fluorescence Spectrometer (CVAFS) were used for total Hg analysis. The instrument was selected because of its low sensitivity for Hg in seawater matrix. The autosampler allows a high throughput of samples with low risk of contamination. Moreover, the potential of carryover is low since gaseous Hg is analyzed (Brooks Rand Instruments, n.d.). With the CVAFS, total Hg is analyzed, i.e., all inorganic and organic Hg species.

Method 1631, developed by United-States Environmental Protection Agency, is a common methodology for Hg analysis in water matrixes (Cossa et al., 2011; Heimbürger et al., 2015). This work followed the user's guide from Brooks Rands Instruments for MERX-T (Brooks Rand Instruments, n.d.) that is based on method 1631. The samples were analyzed four to five months after the experiment was finished. Concentrated BrCl (40 µL) was added to all the samples to reach 0.1 % v/v concentration. The BrCl is a strong oxidizing agent and transforms all Hg to water-soluble Hg(II). The oxidation prevents Hg adsorption on the walls and loss of Hg(0) to the atmosphere (Brooks Rand Instruments, n.d.).

Prior to analysis, approximately 24 to 25 mL sample was pipetted into new, tared vials. The exact weight was noted down. Then, the samples in the new vials were pre-reduced by pipetting 100 µL hydroxylamine hydrochloride ($NH_2OH{\cdot}HCl$) to remove all free halogens, i.e., Cl_2, Br_2, and BrCl, that potentially could damage system components. 100 µL stannous chloride ($SnCl_2$) solution was then added to the sample to reduce all oxidized Hg(II) species to Hg(0). The vial was capped quickly to avoid any loss of gaseous Hg.

The MERX-T configuration consists of an autosampler, purge and trap module, CVAFS and a computer.

Figure 3.12 provides a scheme overview of the purge and trap module. The instrumental analysis of Hg proceeds in the following steps. The module includes the soda lime trap, valves, and the gold amalgamation traps. It controls the gas flow and the absorption and release of Hg on the traps. First, the autosampler probe purges the Hg(0) from the sample into the system. Hg-free nitrogen (N_2) were used as purging gas. The system is driven from the pressure created by the purging gas and therefore a pump is not applied. To prevent liquid injection into the tubing, the sample vial should never be filled more than 2/3, i.e., ca. 25 mL, leaving at least 15 mL headspace in the vial. If the vial is overfilled, a liquid/gas separator will protect the purge and trap module. The separator is connected to

a sensor that will stop the purging. Next, the sample gas passes a soda lime scrubber that absorbs any excess moisture and acid vapor to protect the gold traps (Brooks Rand Instruments, n.d.).

The purge and trap module contains three traps- X, Y, and Z- that preconcentrates atomic Hg on a dual-trap amalgamation system. Trap X and Y are sample traps. The nitrogen gas is removed once the elemental Hg has been amalgamated and adsorbed onto the X trap. Next, the X trap is flushed with the carrier gas simultaneously as the trap is heated to 450 – 500 °C. Here, Hg-free argon gas was applied as carrier gas. The temperature increase causes the Hg to desorb. The Hg is then adsorbed onto the analytical trap, the Z trap. While the X trap is heated, Hg from the next sample is amalgamated onto the Y trap. Finally, the analytical trap is heated, Hg is released, and the carrier gas transports the Hg to the atomic fluorescence spectrometer (Brooks Rand Instruments, n.d.; Fitzgerald & Gill, 1979). This alternation between the X and the Y trap reduces the analytical measurement time.

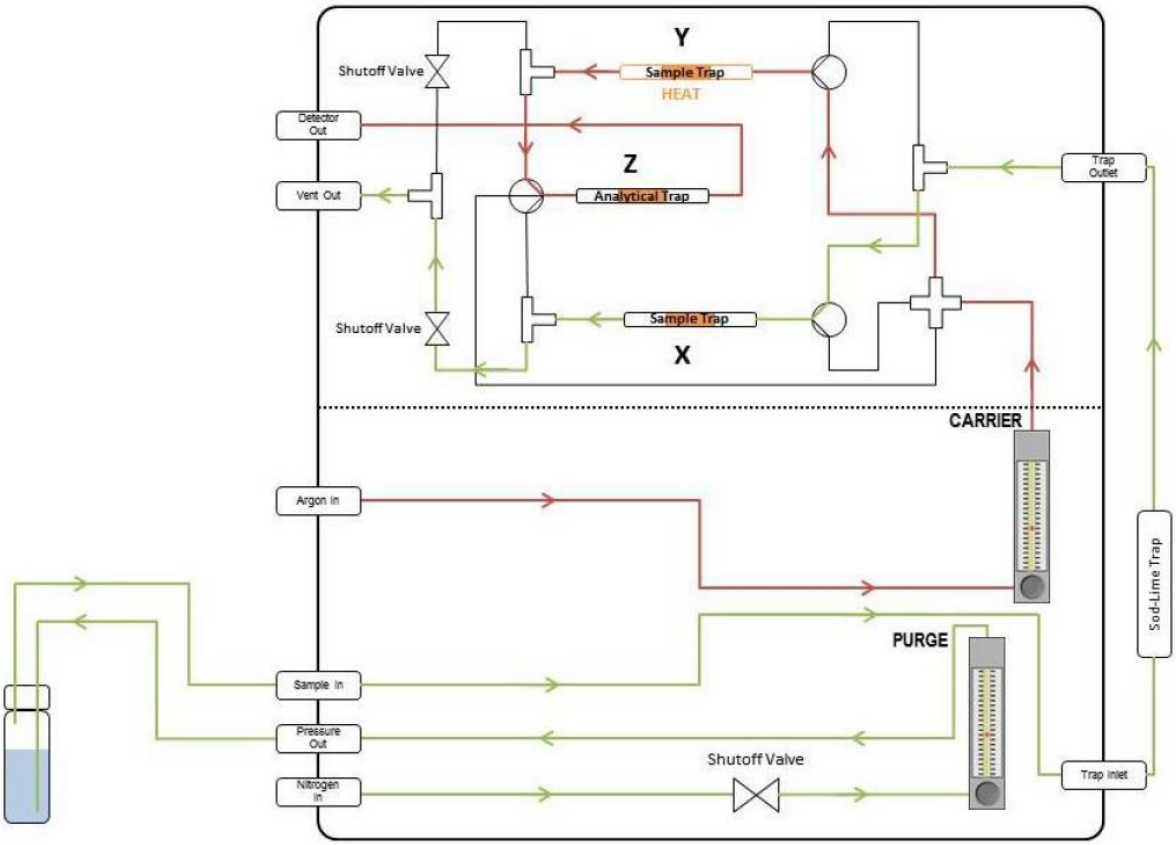

Figure 3.12: Schematic overview of the purge and trap module. The figure is reproduced from Brooks Rand Instruments (n.d.).

The Brooks Rand CVAFS detection system consists of a light source, a collimating optical path, a quartz cell, and a photomultiplier tube (PMT), illustrated in Figure 3.13. The UV light source has a peak emission wavelength at 253.7 nm, which is the optimal fluorescence light intensity of Hg. The photons are directed towards a quartz cell through a collimating optical path. The purpose of the path is to improve the sensitivity in the analysis by reducing light scattering. The Hg and the argon gas- i.e., the carrier gas- enter through the quartz cell (Brooks Rand Instruments, n.d.). Argon gas were used as carrier gas since

it is inert and would not disturb the absorption in the analysis (USEPA, 2002). In the quartz cell, Hg becomes excited and fluoresces light. The emitted light is further filtered at 253.7 nm through an optical band pass before it reaches the photomultiplier tube. The photomultiplier tube detects photons and converts it to an electrical signal which is amplified proportionally to the voltage applied in the PMT. Here, 461.0 V was applied. The signal is sent to a connected computer (Brooks Rand Instruments, n.d.). The detection limit has previously been reported below 0.5 pM in seawater (Cossa et al., 2011; Heimbürger et al., 2015).

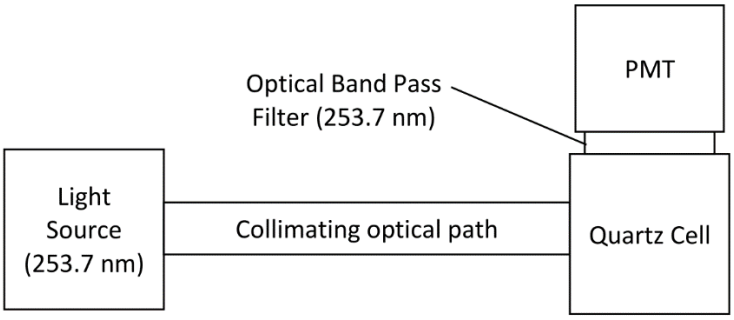

Figure 3.13: Illustration of the CVAFS detection system. The figure is reproduced from Brooks Rand Instruments (n.d.).

3.4.2.3 Total Hg Analysis

Due to limitations on cap septum, the analysis was constrained to sample time 2 hours, 16 hours, 7 days, and the wall desorption test.

40 mL borosilicate glass vials and caps with septum were used in the analysis and cleaned according to Box 3.2.

Reagents were prepared according to Method 1631 (USEPA, 2002).

Box 3.2 Cleaning Procedure of Borosilicate Glass Vials and Caps

1. Empty and rinse used caps and vials in DI water.
2. Submerge caps and vials in 1 % acid detergent bath for at least 24 hours.
3. Rinse caps and vials 3 times in DI water.
4. Dry caps and glassware in oven at 60 °C.
5. Place caps in 1.2 M low Hg concentration HCl bath for at least 24 hours.
6. Combust glass vials at 550 °C for 4 hours.
7. Store glass vials in clean plastic bag.
8. Rinse caps three times with Milli-Q water.
9. Dry the caps in oven at 60 °C.
10. Store caps in clean plastic bag.

Prior to every run, noise and offset were recorded. Fresh soda lime was added to the soda lime trap. The parameter of the batch settings was selected according to (Brooks Rand Instruments, n.d.).

The sequence order of each batch followed (Brooks Rand Instruments, n.d.). First, a rinse solution containing only Milli-Q water was run. Thereafter followed the run of two calibration/reagent blanks. They contained the same reagents as the samples and was prepared by pipetting approximately 25 mL 0.055 µS/cm Milli-Q water into an empty precombusted glass vial. 0.1 % v/v (25 µL) BrCl was pipetted into the vial. When 15 min passed, 100 µL hydroxylamine hydrochloride was added. Finally, 100 µL stannous chloride was added and the vial was capped quickly to avoid any loss of gaseous Hg.

A new calibration curve was made for each analysis run. The stock standards for the calibration curve were prepared as follows; From a 988 µg/L Hg stock solution, a new standard of 25 mL 1 ng/mL was made. From the 1 ng/mL standard, a 5 mL 0.1 ng/mL standard was prepared. The two new standards were prepared by pipetting Milli-Q water and 0.5 % v/v HCl or 0.5 % v/v BrCl to a pre-combusted borosilicate glass prior to the addition of the correct amount of standard. The purpose of HCl and BrCl was to stabilize the Hg in the solution. All the additions were weighted (Sartorius BL210S scale with 0.1 mg readability) to calculate the correct concentration in the standard. The 1 ng/mL and 0.1 ng/mL standards were prepared every day.

The calibration curve was made from the following Hg weights: 2.5, 5, 10, 20, and 40 pg. The reasoning was to include the expected Hg concentration in seawater (1.0 pM) and the intended Hg spike (5.0 pM). In 25 mL glass vials, these concentrations make up 30 pg Hg. Furthermore, the lower range of the calibration curve was intended to include the possible decrease in Hg from the treatments. For the preparation of the calibration curve, approximately 25 mL Milli-Q water was added to the vials. Then, solutions from the standards were pipetted and weighted to get the accurate Hg weight in the standard. 0.1 % v/v (25 µL) BrCl was pipetted into the vial. When 15 min passed, 100 µL hydroxylamine hydrochloride was added. Finally, 100 µL stannous chloride was added and the vials were capped immediately. The calibration curves were corrected for the reagent blanks. The calibration curve from the analysis of the last sample batch is presented in Figure 3.14. Calibration curves of the other analysis runs are given in Appendix C, Figure 0.1.

After the calibration curve was analyzed, two purchased certified reference materials (CRM) from European Reference Materials were run to validate the calibration curve. The reference materials were seawater ERM-CA400 (16.4 ± 1.0 ng/kg) and coastal seawater BCR-579 (1.9 ± 0.5 ng/kg). The ERM-CA400 was prepared by pipetting approximately accurately 0.595 mL of the CRM to approximately 23 mL Milli-Q. The BCR-579 was prepared by pouring approximately accurately 12 mL of the CRM into a vial. Both the ERM-CA400 and BCR-579 was weighted to get an accurate expected value in the analysis. 0.1 % v/v (25 µL) BrCl was pipetted to the vial. When 15 min passed, 100 µL hydroxylamine hydrochloride was added. Finally, 100 µL stannous chloride was added and the vials were capped quickly. The recovery range criteria of the CRM were 77 - 123 %.

One quality control with matrix spike was run every 10^{th} sample in the batch. The matrix spike was a purged sample spiked with 10 pg Hg prepared from the 0.1 ng/mL Hg standard. The recovery range criteria of the matrix spike were 71 – 125 %. Accurately 100 µL stannous chloride was added to the matrix spike and the vial was capped immediately. Every batch was ended with a calibration/reagent blank and a certified reference material.

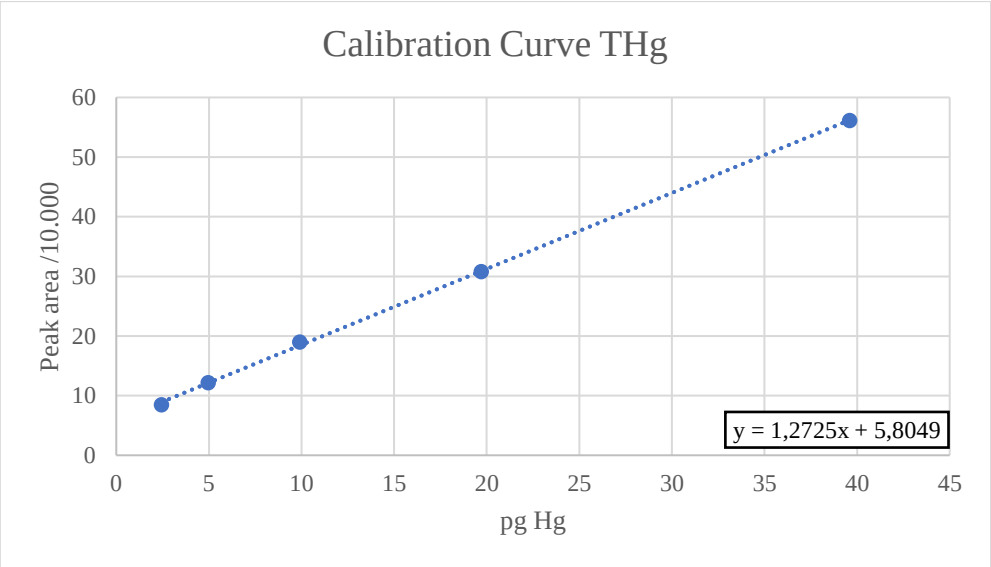

Figure 3.14: Linear regression of a 5-point calibration curve executed prior to analysis of the supernatant and the wall desorbed Hg.

3.5 Data Processing and Statistics

Microsoft Excel was used for data processing and statistics. It was also used to display most of the results. RStudio was used to model the wall adsorption of Pb, Fe, and Mn. All statistical tests and models are presented in Appendix D and Appendix E, respectively.

Precision is defined as the agreement of data that has been analyzed in the same way, and accuracy is defined as the closeness of a measured value to the true value (West et al., 2014, p. 85). In this thesis, the precision of the seaFAST is given as the standard deviation of the measured concentration of NASS-7. The accuracy is expressed as % error of the average measured value to the consensus value.

When performing statistical tests, it is of importance to control whether the data are normally distributed or not. For this purpose, a Shapiro-Wilk test was used. In cases where the data was not normally distributed, the non-parametric Mann-Whitney U test was run. The test assessed whether two independent data sets are equal or not. Data that were normally distributed was statistically tested with a parametric t-test as the true standard deviation was unknown. More specifically, a paired t-test was run when the standard deviation of the two data sets were assumed to be equal (Helbæk, 2011, pp. 76-81).

The models were plotted with 95 % confidence interval, illustrating the range within which the true mean would reside with 95% certainty. The quality of the regression models was tested with analysis of variance. This test assumes normal distribution and independent variables. The regression models were evaluated in multiple ways. Both the p-value of each explanatory variable and that of the overall model should be significant, and as low as possible. In this study, a significance level of 5 % was chosen. Additionally, the adjusted coefficient of determination (R^2_{adj}) should be as close to 1 as possible. Moreover, four diagnostic plots of each model were used to evaluate their fitness. In the residual vs fitted plots, the data should be randomly distributed with an equal distance to 0 on the y- axis. In the Q-Q residuals, the data points should be on a line. In residuals vs. leverage, the leverage should be below 0.50, and any data point above 0.5 cook's distance was considered as an outlier. In the scale location-plot, the mean red line should be a straight line and not a function of the fitted values (Mendenhall & Sincich, 2012, pp. 371-426).

4 Results

4.1 Controls

Table 4.1 presents the time zero results of the TTe in seawater control (Control 1) and the spiked seawater control (Control 2) with respective duplicates. In theory, the spiked concentrations of TPb and THg should be higher than the seawater background in Control 1. However, as the spike concentration was 2 pM Pb and 0.005 pM Hg, the spike was not apparent. TMn and TFe should be the same in the two controls since they were not added. However, Control 2 had higher TFe concentration than Control 1, and TMn had higher concentrations in Control 1 than Control 2. All elements combined, the two controls seemed to be different. Since Control 2 and the treatments originated from the same 100 L barrel, the Control 2 was further comparatively analyzed with the treatments.

Table 4.1: TTe at time zero for both seawater control (Control 1) and spiked seawater (Control 2) with their duplicates A and B. Values are corrected for blanks and preconcentration factor. Note the smaller unit of THg.

	nmol L^{-1} TPb	**pmol L^{-1} THg**	**nmol L^{-1} TMn**	**nmol L^{-1} TFe**
Control 1 A	0.139	1.37	18.15	252.2
Control 1 B	0.141	1.26	18.30	252.7
Control 2 A	0.165	1.11	17.28	331.0
Control 2 B	0.163	1.16	17.76	319.6

4.1.1 Total Pb in Controls

To statistically test whether TPb in the controls differed from each other, a two-way ANOVA at a significance level of 0.05 was tested. To accomplish this objective, both control concentrations were transformed to log scale to make a linear plot, see Figure 4.1. A Shapiro-Wilk test was conducted to confirm the normal distribution of both control groups at a significance level of 0,05, see Appendix D, Table 0.4. The ANOVA test exhibited that the intercepts of the lines were different, whereas the slopes were not. Since the lines were parallel, the concentration was significantly different at any time. The ANOVA statatistics are given in Appendix D, Figure 0.2.

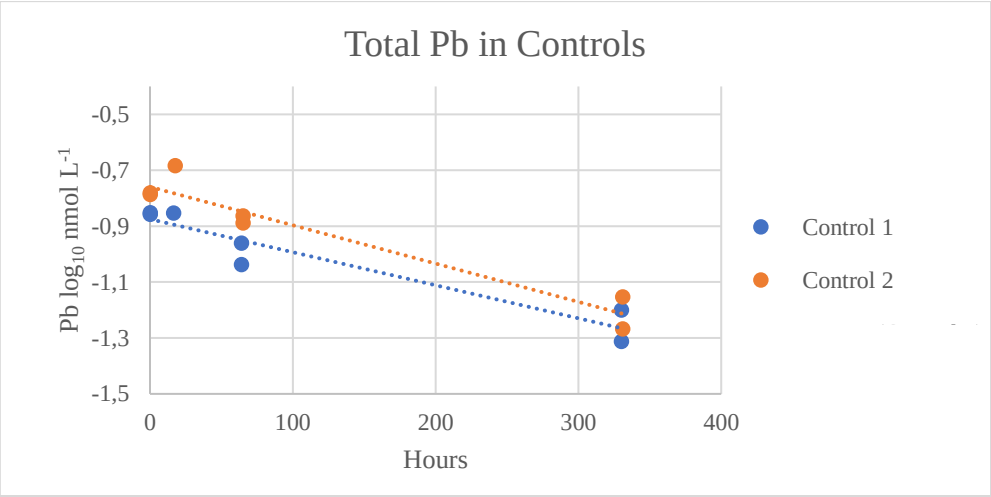

Figure 4.1: TPb in the seawater control 1 and spiked seawater control 2 over time. The concentration is on logarithmic scale. The values are corrected for blanks and preconcentration factor.

4.1.2 Total Hg in Controls

A one-way Mann-Whitney test was carried out to investigate if THg in the controls were significantly different. At a 5 % significance level, the test rejected the null hypothesis that the two controls had the same concentration. Thus, the different THg concentrations in the controls was evident as shown in Figure 4.2. The statistics are given in Appendix D, Table 0.5

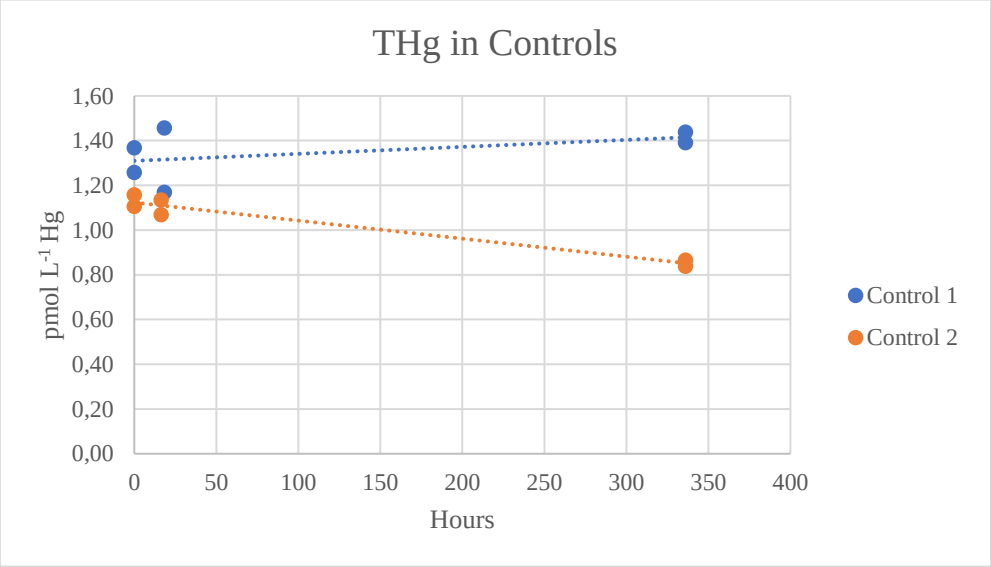

Figure 4.2: THg in the seawater control 1 and spiked seawater control 2 as a function of time.

4.1.3 Total Mn and Total Fe in Controls

The TMn and TFe results in the two controls are shown in Figure 4.3 a) and b), respectively. Almost all the measurements were different between the controls at any time. TMn in Control 1 was consistently higher than Control 2. TFe in Control 2 was consistently higher than Control 1.

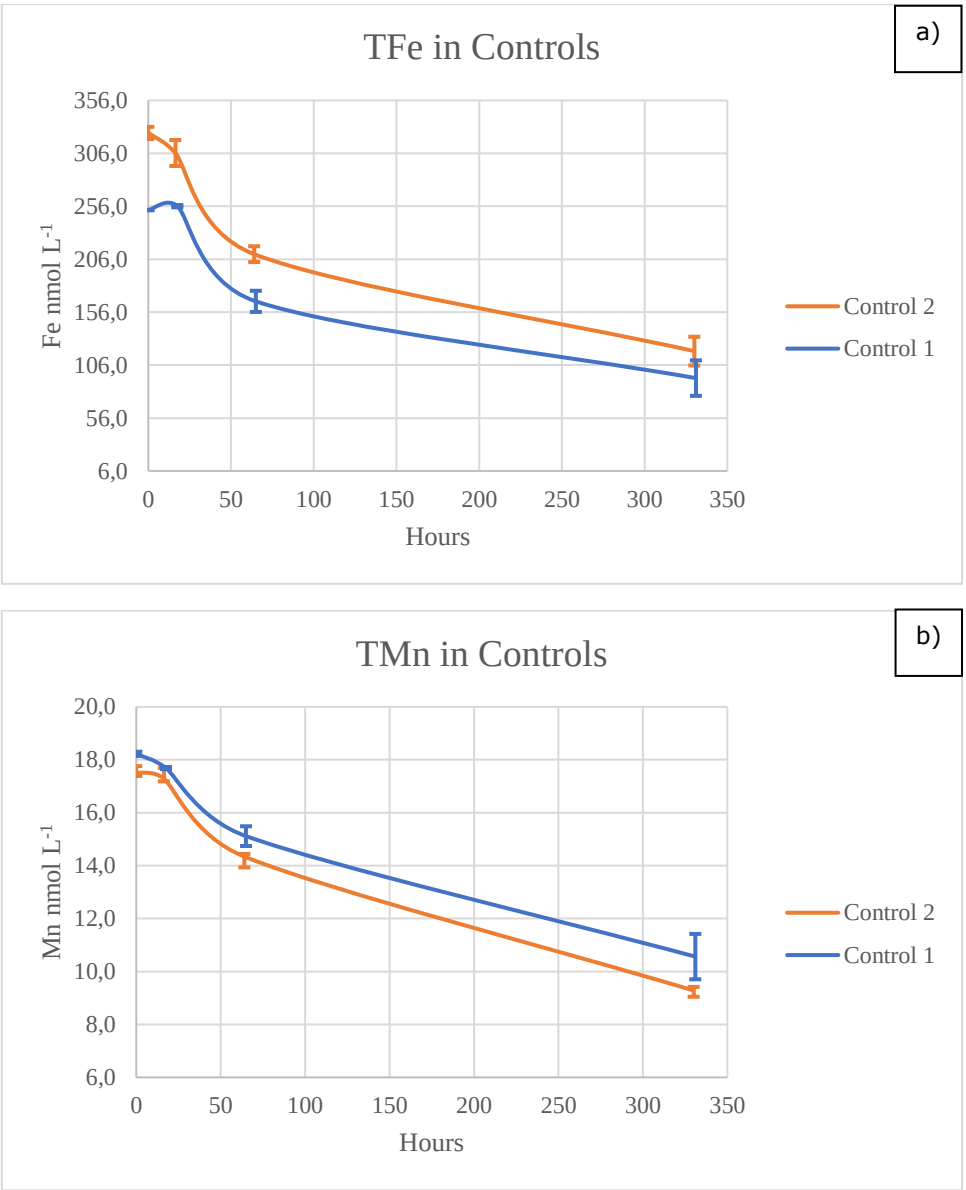

Figure 4.3: TMn and TFe as a function of time in the seawater control 1 and the spiked seawater control 2. The values are corrected for blanks and preconcentration factor.

4.2 Pb

4.2.1 Dissolved Pb

Dissolved Pb concentrations decreased rapidly with time. Consequently, 15 samples of the treatments were above the detection limit (LOD). Even though the majority of samples were below the detection limit, the dPb concentrations were plotted against time to visually present dPb as a function of time. The graphs are shown in Figure 4.4 and demonstrates a rapid removal of dPb in the treatments MnFe (a)), Fe (b)), and Mn (c)). In the figure, the dashed line in the plot represents the average concentrations of the spiked seawater controls. The flat end of the error bars indicates the duplicate concentrations. Common for all the treatments was that the experimental results could not be proven to be any different than the spiked seawater control. Additionally, as the dPb concentrations decreased over time, it was speculated that dPb was rapidly adsorbed onto particles from the seawater.

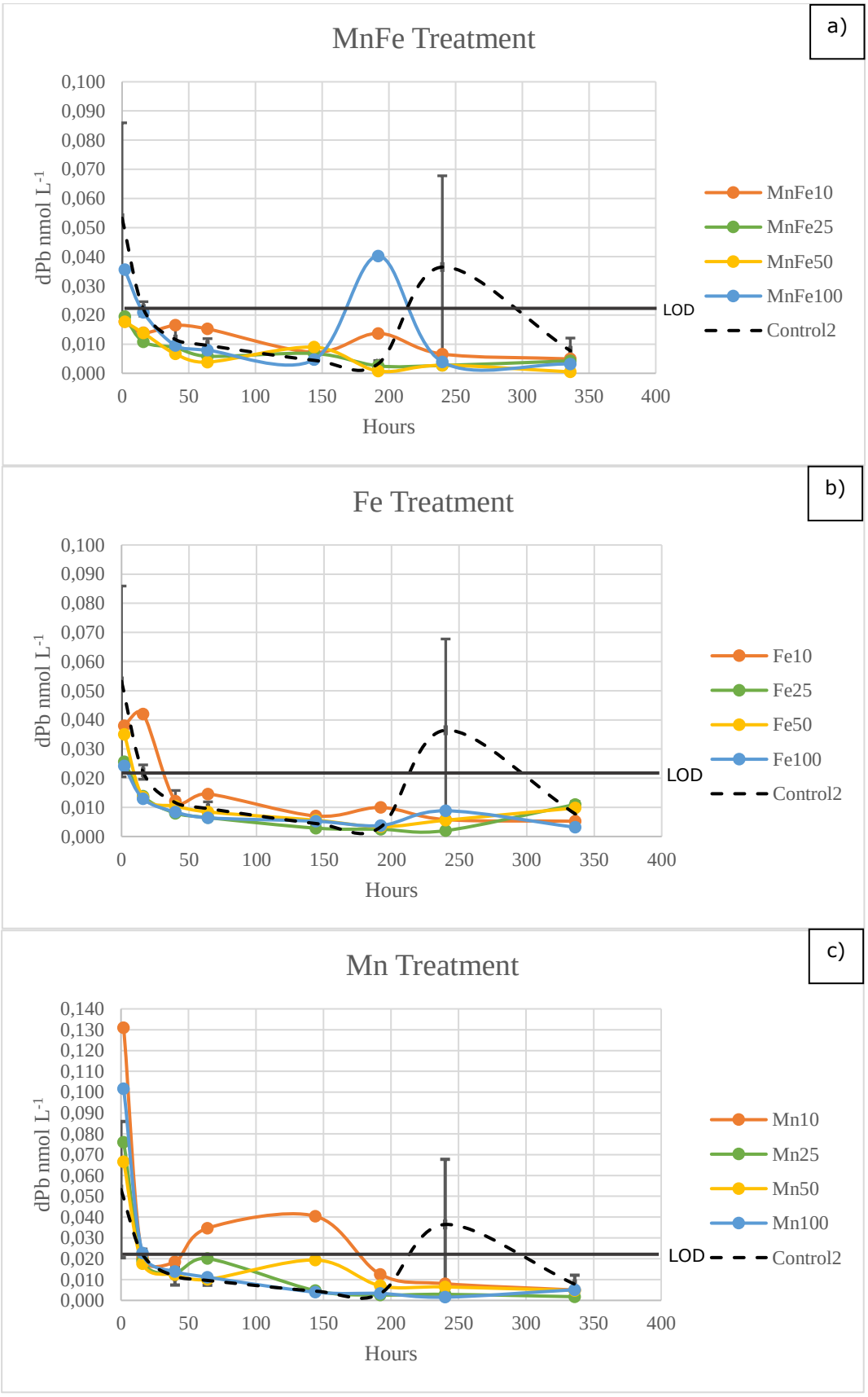

Figure 4.4: dPb as a function of time in MnFe (a), Fe (b), and Mn (c) treatment. The dashed line shows the dPb as a function of time in the spiked seawater control (n=2). The solid black line denotes the limit of detection (0,021 nmol L^{-1}). The figures were made after correction for blanks and preconcentration factor.

4.2.2 Total Pb

The TPb results are shown in Figure 4.5. The dashed line in the plot represents the average concentrations of the spiked seawater controls. The flat end of the error bars indicates the duplicate concentrations. All treatments and controls showed a decline in TPb concentration over the experimental period. Because all sedimented particles would be resuspended after the bottles were inverted, essentially all the Pb would be measured. Since the TPb concentration decreased over time in treatments and controls, it was speculated that wall adsorption served as the explanation for the reduction of TPb.

As shown in Appendix F, Figure 0.11, MnFe treatment at 16 hours was evidently contaminated due to the elevated concentrations. Therefore, this sampling time was excluded from Figure 4.5 a).

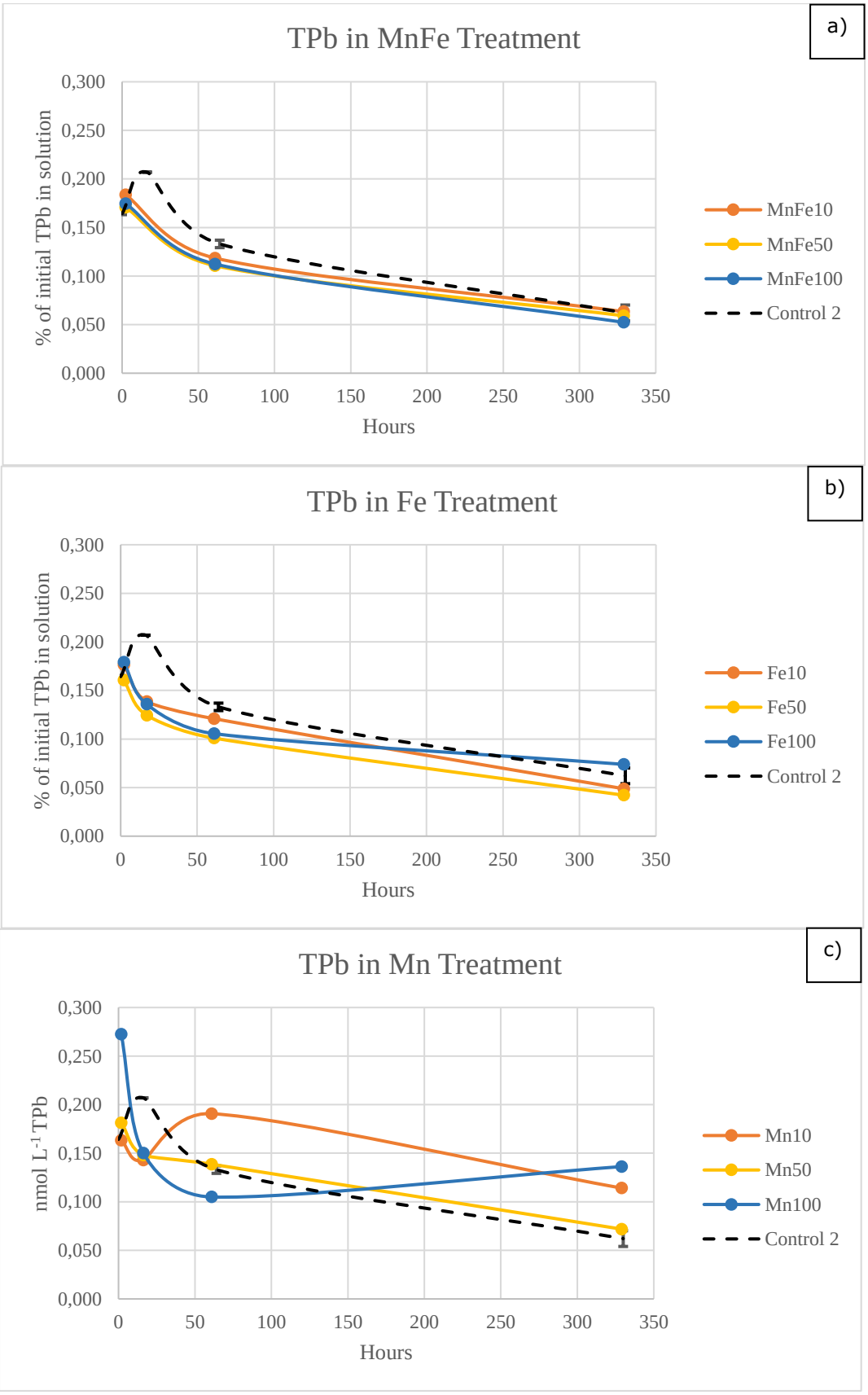

Figure 4.5: TPb concentrations as a function of time at the three treatments MnFe (a), Fe (b), and Mn (c). The values are corrected for blanks and preconcentration factor.

4.2.3 Modeled Wall Adsorption of Total Pb

As previously shown, TPb and dPb concentrations decreased as a function of time in both controls and experimental conditions. Hence, wall adsorption could be the dominating reason for the decrease in TPb and dPb over time. To investigate the influence of wall adsorption, the behavior of Pb in the seawater and the spiked seawater controls were investigated. However, since the dPb concentrations were in proximity and below the detection limit, TPb was modeled.

The model is shown in Figure 4.6. The percent of initial TPb in solution is plotted as a function of hours. To facilitate a meaningful comparison of TPb behavior in the controls, the reduction of TPb was normalized. This was done since the two controls were significantly different. A 95 % confidence interval is darkened around the line. At 336 hours, 38 % of the initial TPb remained in the solution. Two data points at 16 hours are not shown as they were suspected to be contaminated, see Appendix E, Figure 0.3. The statistic of the model is given in Appendix E, Figure 0.5.

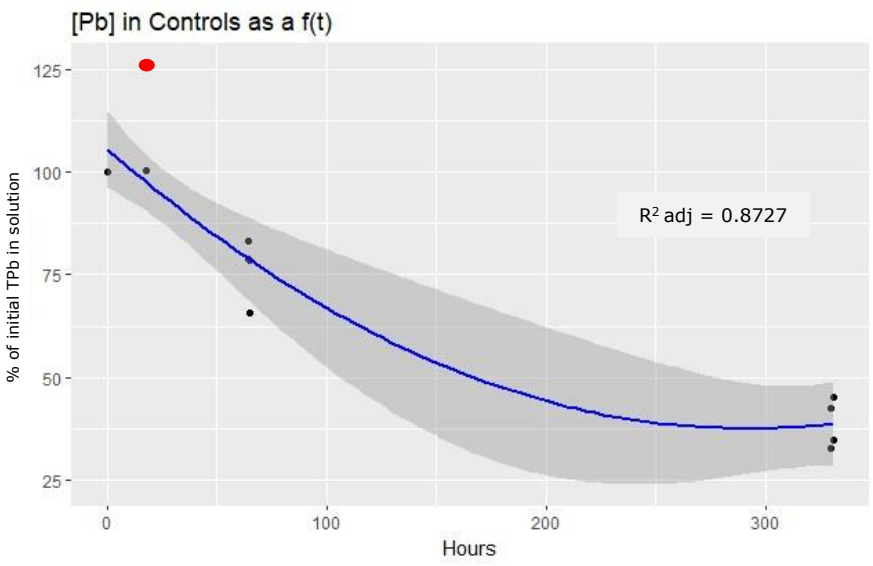

Figure 4.6: Modeled percent TPb of initial concentration in Control1 and Control2 as a function of time at a 95 % confidence interval. The curve follows the function $E(y) = 105,5 - 0,4645x + 0,0007954x^2$. F-statistics p-value = $4,76 * 10^{-6}$.

The data point at 125% could explain why the intercept exceeded 100%. This data point could not be ruled out as an outlier. One limitation with a second-order model is that it is only valid within the time frame of the experiment. Any interpretation at longer time scales cannot be done because of the U- shape of a quadratic function (Mendenhall & Sincich, 2012, p. 259).

4.2.4 Model Compared to Treatments

The model was tested with each treatment in Figure 4.7. The conversion from concentration to percentage was carried out by dividing each treatments sample time point with its time zero concentration. Figure 4.7 a) show that all MnFe treatments at 64 hours was below the 95 % confidence interval of the model, whereas the treatments were within at 336 hours. Concerning the Fe treatments, all the results after 2 hours were below the confidence interval of the model, Figure 4.7 b). The Mn treatment is displayed in Figure 4.7 c). At 336 hours, all Mn treatments had TPb above the model. This was opposite to TPb in Fe and MnFe treatmens which were below.

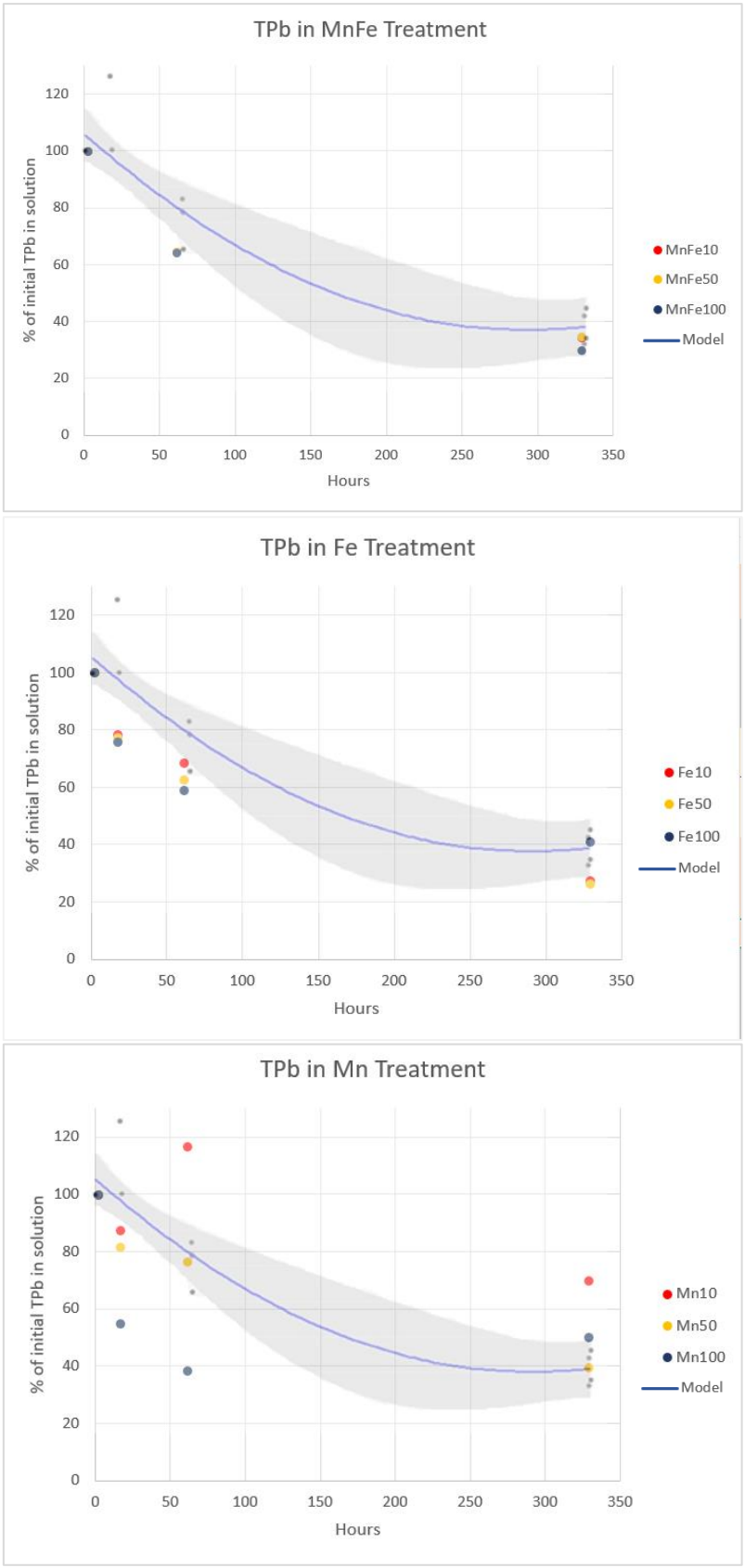

Figure 4.7: Comparison of the % of initial TPb in solution in the model and the treatments: MnFe a), Fe b), and Mn c).

4.2.5 Wall Desorption Test of Pb

The wall desorption test was carried out to measure the amount of Pb on the walls. The results are presented in Figure 4.8. The increased Mn and Fe concentration from 25 to 50 nM seemed to have decreased the amount of Pb desorbed from the bottles. At the 100 nM oxide concentration, the least amount of Pb was desorbed from the walls.

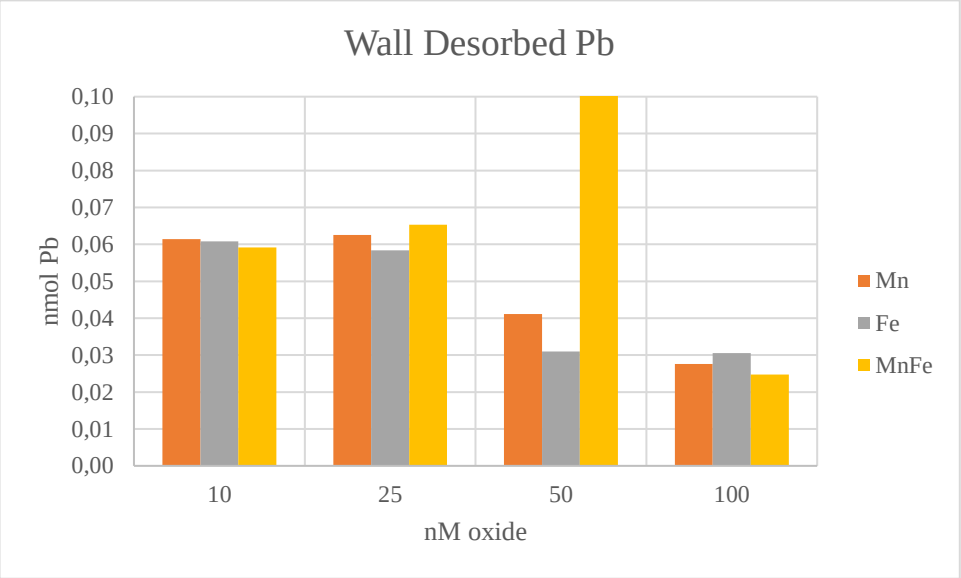

Figure 4.8: Amount of Pb desorbed from experimental bottles as a function of the nM oxide concentration. The results are corrected for blanks and preconcentration factor.

The desorbed Pb from the walls could be used to verify the wall adsorption model. The initial TPb concentration in Control 2 was 0.164 ± 0.001 nM, Table 4.1. Comparably, 0.093 ± 0.010 nmol Pb was desorbed from the walls in the Control 2, see Table 4.2. Thus, 56.7% of the initial TPb concentration was desorbed from the walls in the controls. With the assumption that the remaining TPb was in solution, it can be inferred that approximately 43.3 % of the initial TPb remained in the solution at 336 hours. 43.3 % of initial TPb in solution was within the 95% confidence interval of the modeled TPb concentration at 336 hours (Figure 4.6). The comparability of wall desorbed Pb and the modeled wall adsorption strengthened the model.

Table 4.2: The amount of Pb desorbed from the walls in the two controls with their respective duplicates. The values are corrected for blanks and preconcentration factor.

	Pb (nmole)
Control 1 A	0,061
Control 1 B	0,048
Control 2 A	0,100
Control 2 B	0,085

4.2.6 Mass Balance of Pb

Figure 4.8 raised a new important question; whether there was a mass balance in the system or not. The equation below was applied to calculate the mass balance of each treatment. Thus, the mass balance would equal zero if wall adsorption was the solely explanation for the reduction in TPb concentration.

$$\text{Mass balance} = \text{Initial TPb} - \text{Wall adsorbed Pb} - \text{Final TPb} \quad \textbf{(11)}$$

The results of the mass balance are presented in Figure 4.9. From the figure, it is apparent that there were TPb in the system that was not sampled. The reason being that 7 out of 8 treatments had a positive value. Hence, wall adsorption could not be the solely removal surface of TPb.

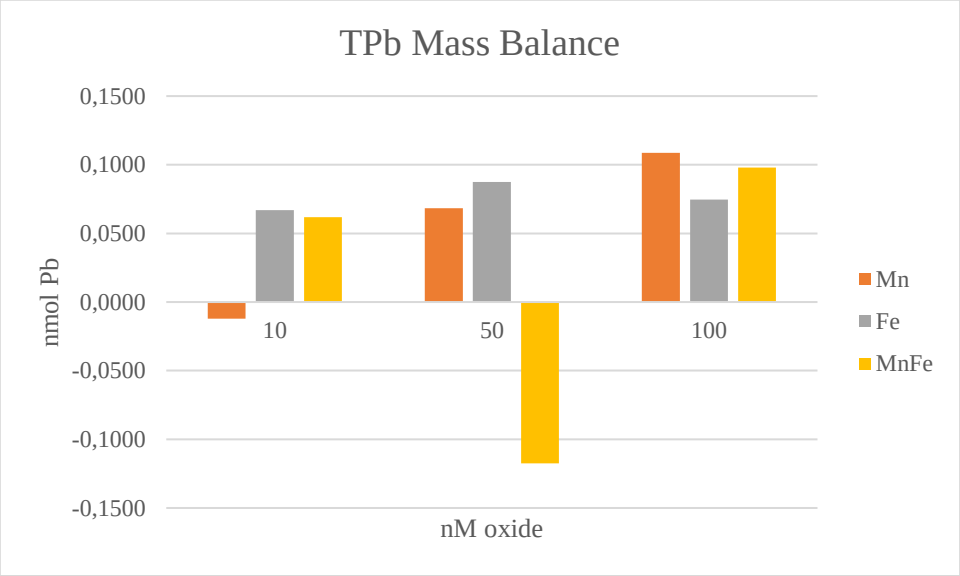

Figure 4.9: Mass balance of TPb in the experimental treatments. The values are corrected for blanks and preconcentration factor.

4.2.7 Percent Dissolved Pb

The percentage dPb to the TPb were plotted as a function of time, and the results are presented in Appendix F, Figure 0.12. Since the dPb values were predominantly below the detection limit, they were not quantifiable. Therefore, the detection limit (0,021 nM) was used for values below the LOD. However, the results were difficult to interpretate because the TPb decreased over time whereas most dPb values were constant (LOD), resulting in increasing % dPb over time. Overall, the treatments were not substantially different to the Control 2.

4.3 Total Hg

The results of THg were plotted as a function of time for the different treatments. The results are presented in Figure 4.10**Feil! Fant ikke referansekilden.** where treatments MnFe, Fe, and Mn are shown in panels a), b), and c), respectively. The dashed line in the plot represents the average concentrations of the spiked seawater controls. The flat end of the error bars indicates the duplicate concentrations. A statistical determination of equilibrium could not be accomplished as there were few data points of each treatment. However, a decreasing trend in THg concentration could be visually seen for some of the treatments, i.e., Mn25, Mn50, Mn100, Fe25, and Fe10. These treatments had lower THg concentration at 336 hours compared to 16 hours, suggesting a minor removal mechanism of THg across the whole time period. On the contrary, the MnFe treatments all increased in THg from 1 to 16 hours. Mn10, Fe10, also went up from 1 to 16 hours and then decreased towards the end of the experiment. Except for Mn10 and Fe10, all Fe and Mn treatments removed more THg than the Control2.

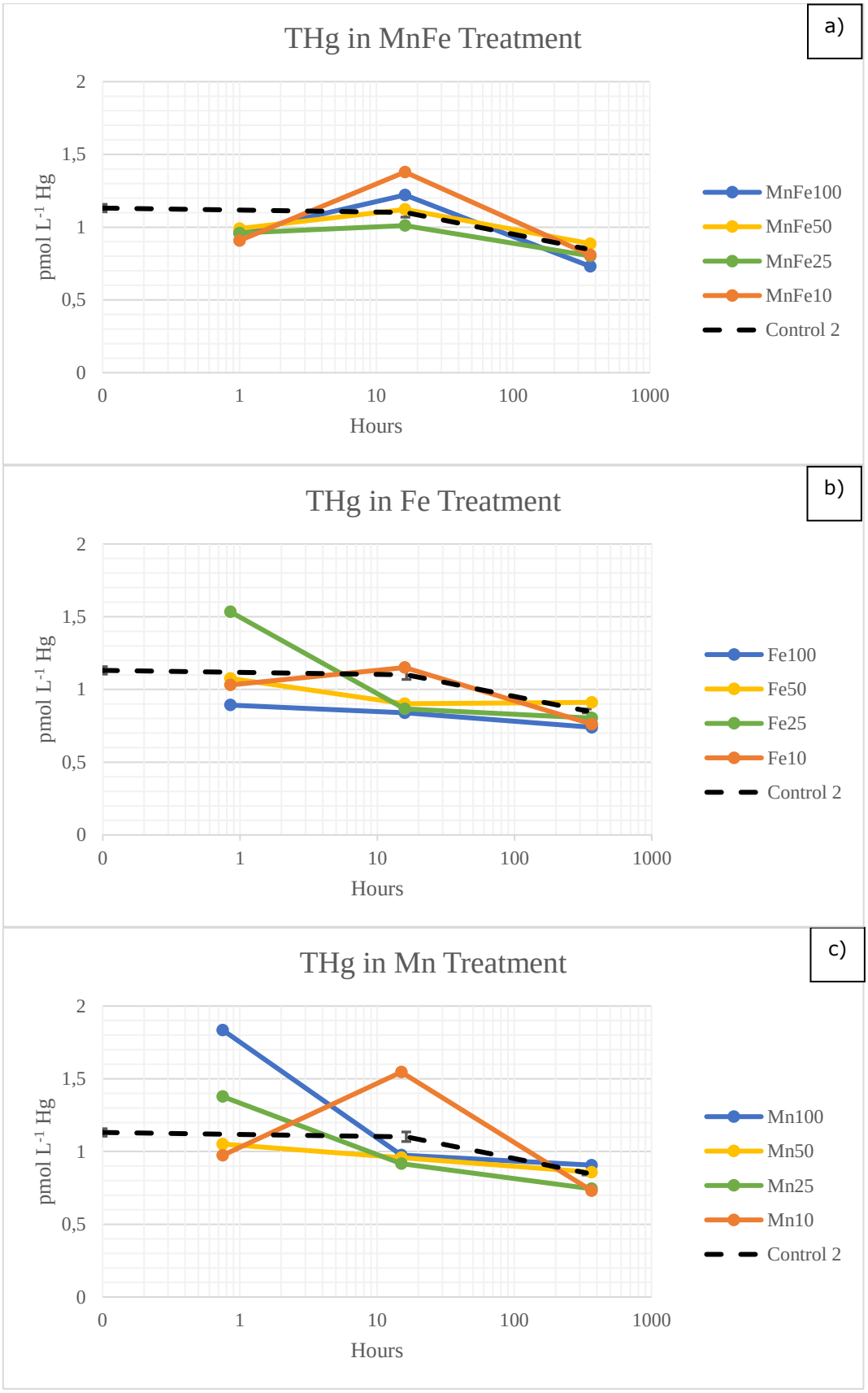

Figure 4.10: THg concentrations as a function of time at the three different treatments: MnFe (a), Fe (b), and Mn (c). Note that the x-axes are on log scale.

4.3.1 Wall Desorption Test of Hg

Figure 4.11 show the results of the wall desorption test of THg. There were no clear trend of the treatments nor oxide concentration.

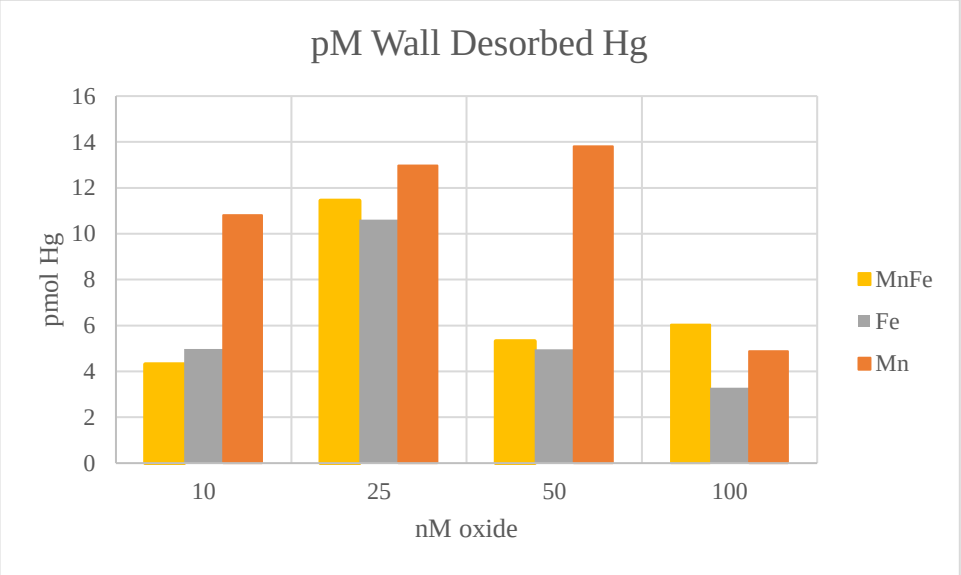

Figure 4.11: Hg desorption from the walls at different oxide concentrations.

Table 4.3 compares THg concentration at the start of the experiment with the amount of desorbed mercury from the walls. In overall, the amount of desorbed THg was almost an order of magnitude larger than the concentration in the bottles.

Table 4.3: Comparison of THg concentrations in the bottles at the start of the experiment and wall desorbed Hg.

	Seawater Samples at 2 hours (pmol L^{-1} Hg) n=16	**Wall Desorption (pmol Hg) n=16**
Average	1.15	8.85
std	0.26	3.62

4.4 Total Fe and Total Mn

The results of TFe and TMn are presented in the figure below. The dashed line in the plot represents the average concentrations of the spiked seawater controls. The flat end of the error bars indicates the duplicate concentrations. As mentioned above for TPb, all TTe were assumed to be analyzed upon the shaking of the experimental bottles. Therefore, the decline in TMn and TFe in treatments and Control 2 were speculated to be influenced by wall adsorption. The graphs in the figure additionally show that the *in situ* Mn treatments were high compared to the seawater background concentration. Comparatively, the background Fe concentration was high compared to the *in situ* concentrations. Thus, the TFe in the Fe10 and Fe50 treatments were not substantially different to TFe in the Control 2.

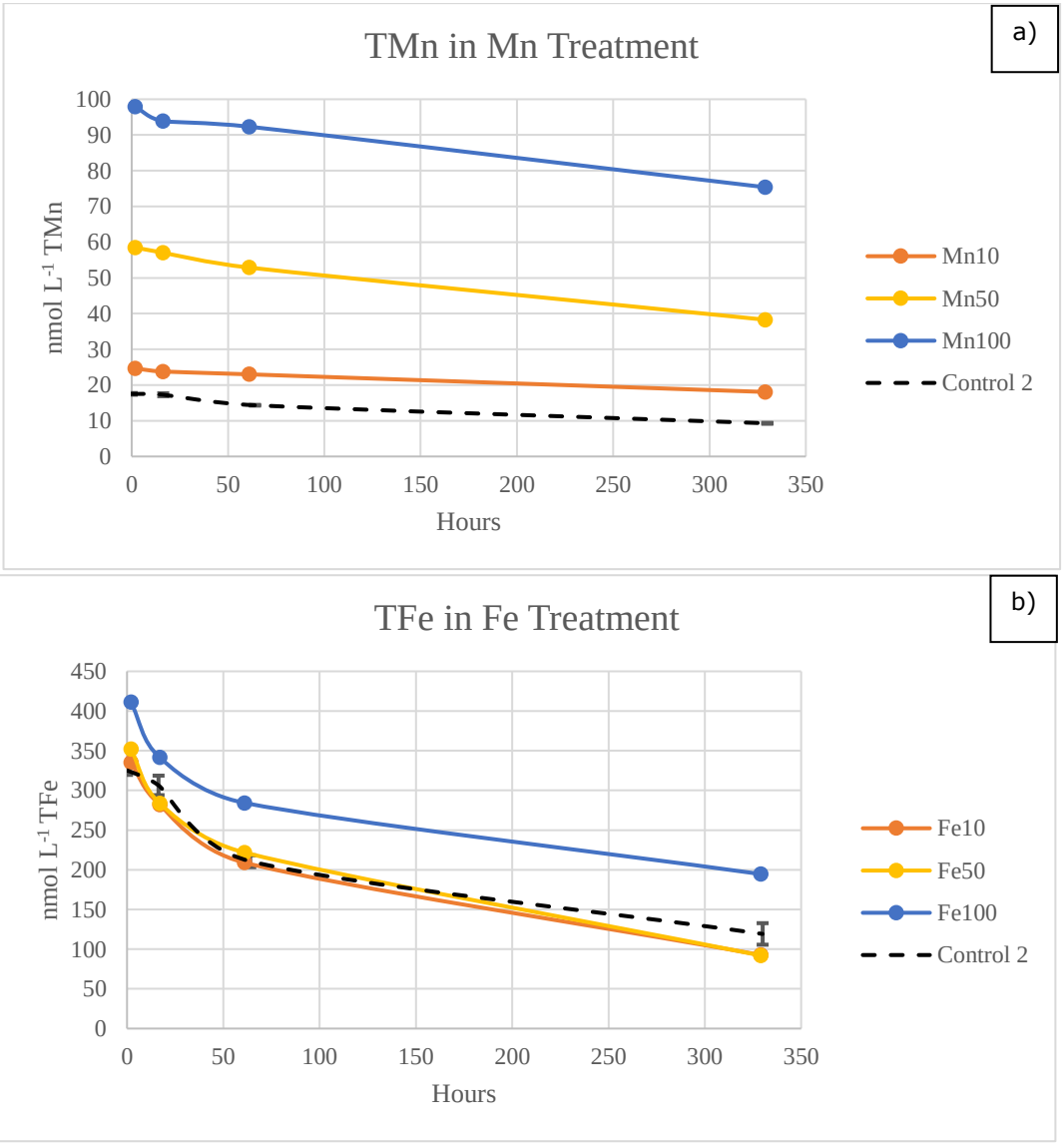

Figure 4.12: TMn a) and TFe b) as a function of time. The values are corrected for blanks and preconcentration factor.

4.4.1 Modeled Wall Adsorption of Total Fe and Total Mn

Since the TMn and TFe concentration was different in the two controls, they were modeled as percent reduction to make them comparable. The two models are shown in Figure 4.13 with 95 % confidence interval. Similar to the TPb model, the TMn and TFe models were quadratic functions with hours as a single quantitative independent variable. One datapoint at 336 hours in the Mn treatment was excluded as it was determined to be an outlier above 0,5 cook's distance from the standardized residuals Appendix E, Figure 0.8. The diagnostic plots of the TFe and TMn models are given in Appendix E, Figure 0.6 and Figure 0.7, respectively.

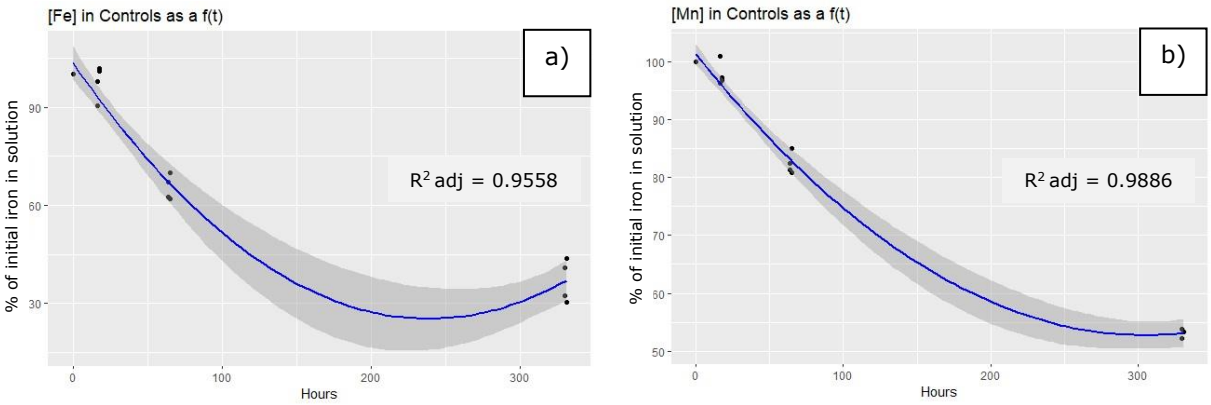

Figure 4.13: Modeled TFe a) and TMn b) concentration in the controls as a function of time at a 95 % confidence interval. The Fe model followed the function $E(y) = 103.5 – 0.6552x + 0.001372x^2$. F-statistics of p-value = $6.142 * 10^{-10}$. The Mn model followed the function $E(y) = 101.3 – 0.3175x + 0.0005193x^2$. F-statistics of p-value = $8.547 * 10^{-13}$. Note the different scales on the y-axis.

4.4.2 Models Compared to Treatments

The figure below compares the modeled wall adsorption with the treatments. TFe in the treatments followed the model more closely than TMn in the Mn treatments. At 64 hours and 336 hours, all data points from the Mn treatments were above the model whereas most TFe was below the model. Furthermore, there were no consistency in the distance to the model as a function of oxide concentration. For instance, a higher percentage TMn in Mn10 treatment was in solution than Mn50. Most TMn was left in the solution in Mn100 treatment. At 16 hours, the TMn in solution was the opposite as 64 and 336 hours.

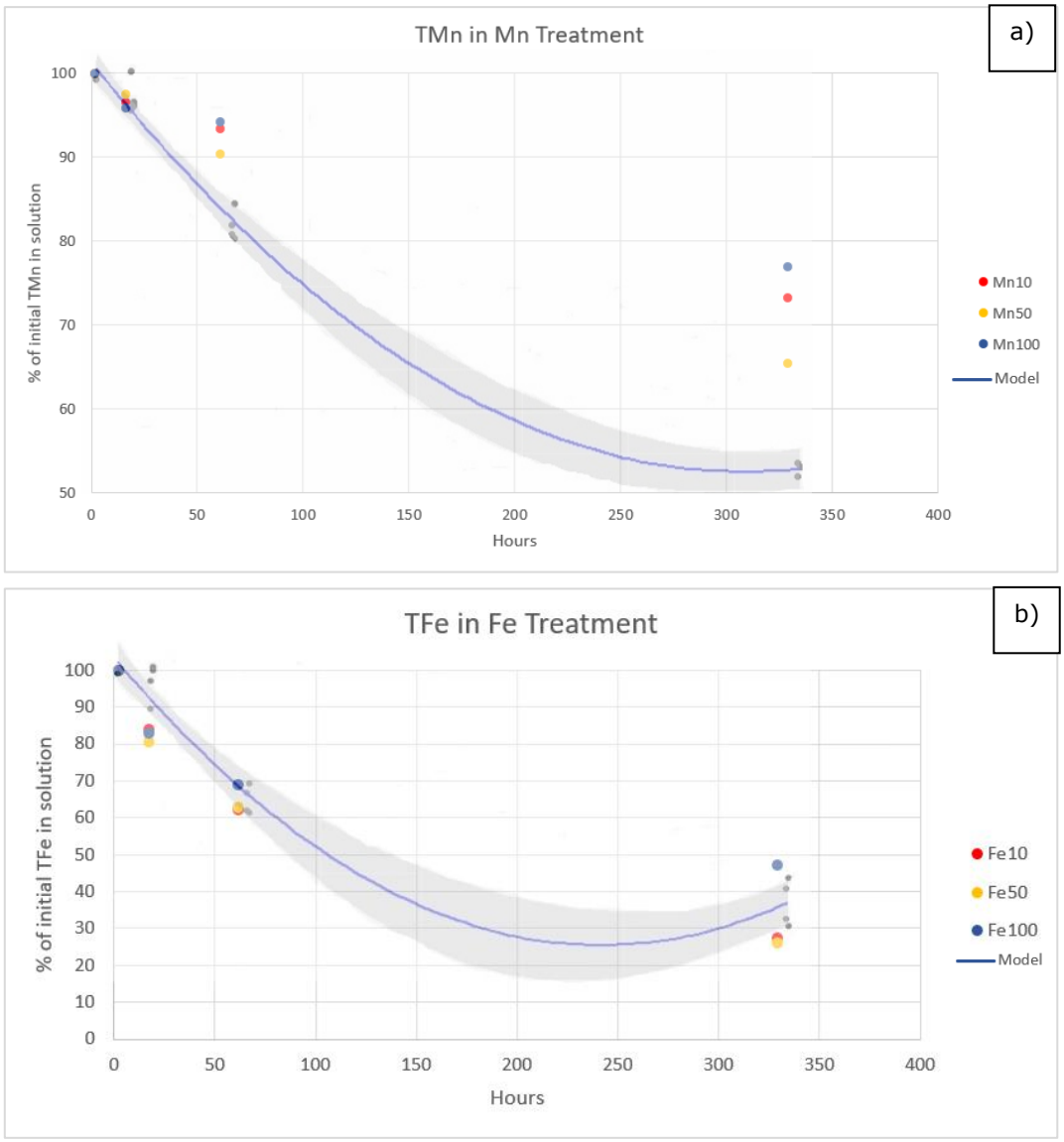

Figure 4.14: Comparison of the modeled TMn a) and TFe b) with the respective treatments. Note the different scale on the y-axis.

4.4.3 Wall Desorption of Fe and Mn

Table 4.4 presents the results of the wall desorption test in the controls, and the percent wall desorbed element of the initial concentration. The percent wall desorption was calculated by dividing the average amount of Fe/Mn in each control with the average initial concentration of each element. Of TMn, wall desorption makes up 15.0 % in Control 1 and 14.6 % Control 2. Of Fe, wall desorption accounts for 7.25 % in Control 1 and 7.59 % in Control 2. This did not fit to the model where 40 % Fe and 54 % Mn was removed at the end of the modeled time period.

Table 4.4: Results of the wall desorption test of Mn and Fe in nmol. The results are corrected for blanks and preconcentration factor.

	Mn		Fe	
	Control 1	**Control 2**	**Control 1**	**Control 2**
Duplicate A (nmol)	1.72	2.76	18.9	27.6
Duplicate B (nmol)	3.76	2.36	17.7	21.8
Wall Desorption %	15.0	14.6	7.25	7.59

4.4.4 Mass Balance of Fe and Mn

The mass balance was calculated as previously described for Pb by subtracting both the wall desorption and the final TMn/TFe from the initial concentration, see equation (11). However, the mass balance was calculated as percentage to the initial concentration because the seawater concentration of TMn was lower than the TFe. By considering the percentage instead of concentration, it was possible to compare the two elements. The mass balance for TFe and TMn are displayed in Figure 4.15 a) and b), respectively.

From the figure below, it is apparent that the analyzed Fe and Mn at the end was less than the initial concentration, although, most profound for Fe. The average Fe deficit was 61.4 ± 7.6 % (n=6), whereas the Mn deficit was 20.2 ± 8.1 % (n=6).

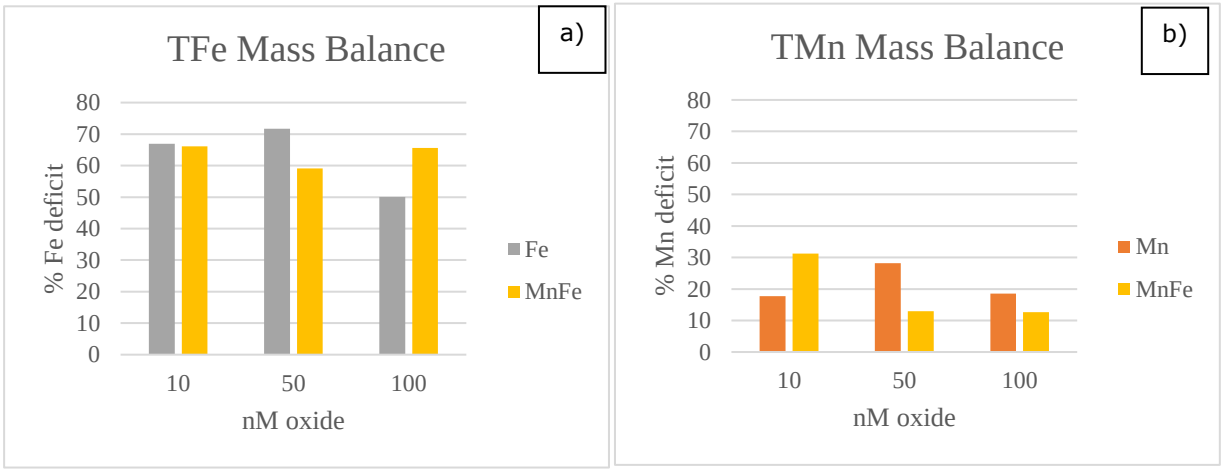

Figure 4.15: Percent deficit Fe a) and Mn b) in the mass balance.

4.4.5 Percent Dissolved Fe and Mn

The percentage dissolved to total trace elements of Fe and Mn in the controls were calculated to reveal the size distribution in the seawater. dMn accounted for 57.3 ± 11.5 % and dFe accounted for 4.3 ± 3.0 %. Hence, approximately 50 % of the Mn pool were in the colloidal size range whilst most of the Fe was present as particulates. The percentage dissolved Te did not change over time for neither Fe nor Mn Appendix F, Figure 0.13.

4.5 Centrifugation Test

Mn obtained similar concentrations in the supernatant and in the precipitate sample. Thus, Mn showed poor separation with the centrifugation technique, the result can be seen in Appendix F, Table 0.7. Fe was more successfully separated with centrifugation. The result

of the centrifugation test of Fe is displayed in Table 4.5. The elevated Fe concentration upon centrifugation compared to the regular samples signifies contamination. However, the fraction dFe in samples were 8.7 %, and fraction Fe in supernatant were 7.5 % which are notably similar values. The values of the precipitate samples were corrected for the filtration blank.

Table 4.5: Centrifugation and filtration of Fe oxides with descriptive statistics. Concentrations are in nmol L^{-1}. n= number of samples. The values are corrected for preconcentration factor and blanks.

	Samples		Centrifugation	
	nmol L^{-1} dFe n=3	**nmol L^{-1} TFe n=2**	**nmol L^{-1} Fe Supernatant n=7**	**nmol L^{-1} Fe Precipitate n=6**
average	11.01	126.73	32.2	426.7
std	3.11	10.19	11.3	172.7
RSD	28.21	8.04	35.2	40.5

The centrifugation results of the toxic trace elements are shown in the table below. Pb concentration in the precipitate samples (0.17 nmol L^{-1}) were approximately three times higher than the TPb in the samples (0.056 nmol L^{-1}). This signifies contamination as well as the large RSD (135 %) of the precipitate samples. Concerning Hg, only supernatant samples were collected. The Hg concentrations were lower in the supernatant compared to the regular samples.

Table 4.6: Centrifugation and filtration of Pb and Hg with descriptive statistics. Concentrations are in nmol L^{-1} for Pb and pmol L^{-1} for Hg. n= number of samples. The Pb values are corrected for preconcentration factor and blanks.

	Samples			Centrifugation		
	nmol L^{-1} dPb n=3	**nmol L^{-1} TPb n=2**	**pmol L^{-1} THg n=2**	**nmol L^{-1} Pb Supernatant n=7**	**nmol L^{-1} Pb Precipitate n=6**	**pmol L^{-1} Hg Supernatant n=4**
average	< LOD	0.056	0.81	< LOD	0.17	0.56
std	na	0.005	0.11	na	0.23	0.08
RSD	na	8.6	13.7	na	135.6	14.3

4.6 pH and Temperature

The pH and temperature throughout the whole experiment was 7.39 ± 0.19 and 9.04 ± 0.96 °C, respectively. The graphs are shown in Appendix F, Figure 0.14 for pH and Figure 0.15 for temperature.

5 Discussion

5.1 Experiment

The original aim of the project was to investigate toxic element adsorption onto *in situ* formed Mn and Fe oxides. Three research questions were sought answered after the incubation experiment was accomplished. The first question was how long time it took for the adsorption of Hg, Pb, As, and Cr onto Fe and Mn to approach equilibrium. The second question was whether Fe or Mn is the better adsorbent of the toxic elements. The last question was which concentration of Fe and Mn that better adsorbed Hg, Pb, As, and Cr.

Some changes during the incubation experiment made the research questions difficult to answer. Cr and As could not be analyzed because of the apparent necessity of preconcentrating the samples with seaFAST. The seaFAST was operated in offline mode, and Cr and As have negligible recovery in this mode of analysis. Concerning Pb and Hg, there was a mistake in the Pb and Hg spike with a factor of 1000. Therefore, 0.002 nM Pb and 0.005 pM Hg was spiked to the experimental bottles instead of 2 nM and 5 pM, respectively. This changed the experiment substantially as the dPb concentration was mainly below the detection limit. Another unforeseen artifact was the wall adsorption of Pb, Fe, and Mn that interfered with the analyzed concentrations.

5.2 Pb

The TPb concentration in the spiked seawater controls was approximately 100 times higher than the spiked Pb. Therefore, the *in situ* Pb had a low contribution to the total Pb pool in the bottles. For this reason, seawater originating Pb was addressed in the discussion. Pb has in previous studies shown to exhibit a reactive nature towards a variety of surfaces in the marine environment (Koschinsky et al., 2003; Wang et al., 2019; Yang et al., 2013). Thus, the Pb present in the seawater was considered to be associated with colloids and particles before the experiment had started.

5.2.1 Dissolved Pb

dPb was rapidly removed from the solution as dPb was in proximity and below detection limit after 16 hours. The finding is in accordance with Koschinsky et al. (2003), who also measured dPb below detection limit after one day. Although, it should be noted that they had a much higher adsorbent particulate concentration of 1 g/L and high detection limits, using voltametric measurements. Since dPb was sampled by pouring undisturbed experimental bottles, another explanation for its rapid removal could be its association with sinking colloids. Although, colloids are recognized by settling velocities less than 0.01 cm s^{-1} (Chattopadhyay & Chattopadhyay, 1978, p. 248), larger colloids close to the filter pore size (0.2 µm) could have had time to sink below the upper part of the bottle until the second sampling at 16 hours. On the contrary, these colloids would easily have been mixed in the experimental bottles and plausibly collected when the sampling was performed. A more probable explanation could be that dPb adsorbed onto the polyethylene wall which has been described in other studies (Jensen et al., 2020; Koschinsky et al., 2003). Out of the Pb pool, dPb would adsorb faster to the walls compared to particulate Pb that would settle through gravitational force (Turner & Hunter, 2001, pp. 204-207).

5.2.2 Effect of Oxide and Oxide Concentration on Pb

Since the dPb was quickly removed from the solution, the oxide concentration could be evaluated based on the wall desorption test. The test showed a decrease in the amount of Pb desorbed from the experimental bottles between 25 and 50 nM oxide. The difference between oxides was not pronounced. However, one limitation when interpreting the results of the wall desorption test was that the test was performed 16 weeks after the experiment was started and 14 weeks after the experiment was ended. Therefore, any processes that occurred in between has not been accounted for. Additionally, the test was done once, meaning that the data are scarce because there are one sample from each bottle.

Even though the effect of oxide concentration was inconclusive, other studies have shown that sorption of Pb increases with particle concentration (Koschinsky et al., 2003; Lu et al., 2014; Swallow et al., 1980). There could be several reasons why the oxide and oxide concentrations did not show any effect on the dPb concentration. Obviously, the mistake in the Pb spike essentially altered the study as the Pb present in the seawater plausibly was associated with particles before the experiment started. Additionally, the low concentrations of dPb in the seawater went quickly below the detection limit. Because of this, the time interval between the first two sampling moments was too long to measure difference between the treatments. Another explanation could be that the Fe concentration in the seawater (288.9 ± 42.3 nM) was higher than the *in situ* Fe (10 to 100 nM). In that way, Fe to Pb ratio did not change substantially with treatments. Swallow et al. (1980) measured that adsorption of Pb increased with the Fe to Pb ratio 100x > 10x > 5x. They had a much larger variety in Fe to Pb ratios than applied in the present study. Furthermore, the relatively small difference in Fe concentration between the controls and the experiment could explain why the dPb in the experiment was not any different to the spiked seawater controls. As for Mn treatments there was not seen any effect of oxide concentration neither. It could be explained by the TPb introduction with the *in situ* Mn additions. This made the comparison with the Fe and MnFe treatments difficult. In summary, dPb should in theory have been adsorbed with increasing concentrations of oxides but for reasons mentioned, it was not evident in the study.

5.2.3 Mass Balance of Pb

With the exception of the Pb adsorbed onto the bottle walls, essentially all Pb present was considered to be analyzed, as the bottles were shaken prior to sampling. Therefore, the mismatch in the mass balance was surprising. The disagreement with the mass balance was supported by the lower TPb in the Fe and MnFe treatments compared to the modeled TPb in the controls (Figure 4.7). TPb does not form any gaseous species so Pb could not have evaded to the headspace. Analytical issues were not considered to explain the mismatch because the samples were preconcentrated with seaFAST and analyzed with ICP-MS together with the other samples. Furthermore, as the bottles were rinsed with 0.12 M UP HNO_3, the wall adsorbed Pb was expected to be sampled. Although, the true recovery of Pb on the walls was unknown due to the mistake in the spike. Another plausible explanation could be that all the particulate Pb did not resuspend completely during sampling so that the TPb was not homogenized in the bottle.

5.2.4 Modeled Wall Adsorption of Pb

The second order polynomial model that explains Pb sorption in controls was the best describing model tested. The model aligned with the findings of Koschinsky et al. (2003), who reported 40% adsorption of Pb after a duration of 7 days. Although, the model had a drawback in that the p-value of the squared term was slightly above 5 % significance level.

Because it was not significant at 5 %, a linear model excluding the squared term was tested. The explanatory variables were significant with a p-value of $2{,}53 \times 10^{-6}$. However, as shown in Appendix E, Figure 0.9, the R^2 adj became lower and residual standard error increased. The plot of "residuals vs. fitted" additionally displayed a biased distribution. The curvature of the applied model is supported by other studies (Cuculić & Branica, 1996; Koschinsky et al., 2003).

5.3 Total Hg

5.3.1 Effect of Oxide, Oxide Concentration and Wall Adsorption

Due to the low Hg concentration in the spike (0.002 pM), most Hg in the experiment originated from the seawater (1.35 ± 0.112 pM). As for Pb, Hg has a reactive nature, and the seawater originated Hg was therefore expected to be predominantly associated with colloids and particles before the experiment started. A proposed THg budget is as follows.

$$\text{Total Hg} = \text{colloidal Hg} + \text{particulate Hg} + \text{wall adsorbed Hg} \quad \textbf{(12)}$$

The experimental bottles were left untouched from the start of the experiment until the sampling from each individual bottle. During sampling, the THg was collected from undisturbed experimental bottles by pouring the seawater into the glass vials. That implies that the THg sampled, was the Hg that was suspended as colloids in the bottle. Any decrease in the analyzed THg could be explained in two ways, i.e., Hg removed with particles at the bottom of the bottle or wall adsorption. One uncertainty concerning this sampling method was that it required steady handling. Any unintended movement of the bottle could resuspend colloids or particles and thereby theoretically increase the analyzed THg. Resuspension could possibly explain some of the variability in the measured THg in Figure 4.10.

As shown in Figure 4.10, the THg concentration declined as a function of time, although, the decrease was not appreciably unlike the spiked seawater control. The amount of Hg desorbed from the walls (8.85 ± 3.62 pmol) were considerably higher than the initial concentration (1.15 ± 0.26 pM) in the experiment. Hence, the wall desorption test could not be interpreted in a meaningful way with respect to mass balance. This is further addressed in the section below. Due to the incomplete mass balance, the reason for the decrease could not be determined whether it was due to wall adsorption or mercury adsorption onto Fe and Mn oxides.

While it was difficult to ascertain the dominant THg adsorbent, the decline in THg could plausibly be attributed to both oxide and wall adsorption rather than one specific mechanism. Multiple studies have investigated wall adsorption of Hg in seawater onto polyethylene bottles (Creswell et al., 2016; Guevara & Horvat, 2013). Guevara and Horvat (2013) measured wall adsorption of 3 to 13 ng/L Hg at 5 °C over 13 days. They found that 40 % Hg was adsorbed over the time period. Comparatively, Creswell et al. (2016) assessed bias in THg after removal of a subsample from polyethylene bottles. Their bottles contained approximately 1.5 ng/L Hg, and they found significant adsorption of THg. Although wall adsorption probably could explain some of the reduction in THg, other studies have shown that Mn and the combination of MnFe are good adsorbents of Hg (Lockwood & Chen, 1973; Lu et al., 2014). Liang et al. (2013) showed that Hg adsorb well onto crystalline Fe structures. In this study, analyzed dFe accounted for 4.3 ± 3.0 % of the total Fe pool in seawater. Thus, most Fe was in the particulate fraction, possibly as crystal

oxides, and this could have adsorbed Hg. In overall, the Hg adsorption could be considered as a competitive process between the wall and the oxides.

Reduction of Hg(II) to Hg(0) could potentially have been an explanation factor for the reduction in THg concentration. Hg(0) is a gaseous, volatile element that can evade from the water phase into the headspace. Previous studies have investigated the reduction of Hg(II) to Hg(0) in incubation experiments (Amyot et al., 1997; Lalonde et al., 2001). Lalonde et al. (2001) saw no formation of dissolved gaseous Hg in dark control bottles. Amyot et al. (1997) saw only dissolved gaseous Hg formation that were induced by sunlight. These findings are in accordance with the review paper by Batrakova et al. (2014) that shows that dark Hg reduction is a slow process in the environment. Furthermore, Creswell et al. (2016) investigated THg in seawater stored on bottles. They did not measure gaseous elemental Hg but thought the evasion to headspace would be unlikely to explain any bias in the results. Their Hg concentration was higher than in the present study. Hence, Hg evasion to headspace was considered as negligible in the incubation experiment.

5.3.2 Wall Desorbtion Test of Hg

The amount of Hg desorbed from the walls of the experimental bottles (8.85 ± 3.62 pmol) was much larger than the initial concentrations (1.15 ± 0.26 pmol). The diffusivity of Hg(0) across polyethylene bottles have previously been investigated. Parker and Bloom (2005) performed a test on mercury stored in polyethylene bottles utilizing ultra-clean techniques in a laboratory with low mercury content (5-10 ng m^{-3} Hg(0)). Their results found a significant increase in mercury content over few weeks storage. Moreover, the contamination depends on the mercury concentration in the laboratory, and as most laboratories have a concentration of 50-500 ng m^{-3} Hg(0), it could pose a contamination introduction (Parker & Bloom, 2005). Similarly, another study found a significant increase in Hg concentration in seawater samples stored on polyethylene bottles (Hammerschmidt et al., 2011). Since the wall desorption test was performed 19 weeks after the experiment, diffusive mercury was the most likely explanation for the elevated mercury concentration on the bottle walls. For this reason, the wall desorption test could neither be used to calculate mass balance nor as an indicator of adsorption because the concentration had most likely increased over the storage period.

Contamination from the bottles themselves were considered unlikely since the bottles were brand new and underwent 8 days of acid washing. Concerning the wall desorption test, Hammerschmidt et al. (2011) showed that BrCl sufficiently removed low level Hg adsorbed onto low density polyethylene. All wall adsorbed Hg was therefore considered to have been recovered and analyzed as shown in the results.

5.4 Fe and Mn Oxides

5.4.1 Wall Adsorption of Fe and Mn

Wall adsorption was postulated to be the explanation for the decline in TFe and TMn concentrations in the controls. To investigate this hypothesis, the findings in the present study was compared to other studies. Fischer et al. (2007) measured Fe in seawater samples stored on polyethylene bottles. They measured that 50 % of the TFe adsorbed onto the walls over 70 hours. In another study, it was observed that 18% of Fe in seawater was adsorbed within 29 hours by using 1 L bottles (Fitzsimmons & Boyle, 2012). Both these studies were similar to the Figure 4.13 a).

The adsorption of Mn onto polyethylene bottles which contains seawater are limitedly studied. Although, Jensen et al. (2020) found that unacidified seawater samples did not significantly adsorb Mn onto polyethylene over 40 weeks. This is contradicting to the findings in the present study where 14.8 % Mn was adsorbed over 16 weeks. Although, both Mn oxides (Lu et al., 2014) and polyethylene (Xu et al., 2018) have a negative surface charge, theoretically implying they would repel each other, supporting the findings of Jensen et al. (2020). However, as mentioned for Pb, the wall desorption data are limited because it was carried out 14 weeks after the experiment was finished. Moreover, only one sample of each treatment was gathered, thereby, the data in the present study are too few to make a conclusion.

5.4.2 Modeled Wall Adsorption of Fe and Mn

The modeled TFe concentrations in the controls showed an increase in concentrations after approximately 250 hours. There could be three reasons for this artifact, either the quadratic model was insufficient, bacteria growth changed the environment or contamination caused the changes. It is well established knowledge that bacteria in seawater alter the chemistry of Fe in their microenvironment by releasing organic molecules that solubilize sorbed Fe (Buck et al., 2010; Leventhal et al., 2019). However, the concentration did not measurably increase over the time-period in the experiment. Additionally, as shown in the Q-Q plot in the Appendix E, Figure 0.6, the data points appeared to be biased as they did not follow a straight line. Thus, the insufficiency of the quadratic function was a more probable explanation rather than contamination and the effect of microorganisms.

The quadratic function explained the TMn adsorption in a more efficient manner than TFe. The p-value were lower, R^2adj was higher, and the confidence interval was narrower, see Appendix E, Figure 0.7 for the model parameters.

As shown in Figure 4.14, TMn in the controls showed poor conformity with the experiment, whereas Fe in the treatments and controls was similar. It can be speculated that *in situ* Mn adsorbed less effectively to the walls than aged Mn oxides. The reason being that more Mn was in the solution in the treatments than in the controls. The different results for Fe and Mn could be explained by the ratio of oxides in seawater to the *in situ* concentrations. The Mn concentration in seawater was lower than the *in situ* concentration whereas the Fe concentration in seawater was higher than any *in situ* additions. Thus, the difference between the controls and the treatments was more evident for Mn than Fe.

5.4.3 Mass Balance of Fe and Mn

As mentioned for TPb samples, all TMn and TFe, except for wall adsorbed elements, were expected to be sampled because of the resuspension before sampling. Regardless, both Fe and Mn had a deficit in the mass balance, Figure 4.15. Therefore, there was plausible that not all Fe and Mn had been recovered in the wall desorption test. Few studies are conducted on the desorption of trace elements in seawater from polyethylene bottles. Jensen et al. (2020) performed a study comparatively to the present one. In their study, 53 % Fe was remaining on the wall after they had acidified the seawater in the bottles with 0.024 M HCl. In this desorption test, the walls were rinsed twice with 15 mL 0.12 M HNO_3. Therefore, the wall adsorbed Fe was plausibly not recovered completely by this method. The 53 % loss of Fe in the study of Jensen et al. (2020) is comparable to the deficit in the mass balance, i.e., 61.4 ± 7.6 %

A higher percentage Mn was recovered from the wall compared to Fe. One explanation could be that the ratio of adsorbate (oxide) to adsorbent (polyethylene) was lower for Mn (17.9 ± 0.46 nM) compared to Fe (288.9 ± 42.3 nM) in the seawater. Additionally, a higher percentage of Mn was measured in the dissolved phase compared to Fe. Thus, dMn would have had time to adsorb onto the walls, while particulate Fe would be too large and settle at the bottom of the bottle.

Another explanation for the deficit in the mass balance could be explained by the wall desorption test itself. One uncertainty was that the desorption was performed 14 weeks after the experiment was ended. Thus, any adsorption or desorption that occurred after the experiment was finished would not have been measured.

5.5 Centrifugation Test

The centrifugation had a better success in separating Fe than Mn. The explanation could be that most of the Fe pool in the incubation experiment originated from the seawater whilst most of the Mn pool was introduced with the *in situ* addition. Moreover, a dominating fraction of the seawater Fe oxides was in the particulate phase. Because of the crystalline nature of aged oxides compared to initially formed oxides, they have less pore volume (Liang et al., 2013), resulting in higher density. Hence, the Fe oxide particles were efficiently sedimented during centrifugation whereas Mn was not.

The THg concentration was lower in the supernatant than in the other samples. There could be more reason for this result. Liang et al. (2013) saw that Hg adsorbs stronger to crystalline structures over amorphous hydroxides. The depletion in Hg could be explained by adsorption onto the sedimented Fe crystals. However, since the extent of wall adsorption of Hg was unknown, it could not be known if the result was influenced by this artifact.

However, there were few weaknesses with the centrifugation experiment. One weakness was that the correction was performed with one method blank. For a more reliable result, the correction should have been carried out as an average of three blanks. Especially since the precipitate samples were filtrated over a previously used filter. Although the filter was rinsed with UP HNO_3 and Milli-Q water, contamination of Pb was evident. Moreover, the increased Fe concentrations could be attributed to the additional handling steps involved with the centrifugation.

5.6 Particle Dynamic Model

A particle dynamic model is proposed in Figure 5.1 to explain the major chemical and physical processes that occurred in the experimental bottles. The model was based on the findings in the present experiment as well as relevant literature by scholars.

The experiment was initiated by the addition of *in situ* Fe(II) and Mn(II) to the closed system. Fe oxidation is a rapid reaction in oxic waters (Fischer et al., 2007) relative to Mn oxidation that is slow and catalyzed by microbial activity (Tebo, 1991). Importantly, the initially formed oxidized species of Fe and Mn were not truly soluble (Byrne & Kester, 1976). They formed colloids smaller than 0.2 µm and could stay suspended in solution. Furthermore, they underwent multiple processes once oxidized. They adsorbed onto polyethylene (Fischer et al., 2007; Jensen et al., 2020), they coagulated to larger particles (Lu et al., 2014) which sedimented, and they adsorbed Hg and Pb (Liang et al., 2013; Yang et al., 2013). The major pathway of the particles was thought to be sedimentation as they had faster gravitational settling and less affinity for the walls compared to the colloidal Fe

and Mn oxides. The settling velocity of the oxides was a function of the size. The larger the particle, the more rapid it would sink and settle the toxic elements to the bottom of the bottle (Turner & Hunter, 2001, pp. 204-207).

Similar chemical and physical processes were thought to occur for the Fe/Mn oxide pool originating from the seawater. Since the morphological composition of these oxides were unknown, they were combined into one unit in the particle dynamic model. However, by filtrating the control samples, information about the size distribution was gathered. As shown in section 4.4.5 and Appendix F, Figure 0.13, dMn accounted for approximately half of the TMn whereas dFe made up 4.3 ± 3.0 % of the TFe. According to scholars, dissolved Fe is the dominating fraction in surface coastal seawater owing to the organic ligands in seawater (Kuma et al., 1998) as inasmuch 99.9 % of all dissolved Fe can be chelated by organic ligands (Turner & Hunter, 2001, pp. 313-315). Similar results are found for Mn (Oldham et al., 2017). One explanation for the discrepancy between the results and other research could be contamination from the handling when the barrels were filled or contamination could originate from the barrels themselves.

Because of the co-existence of *in situ* Fe/Mn oxides and oxides in the seawater, they could be considered as competing processes in adsorbing the toxic elements. Another competing process of Hg and Pb sorption was the adsorption onto the container walls (Guevara & Horvat, 2013; Jensen et al., 2020). Organic ligands bound to colloidal elements could be attracted to the walls through charge-charge attraction, hydrogen bonding, or van der Waals forces depending on their speciation and ligands (Fitzsimmons & Boyle, 2012). According to Xu et al. (2018), polyethylene exhibits a negative charge when the pH exceeds 4.30. This intriguing property makes it prone to be a competitive adsorbent to elements with the same charge, such as Mn oxides (Lu et al., 2014). Moreover, wall adsorption is influenced by elemental concentration, temperature, bottle material, and surface to volume ratio of the bottle. For instance, lower concentration and smaller bottles results in a higher relative adsorption (Fischer et al., 2007; Fitzsimmons & Boyle, 2012; Jensen et al., 2020; Krauskopf, 1956).

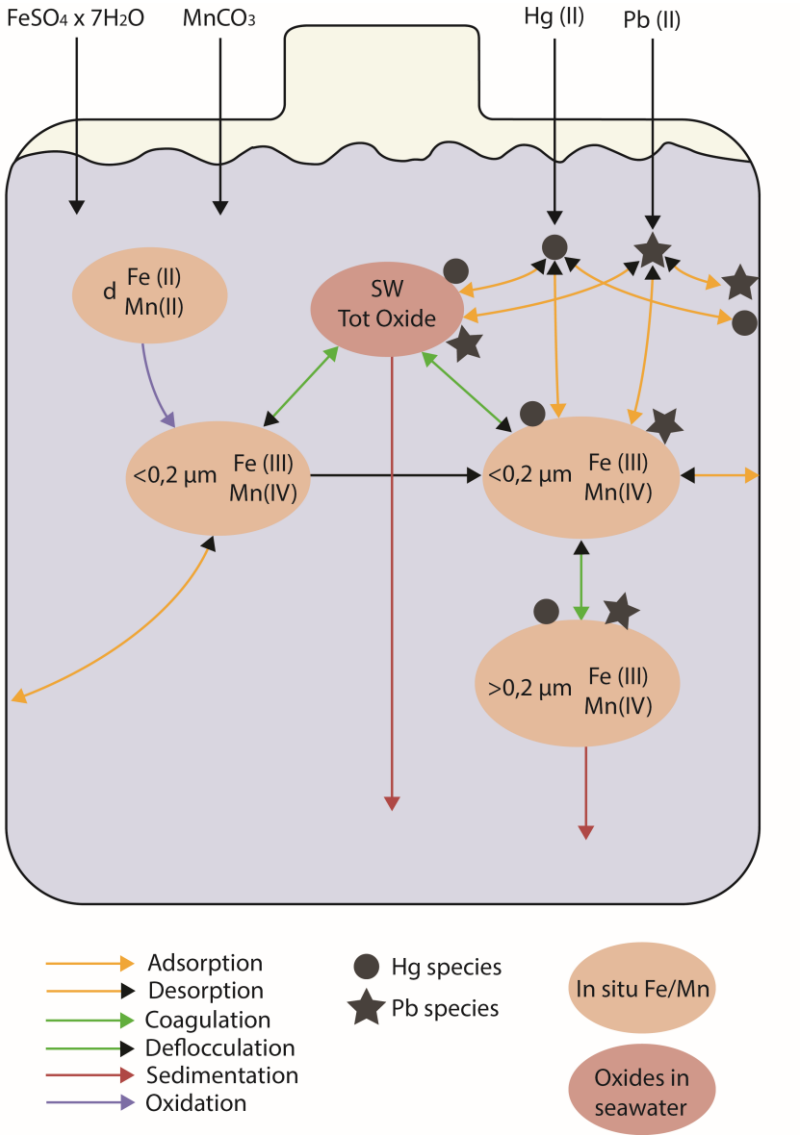

Figure 5.1: Schematic overview over the main processes in the experiment. Brown circles signify *in situ* Mn and Fe. The red circle signifies a representation of all colloidal and particulate oxides present in seawater. The figure was inspired by (Creswell et al., 2016; Fischer et al., 2007; Lamborg et al., 2016; Liu et al., 2012; Lu et al., 2014).

5.7 Analysis

When working with trace elements, possible contamination from multiple sources arises. To have control of contamination, blank samples are commonly used. However, instead of blank samples in the present study, controls with seawater and spiked seawater were imbedded to correct the treatments from the background processes. A systematic error was introduced from the barrels as the trace element concentrations in the two barrels were statistically significant different. The difference between the barrels could not be explained by the spike addition. Anyhow, the measured TPb and THg in the present study was within the concentration range that could be expected from literature. As shown in Table 2.1, TPb concentrations are between 0.013 nM and 2.4 nM, and THg is within 0.10 pM and 3.2 pM in marine waters. Comparably in this study, the highest measured TPb concentration was 0.272 nM, and the highest THg concentration was 1.84 pM, which is

shown in Figure 4.5 and Figure 4.10, respectively. This indicates that it has not been any systematic contamination during the incubation period, during the sample handling, nor from the preconcentration and analysis.

Concerning Fe and Mn oxides, these are elements with high variation in special distribution in the environment. The variability is reflected by the literature in Table 2.1, as there is a large difference between the lowest and the highest value. From the literature, the findings by Bruvold et al. (2023) is comparable because they conducted a recent study in another Norwegian fjord with low anthropogenic impact. Their TMn concentration (~14-27) are similar to the Mn concentration in this study, implying no significant contamination during the incubation experiment. TFe on the contrary, had a higher concentration in this study. Additionally, there was a large difference of TFe between the barrels. At time zero, the duplicate samples in the seawater control barrel were 252.2 nM and 252.7 nM, whereas the other barrel had a concentration of 331.0 nM and 319.6 nM. The barrel with the higher TFe concentration was used to store the seawater in which the treatments were conducted on. Contamination of the barrel could pose as an explanation to why the percent dFe was lower than expected. Overall, TFe showed larger difference between the barrels than TMn.

5.7.1 Pb, Fe, and Mn

5.7.1.1 Storage Conditions

The storage conditions were not thought to have any considerable impact on the results. Since the samples were acidified to pH below 1.8 immediately upon sampling, there were presumably no wall adsorption onto the falcon tubes (Jensen et al., 2020). As an example, Kanna et al. (2020) acidified seawater samples with UP HNO_3 to pH < 1.8 and stored it more than two months in room temperature prior to analysis. Moreover, the acidified samples were stored dark in each individual zip lock bag as recommended by Method 1640 (USEPA, 1995). These actions mitigated the possibility of contamination during storage.

5.7.1.2 Method Performance

The method performance was evaluated through the detection limits and the precision and the accuracy of the certified reference material, NASS-7. The accuracy, precision, and detection limit obtained in the present study were compared with literature that have used the NOBIAS chelate-PA1 resin and the NASS seawater reference material.

5.7.1.3 Detection Limits

The detection limit for Mn and Fe was an order of magnitude higher than detection limits reported elsewhere, whilst Pb had a detection limit approximately 20 times higher than previous studies (Middag et al., 2015; Rapp et al., 2017; Wuttig et al., 2019). If the detection limit had been lower, the measurements of NASS-7 would plausibly have been above the detection limit. This would have given more information on the method performance of Pb. Additionally, more dPb measurements would have been quantified, and the treatments could have been compared statistically.

The detection limit was calculated as 3 times the standard deviation of the blanks, and therefore, directly influenced by random contamination of these. Explanations could be that even though the falcon tubes were metal free clear sterile, they were not acid washed prior to usage. Furthermore, they were taken from a 500 pcs box in a regular laboratory and brought to the pressurized laboratory. The lack of acid washing and the transport between the labs could pose two sources for contamination. Moreover, Pb contamination in the blanks may be a attributed in sample fluctuations and sample processing (Ge et al.,

2022) since the samples were processed by the seaFAST in 12 runs over five weeks. Hence, various factors could explain the high detection limit.

5.7.1.4 Accuracy

Good accuracy of Fe and Mn measurements was obtained and was comparable to values reported elsewhere for NASS reference materials, i.e., 95.9 % - 99.7 % for Mn and 93.6 % - 96.0 % for Fe (Ge et al., 2022; Samanta et al., 2021; Wuttig et al., 2019). The accuracy of Mn was similar to the value obtained in present study (92.2 %) whilst the accuracy for Fe was lower (83.1 %). The accuracy for Fe is supported by Rapp et al. (2017) that obtained the same recovery for Fe at pH 6.1.

5.7.1.5 Precision

The precision, expressed as the relative standard deviation of the analyzed CRM, was 8.3 % for Fe and 7.1 % for Mn. The modest precision could be attributed in the previous discussed contamination risks. However, the precision can be regarded as fair, taken the experimental conditions and the time lag between experiment and analysis into consideration. Comparatively, performed the analysis in ISO 6 (Class 1000 cleanroom) and obtained relative standard deviations of 1.5 % and 2.6 % on NASS-6 CRM.

5.7.1.6 Preconcentration Factor

The 10 times preconcentration factor was chosen because of the expected concentration of TPb in seawater and that of the spike. Thus, the preconcentration factor could have been increased if the mistake in spike concentration and the artifact of wall adsorption was known. An increased preconcentration factor would preferably also have resulted in lower detection limits (Wuttig et al., 2019). However, the preconcentration factor was a tradeoff with the other elements analyzed. TFe, for instance, had a concentration between 252.2 and 319.6 nM in the seawater. Any up concentration of Fe would plausibly have approached saturation of the resin and exceeded the linear range over which Fe is recovered (Wuttig et al., 2019). Samples could have been analyzed twice with two different preconcentration factors, but this would have been time consuming. Overall, it was decided not to increase the preconcentration factor due to the large difference in elemental concentrations.

5.7.1.7 Recovery

The recovery of elements on the resins is mainly influenced by the pH of the buffer. (Rapp et al., 2017). Comparison of recoveries between studies have to be treated carefully as the recovery of each resin is influenced by the storage time of the resin, flow rates, the resin volume, and the concentration of analytes (Rapp et al., 2017). However, previous studies have shown that optimum pH recovery of Pb is achieved over the pH range 5 to 7.9, Fe had best recovery over pH 5.6 and 7.4, whilst Mn had best recovery up to pH 7.1 (Rapp et al., 2017). The buffer pH applied in this study was ~ 5.7.

Pb showed a linear behavior over the concentration range applied in the experiment as the R^2 value for all the calibration points was 0,999. This verifies that the adsorption sites of the functional groups on the resin did not approach saturation over the entire concentration range applied. A calibration curve for Fe and Mn were also run by laboratory technicians upon the analysis but was excluded due to the low concentration range of the elements. However, Mn recovery of the NOBIAS Chelate-PA1 resin has previously been verified to be linear over the concentration range applied (Rapp et al., 2017). Rapp et al. (2017) found a slight decrease in Fe recovery at concentrations above 200 nmol L^{-1} which potentially could have had an impact on the results for Fe in the present study since all samples were above this concentration level.

5.7.2 Total Hg

5.7.2.1 Storage Conditions

The different storage conditions of mercury have previously been discussed by scholars. The Hg storage in borosilicate glass vials is of importance for the analysis. According to EPA Method 1631, seawater samples should be acid preserved if the storage time exceeds 48 hours (USEPA, 2002). However, Parker and Bloom (2005) saw that the Hg(II) is stable in solution and may be stored unpreserved over weeks. Additionally, the sample vials were filled to top so that the Hg(0) could not equilibrate with the headspace (Parker & Bloom, 2005). Since the Hg in the samples was in the pM range, a preservative was not used because the low Hg concentrations could have been modified in the solutions. Due to the absence of a preservative, Hg in the glass vials would be adsorbed onto the walls (Guevara & Horvat, 2013). Anyhow, this had no implications on the analyzed results as BrCl was added directly to the sample vial more than 24 hours prior to the analysis. This recovered all the mercury back into solution (Parker & Bloom, 2005).

5.7.2.2 Analysis

The wall adsorption in glass vials and contamination from HCl and BrCl reagents during analysis was evident. Before running the samples for Hg analysis, the Hg in the standards was stabilized by adding 0.5% v/v HCl (Guevara & Horvat, 2013). The same standards were then used over multiple days. However, there was seen that the slope of the calibration curve decreased over time as the mercury adsorbed onto the walls. The reduced concentration in the standards resulted in gradual steepness of the calibration curve and high recovery of the reference material. In order to stabilize the mercury in the solution over days, 2 % v/v HCl was added to keep the mercury in solution. The UP HCl was not free from Hg which resulted in increased steepness of the calibration curve and accuracy of the reference material below the criteria. Therefore, the analysis was proceeded with the preparation of new standards every day containing 0.5 % v/v HCl.

The steepness of the calibration curve could have impacted the accuracy in the results. Samples run 19th of April (sampling time z duplicates) had a slope of 1.5, with the recovery of mercury in the seawater being 89.8 %. The recovery was close to the expected value of the method (90 %) (Brooks Rand Instruments, n.d.). The four certified reference material April 19th had an average recovery of 96.8. In comparison, on the 27th of April (samples at 336 hour), the steepness was the most gradual among all sample runs with a slope of 1.1. Because of the gradual slope, the ERM were in the upper range of the quality control area [77-123]. Hence, the accuracy would be influenced by the calibration curve. The actual concentration in the samples at 336 hours could therefore be lower than the measured values. More samples could have been analyzed but it was decided not to due to the high wall desorption of mercury.

One uncertainty with the analysis was that the probe was broken, and the tip had to be manually put back on between every sample run. Protective measures were taken by using clean gloves. The constant fixing of the probe could have resulted in potential contamination of random samples, e.g., the elevated concentrations in treatment Mn100 at 2 hours and Mn10 at 16 hours. Another concern was the Hg introduction with the HCl. Additionally, BrCl also proved not to be entirely mercury free, however, the Hg introduction in the reagents was accounted for in the calibration blanks. The cleaning of the glass vials and caps was considered as acceptable as the calibration blanks were below the criteria.

5.8 Experiment Evaluation

As addressed in section 5.7, the measured seawater concentrations of TPb and THg were as expected for coastal seawater. Thus, seawater collected from 80 meters depth in the Trondheim Fjord can be used as matrix in experiments with Pb, Hg, Mn, and Fe. If the mistake with the spike had been avoided, the THg concentration would have been approximately 5 times higher than that of the seawater. TPb would have been 10 times higher. Further studies should therefore aim for spikes with 2 nM Pb and 5 pM Hg concentration. Furthermore, the background TMn concentration (17.28 nM - 18.30 nM) was relatively low compared to the *in situ* concentrations (10 nM – 100 nM). Thus, the *in situ* concentrations of Mn can be used for future work. The Fe concentration, however, was higher than any of the *in situ* concentrations. If future studies investigate Fe as adsorbent, higher concentrations or artificial seawater should be the matrix.

Concerning sampling times, dPb should be sampled more frequently at the beginning of the experiment due to its rapid rate of decrease. Similarly, a higher sampling frequency for THg is warranted as well due to its particle reactivity.

Overall, polyethylene should not have been used as storage container for neither Hg, Pb, Mn, nor Fe in seawater because of the wall adsorption, the uncertain recovery upon desorption, and the diffusivity of Hg(0). However, as the wall adsorption was an evident artifact in the experiment, wall desorption samples should have been taken the last day of the incubation period. The uncertainty introduced between the incubation period and the wall desorption sampling would then have been mitigated, e.g., contamination by diffusive Hg(0). Furthermore, wall desorption should have been measured after the acid washing to control that the walls were clean for trace elements. Additionally, two more desorption tests within the incubation period would have given information about the rate of wall adsorption.

The bottles were preconditioned with the seawater before the experiment was started. However, one way to avoid wall adsorption could be to saturate the walls in an elevated solution of Hg, Pb, Mn, and Fe. Then, the elements would theoretically not adsorb to the walls. Another approach to address the challenges associated with wall adsorption could involve using one single, large storage container, rather than multiple experimental bottles. All samples derived would then be subsampled from the container. Compared with 1 L experimental bottles, the surface area to volume would have been smaller, and the wall adsorption would be less pronounced.

Conclusion

Hg and Pb are known to be extremely harmful to marine organisms. It is of importance to understand their geochemical interaction with colloids and particles in the marine environment. Fe and Mn particles are known to be effective scavengers of Hg and Pb in seawater. Therefore, the present study was designed to examine the effect of *in situ* oxidized Mn and Fe on adsorption of Hg and Pb in seawater.

The polyethylene walls on the storage bottles used in the incubation experiment appeared to be an important artifact for Pb. The wall desorption test indicated that the oxide concentration had an influence on the Pb concentration at the 50 and 100 nM Fe and Mn concentration. However, limited data samples on wall desorption made it impossible to test statistically. A mass balance was conducted on Pb, Mn, and Fe, revealing a deficit of all the elements for most of the treatments. One plausible explanation was that the elements had poor recovery by the method applied. The Mn, Hg, and Pb samples were measured to be within the expected concentrations found in natural seawater. Thus, contamination of these were not evident. The centrifugation method indicated that the particulate Fe was separated as efficiently as 0.2 µm filtration. However, it could not be concluded due to contamination. A particle dynamic model is proposed to explain the processes during the incubation period.

One limitation with the study was a mistake in the Hg and Pb spike, being negligible to the Hg and Pb background concentration in the seawater. Because of wall adsorption, the dPb concentration decreased quickly below detection limit between the sampling point at 2 hours and 16 hours. Thus, the time intervals between the two first sampling times were not sufficient to measure any effect of the treatments. Furthermore, because of the low elemental concentration, preconcentration with seaFAST was a necessity. The seaFAST was operated in offline mode resulting in that Cr and As could not be analyzed. Another limitation was that the wall desorption test was performed 14 and 17 weeks after the incubation experiment was finished. Introducing uncertainty in interpreting the results obtained. The background Fe concentration in seawater interfered with the experiment as it was higher than the *in situ* concentrations.

Because of the particle reactivity of dPb, more frequent samples should be collected within the first 16 hours of the experiment. Wall desorption test should at least be performed at the start and at the end of the experiment. Polyethylene bottles should not be used as storage material due to the diffusiveness of Hg(0), adsorption of Pb, and low recovery of Fe. Furthermore, more research should investigate the recovery of Fe, Mn, and Pb from polyethylene bottles in seawater. Although, one mitigation method could be to precondition the bottles in a high elemental solution prior to the experiment as this would saturate the walls. Alternatively, one large storage container could be used as this would increase the volume to surface area.

References

AMAP. (2018). *AMAP Assessment 2018: Arctic Ocean Acidification.* Arctic Monitoring and Assessment Programme (AMAP), Tromsø, Norway. vi+187pp.

AMAP. (2021). *AMAP Assessment 2021: Mercury in the Arctic.* Arctic Monitoring and Assessment Programme (AMAP), Tromsø, Norway. viii + 324pp.

Amyot, M., Gill, G. A., & Morel, F. M. (1997). Production and loss of dissolved gaseous mercury in coastal seawater. *Environmental Science & Technology*, *31*(12), 3606-3611.

Andreae, M. O. (1979). Arsenic speciation in seawater and interstitial waters: The influence of biological-chemical interactions on the chemistry of a trace element 1. *Limnology and Oceanography*, *24*(3), 440-452.

Antonopoulou, E., Rohmann-Shaw, C. F., Sykes, T. C., Cayre, O. J., Hunter, T. N., & Jimack, P. K. (2018). Numerical and experimental analysis of the sedimentation of spherical colloidal suspensions under centrifugal force. *Physics of Fluids*, *30*(3), 030702.

Azad, A. M., Frantzen, S., Bank, M. S., Johnsen, I. A., Tessier, E., Amouroux, D., Madsen, L., & Maage, A. (2019). Spatial distribution of mercury in seawater, sediment, and seafood from the Hardangerfjord ecosystem, Norway. *Science of the Total Environment*, *667*, 622-637.

Bam, W., Maiti, K., Baskaran, M., Krupp, K., Lam, P. J., & Xiang, Y. (2020). Variability in 210Pb and 210Po partition coefficients (Kd) along the US GEOTRACES Arctic transect. *Marine Chemistry*, *219*, 103749.

Batrakova, N., Travnikov, O., & Rozovskaya, O. (2014). Chemical and physical transformations of mercury in the ocean: a review. *Ocean Science*, *10*(6), 1047-1063.

Beauchemin, D. (2000). *Discrete sample introduction techniques for inductively coupled plasma mass spectrometry* (Vol. Vol. 34). Elsevier.

Berger, C. J., Lippiatt, S. M., Lawrence, M. G., & Bruland, K. W. (2008). Application of a chemical leach technique for estimating labile particulate aluminum, iron, and manganese in the Columbia River plume and coastal waters off Oregon and Washington. *Journal of Geophysical Research: Oceans*, *113*(C2).

Biller, D. V., & Bruland, K. W. (2012). Analysis of Mn, Fe, Co, Ni, Cu, Zn, Cd, and Pb in seawater using the Nobias-chelate PA1 resin and magnetic sector inductively coupled plasma mass spectrometry (ICP-MS). *Marine Chemistry*, *130*, 12-20.

Boyle, E. A., Lee, J.-M., Echegoyen, Y., Noble, A., Moos, S., Carrasco, G., Zhao, N., Kayser, R., Zhang, J., & Gamo, T. (2014). Anthropogenic lead emissions in the ocean: The evolving global experiment. *Oceanography*, *27*(1), 69-75.

Breitbarth, E., Achterberg, E. P., Ardelan, M., Baker, A. R., Bucciarelli, E., Chever, F., Croot, P. L., Duggen, S., Gledhill, M., & Hassellöv, M. (2010). Iron biogeochemistry across marine systems–progress from the past decade. *Biogeosciences*, *7*(3), 1075-1097.

Bridgestock, L., Van De Flierdt, T., Rehkämper, M., Paul, M., Middag, R., Milne, A., Lohan, M. C., Baker, A. R., Chance, R., & Khondoker, R. (2016). Return of naturally sourced Pb to Atlantic surface waters. *Nature Communications*, *7*(1), 12921.

Brooks Rand Instruments. (n.d.). User's Guide MERX-T.

Bruvold, A. S., Bienfait, A. M., Ervik, T. K., Loeschner, K., & Valdersnes, S. (2023). Vertical distribution of inorganic nanoparticles in a Norwegian fjord. *Marine Environmental Research*, *188*, 105975.

Buck, K. N., Selph, K. E., & Barbeau, K. A. (2010). Iron-binding ligand production and copper speciation in an incubation experiment of Antarctic Peninsula shelf waters

from the Bransfield Strait, Southern Ocean. *Marine Chemistry*, *122*(1-4), 148-159.
Byrne, R. H., & Kester, D. R. (1976). Solubility of hydrous ferric oxide and iron speciation in seawater. *Marine Chemistry*, *4*(3), 255-274.
Carter, S., Lu, W., Moore, M., Granchelli, J., & Neeley, C. (n.d). *Considerations When Selecting Conical Tubes for Centrifugation Applications* https://assets.thermofisher.com/TFS-Assets/LCD/Application-Notes/ANLSPCONICALTUBES%201112.pdf
Castelle, S., Schäfer, J., Blanc, G., Dabrin, A., Lanceleur, L., & Masson, M. (2009). Gaseous mercury at the air–water interface of a highly turbid estuary (Gironde Estuary, France). *Marine Chemistry*, *117*(1-4), 42-51.
Charette, M. A., Kipp, L. E., Jensen, L. T., Dabrowski, J. S., Whitmore, L. M., Fitzsimmons, J. N., Williford, T., Ulfsbo, A., Jones, E., & Bundy, R. M. (2020). The transpolar drift as a source of riverine and shelf-derived trace elements to the central Arctic Ocean. *Journal of Geophysical Research: Oceans*, *125*(5), e2019JC015920.
Chattopadhyay, S., & Chattopadhyay, D. (1978). Colloidal properties of sediments. In *Sedimentology* (pp. 248-251). Berlin, Heidelberg: Springer Berlin Heidelberg. https://doi.org/10.1007/3-540-31079-7_51
Coquery, M., & Cossa, D. (1995). Mercury speciation in surface waters of the North Sea. *Netherlands Journal of Sea Research*, *34*(4), 245-257.
Cornell, R. M., & Schwertmann, U. (2003). *The iron oxides : structure, properties, reactions, occurences and uses* (2nd, completely rev. and extended ed.). Wiley-VCH.
Cossa, D., Coquery, M., Gobeil, C., & Martin, J.-M. (1996). Mercury fluxes at the ocean margins. *Global and regional mercury cycles: sources, fluxes and mass balances*, 229-247.
Cossa, D., Heimbürger, L.-E., Lannuzel, D., Rintoul, S. R., Butler, E. C., Bowie, A. R., Averty, B., Watson, R. J., & Remenyi, T. (2011). Mercury in the southern ocean. *Geochimica et Cosmochimica Acta*, *75*(14), 4037-4052.
Creswell, J. E., Carter, A., Chen, B., DeWild, J., Fajon, V., Rattonetti, A., Saffari, M., Tsui, M. T.-K., Živković, I., & Braaten, H. F. V. (2016). Assessing bias in total mercury results after removing a subsample from the bottle. *International Journal of Environmental Analytical Chemistry*, *96*(11), 1038-1047.
Cuculić, V., & Branica, M. (1996). Adsorption of trace metals from sea-water onto solid surfaces: analysis by anodic stripping voltammetry. *Analyst*, *121*(8), 1127-1131.
Cui, X., Lamborg, C. H., Hammerschmidt, C. R., Xiang, Y., & Lam, P. J. (2021). The effect of particle composition and concentration on the partitioning coefficient for mercury in three ocean basins. *Frontiers in Environmental Chemistry*, *2*, 660267.
Cullen, J. T., Bergquist, B. A., & Moffett, J. W. (2006). Thermodynamic characterization of the partitioning of iron between soluble and colloidal species in the Atlantic Ocean. *Marine Chemistry*, *98*(2-4), 295-303.
Elemental Scientific-2 (n.d). *seaFAST – Automated Preconcentration System for Undiluted Seawater*. https://www.icpms.com/products/online-matrix-removal/seafast-seawater-high-matrix-icpms/
Elemental Scientific (n.d.). SC-DX seaFAST-pico Method Guide.
Everett, D. H. (1972). Manual of symbols and terminology for physicochemical quantities and units, appendix II: Definitions, terminology and symbols in colloid and surface chemistry. *Pure and Applied Chemistry*, *31*(4), 577-638.
Fischer, A., Kroon, J., Verburg, T., Teunissen, T., & Wolterbeek, H. T. (2007). On the relevance of iron adsorption to container materials in small-volume experiments on iron marine chemistry: 55Fe-aided assessment of capacity, affinity and kinetics. *Marine Chemistry*, *107*(4), 533-546.
Fitzgerald, W. F., & Gill, G. A. (1979). Subnanogram determination of mercury by two-stage gold amalgamation and gas phase detection applied to atmospheric analysis. *Analytical chemistry*, *51*(11), 1714-1720.

Fitzsimmons, J. N., & Boyle, E. A. (2012). An intercalibration between the GEOTRACES GO-FLO and the MITESS/Vanes sampling systems for dissolved iron concentration analyses (and a closer look at adsorption effects). *Limnology and Oceanography: Methods*, *10*(6), 437-450.
Gao, W., Qu, B., Yuan, H., Song, J., & Li, W. (2023). Heavy metal mobility in contaminated sediments under seawater acidification. *Marine Pollution Bulletin*, *192*, 115062.
Ge, Y., Zhang, R., Jiang, Z., Shen, Z., & Yan, M. (2022). Determination of Fe, Ni, Cu, Zn, Cd and Pb in seawater by isotope dilution automatic solid-phase extraction—ICP-MS. *Acta Oceanologica Sinica*, *41*(8), 129-136.
Gianguzza, A., Pelizzetti, E., Sammartano, S., & International School on Marine, C. (2000). *Chemical processes in marine environments*. Springer.
Grassi, S., & Netti, R. (2000). Sea water intrusion and mercury pollution of some coastal aquifers in the province of Grosseto (Southern Tuscany—Italy). *Journal of Hydrology*, *237*(3-4), 198-211.
Gruber, N., Boyd, P. W., Frölicher, T. L., & Vogt, M. (2021). Biogeochemical extremes and compound events in the ocean. *Nature*, *600*(7889), 395-407.
Guevara, S. R., & Horvat, M. (2013). Stability and behaviour of low level spiked inorganic mercury in natural water samples. *Analytical Methods*, *5*(8), 1996-2006.
Hammerschmidt, C. R., Bowman, K. L., Tabatchnick, M. D., & Lamborg, C. H. (2011). Storage bottle material and cleaning for determination of total mercury in seawater. *Limnology and Oceanography: Methods*, *9*(10), 426-431.
Heimbürger, L.-E., Sonke, J. E., Cossa, D., Point, D., Lagane, C., Laffont, L., Galfond, B. T., Nicolaus, M., Rabe, B., & van Der Loeff, M. R. (2015). Shallow methylmercury production in the marginal sea ice zone of the central Arctic Ocean. *Scientific Reports*, *5*(1), 10318.
Helbæk, M. (2011). *Statistikk : kort og godt* (3. utg. ed.). Universitetsforl.
Hurst, M. P., Aguilar-Islas, A. M., & Bruland, K. W. (2010). Iron in the southeastern Bering Sea: elevated leachable particulate Fe in shelf bottom waters as an important source for surface waters. *Continental Shelf Research*, *30*(5), 467-480.
Jensen, L., Wyatt, N., Landing, W., & Fitzsimmons, J. (2020). Assessment of the stability, sorption, and exchangeability of marine dissolved and colloidal metals. *Marine Chemistry*, *220*, 103754.
Joksič, A. š., Katz, S. A., Horvat, M., & Milačič, R. (2005). Comparison of single and sequential extraction procedures for assessing metal leaching from dredged coastal sediments. *Water, Air, and Soil Pollution*, *162*, 265-283.
Jones, C., Crowe, S. A., Sturm, A., Leslie, K. L., MacLean, L., Katsev, S., Henny, C., Fowle, D. A., & Canfield, D. E. (2011). Biogeochemistry of manganese in ferruginous Lake Matano, Indonesia. *Biogeosciences*, *8*(10), 2977-2991.
Kanna, N., Sugiyama, S., Fukamachi, Y., Nomura, D., & Nishioka, J. (2020). Iron supply by subglacial discharge into a fjord near the front of a marine-terminating glacier in northwestern Greenland. *Global Biogeochemical Cycles*, *34*(10), e2020GB006567.
Kohler, S. G., Heimbürger-Boavida, L.-E., Petrova, M. V., Digernes, M. G., Sanchez, N., Dufour, A., Simić, A., Ndungu, K., & Ardelan, M. V. (2022). Arctic Ocean's wintertime mercury concentrations limited by seasonal loss on the shelf. *Nature Geoscience*, *15*(8), 621-626.
Kohler, S. G., Kull, L. M., Heimbürger-Boavida, L.-E., de Freitas, T. R., Sanchez, N., Ndungu, K., & Ardelan, M. V. (2022). Distribution pattern of mercury in northern Barents Sea and Eurasian Basin surface sediment. *Marine Pollution Bulletin*, *185*, 114272.
Koschinsky, A., Winkler, A., & Fritsche, U. (2003). Importance of different types of marine particles for the scavenging of heavy metals in the deep-sea bottom water. *Applied Geochemistry*, *18*(5), 693-710.
Kosmulski, M. (2002). The pH-dependent surface charging and the points of zero charge. *Journal of colloid and interface science*, *253*(1), 77-87.

Krauskopf, K. B. (1956). Factors controlling the concentrations of thirteen rare metals in sea-water. *Geochimica et Cosmochimica Acta*, *9*(1-2), 1-B32.
Krisch, S., Hopwood, M. J., Schaffer, J., Al-Hashem, A., Höfer, J., Rutgers van der Loeff, M. M., Conway, T. M., Summers, B. A., Lodeiro, P., & Ardiningsih, I. (2021). The 79 N Glacier cavity modulates subglacial iron export to the NE Greenland Shelf. *Nature Communications*, *12*(1), 3030.
Kuma, K., Katsumoto, A., Nishioka, J., & Matsunaga, K. (1998). Size-fractionated iron concentrations and Fe (III) hydroxide solubilities in various coastal waters. *Estuarine, Coastal and Shelf Science*, *47*(3), 275-283.
Lalonde, J. D., Amyot, M., Kraepiel, A. M., & Morel, F. M. (2001). Photooxidation of Hg (0) in artificial and natural waters. *Environmental Science & Technology*, *35*(7), 1367-1372.
Lamborg, C., Bowman, K., Hammerschmidt, C., Gilmour, C., Munson, K., Selin, N., & Tseng, C.-M. (2014). Mercury in the anthropocene ocean. *Oceanography*, *27*(1), 76-87.
Lamborg, C. H., Hammerschmidt, C. R., & Bowman, K. L. (2016). An examination of the role of particles in oceanic mercury cycling. *Philosophical Transactions of the Royal Society A: Mathematical, Physical and Engineering Sciences*, *374*(2081), 20150297.
Leventhal, G. E., Ackermann, M., & Schiessl, K. T. (2019). Why microbes secrete molecules to modify their environment: the case of iron-chelating siderophores. *Journal of the Royal Society Interface*, *16*(150), 20180674.
Liang, P., Li, Y.-C., Zhang, C., Wu, S.-C., Cui, H.-J., Yu, S., & Wong, M. H. (2013). Effects of salinity and humic acid on the sorption of Hg on Fe and Mn hydroxides. *Journal of Hazardous Materials*, *244*, 322-328.
Liu, G., Li, Y., & Cai, Y. (2012). *Environmental Chemistry and Toxicology of Mercury* (G. Liu, Y. Cai, & N. O'Driscoll, Eds.). Wiley.
Liu, J., Chen, Q., Yang, Y., Wei, H., Laipan, M., Zhu, R., He, H., & Hochella Jr, M. F. (2022). Coupled redox cycling of Fe and Mn in the environment: The complex interplay of solution species with Fe-and Mn-(oxyhydr) oxide crystallization and transformation. *Earth-Science Reviews*, *232*, 104105.
Lockwood, R. A., & Chen, K. Y. (1973). Adsorption of mercury (II) by hydrous manganese oxides. *Environmental Science & Technology*, *7*(11), 1028-1034.
Lu, X., Huangfu, X., & Ma, J. (2014). Removal of trace mercury (II) from aqueous solution by in situ formed Mn–Fe (hydr) oxides. *Journal of Hazardous Materials*, *280*, 71-78.
Mendenhall, W., & Sincich, T. (2012). *A second course in statistics : regression analysis* (7th ed.). Pearson/Prentice Hall.
Middag, R., Séférian, R., Conway, T. M., John, S. G., Bruland, K. W., & de Baar, H. J. (2015). Intercomparison of dissolved trace elements at the Bermuda Atlantic Time Series station. *Marine Chemistry*, *177*, 476-489.
Millero, F. J., Yao, W., & Aicher, J. (1995). The speciation of Fe (II) and Fe (III) in natural waters. *Marine Chemistry*, *50*(1-4), 21-39.
Nealson, K. H., & Saffarini, D. (1994). Iron and manganese in anaerobic respiration: environmental significance, physiology, and regulation. *Annual review of microbiology*, *48*(1), 311-343.
Nriagu, J. O. (1989). A global assessment of natural sources of atmospheric trace metals. *Nature*, *338*, 47-49.
Oldham, V. E., Mucci, A., Tebo, B. M., & Luther III, G. W. (2017). Soluble Mn (III)–L complexes are abundant in oxygenated waters and stabilized by humic ligands. *Geochimica et Cosmochimica Acta*, *199*, 238-246.
Pacyna, J. M., & Pacyna, E. G. (2001). An assessment of global and regional emissions of trace metals to the atmosphere from anthropogenic sources worldwide. *Environmental reviews*, *9*(4), 269-298.
Parker, J. L., & Bloom, N. S. (2005). Preservation and storage techniques for low-level aqueous mercury speciation. *Science of the Total Environment*, *337*(1-3), 253-263.

Powell, K. J., Brown, P. L., Byrne, R. H., Gajda, T., Hefter, G., Leuz, A.-K., Sjöberg, S., & Wanner, H. (2009). Chemical speciation of environmentally significant metals with inorganic ligands. Part 3: The Pb2++ OH−, Cl−, CO32−, SO42−, and PO43− systems (IUPAC Technical Report). *Pure and Applied Chemistry*, *81*(12), 2425-2476.

Raiswell, R., & Canfield, D. E. (2012). The iron biogeochemical cycle past and present. *Geochemical perspectives*, *1*(1), 1-2.

Rapp, I., Schlosser, C., Rusiecka, D., Gledhill, M., & Achterberg, E. P. (2017). Automated preconcentration of Fe, Zn, Cu, Ni, Cd, Pb, Co, and Mn in seawater with analysis using high-resolution sector field inductively-coupled plasma mass spectrometry. *Analytica Chimica Acta*, *976*, 1-13.

Ross, D. A., Guzman, H. M., Potvin, C., & van Hinsberg, V. J. (2017). A review of toxic metal contamination in marine turtle tissues and its implications for human health. *Regional Studies in Marine Science*, *15*, 1-9.

Samanta, S., Cloete, R., Loock, J., Rossouw, R., & Roychoudhury, A. N. (2021). Determination of Trace Metal (Mn, Fe, Ni, Cu, Zn, Co, Cd and Pb) Concentrations in Seawater Using Single Quadrupole ICP-MS: A Comparison between Offline and Online Preconcentration Setups. *Minerals*, *11*(11), 1289.

Schaule, B. K., & Patterson, C. C. (1981). Lead concentrations in the northeast Pacific: evidence for global anthropogenic perturbations. *Earth and Planetary Science Letters*, *54*(1), 97-116.

Schwertmann, U., Stanjek, H., & Becher, H.-H. (2004). Long-term in vitro transformation of 2-line ferrihydrite to goethite/hematite at 4, 10, 15 and 25 C. *Clay Minerals*, *39*(4), 433-438.

Seo, H., Kim, G., Kim, Y.-I., & Kim, I. (2021). Tracing the atmospheric input of seawater-dissolvable Pb based on the budget of 210Pb in the East Sea (Japan Sea). *Frontiers in Marine Science*, *8*, 756076.

Stumm, W., & Morgan, J. J. (1996). *Aquatic chemistry : chemical equilibria and rates in natural waters* (3rd ed.). Wiley.

Swallow, K. C., Hume, D. N., & Morel, F. M. (1980). Sorption of copper and lead by hydrous ferric oxide. *Environmental Science & Technology*, *14*(11), 1326-1331.

Tang, Y., Stewart, G., Lam, P. J., Rigaud, S., & Church, T. (2017). The influence of particle concentration and composition on the fractionation of 210Po and 210Pb along the North Atlantic GEOTRACES transect GA03. *Deep Sea Research Part I: Oceanographic Research Papers*, *128*, 42-54.

Tebo, B. M. (1991). Manganese (II) oxidation in the suboxic zone of the Black Sea. *Deep Sea Research Part A. Oceanographic Research Papers*, *38*, S883-S905.

Tiffreau, C., Lützenkirchen, J., & Behra, P. (1995). Modeling the adsorption of mercury (II) on (hydr) oxides: I. Amorphous iron oxide and α-quartz. *Journal of colloid and interface science*, *172*(1), 82-93.

ToolBox, E. (2005). *Seawater - Properties*. Retrieved 12.01.2023 from https://www.engineeringtoolbox.com/sea-water-properties-d_840.html

Trivedi, P., & Axe, L. (2001). Ni and Zn sorption to amorphous versus crystalline iron oxides: macroscopic studies. *Journal of colloid and interface science*, *244*(2), 221-229.

Turner, D. R. (1987). Speciation and cycling of arsenic, cadmium, lead and mercury in natural waters. *Lead, mercury, cadmium and arsenic in the environment*, 175-186.

Turner, D. R., & Hunter, K. A. (2001). *The Biogeochemistry of iron in seawater* (Vol. vol. 7). Wiley.

United Nations (n.d.). *Conserve and sustainably use the oceans, seas and marine resources for sustainable development*. Retrieved 12.08 from https://sdgs.un.org/goals/goal14

USEPA. (1995). METHOD 1640: DETERMINATION OF TRACE ELEMENTS IN WATER BY PRECONCENTRATION AND INDUCTIVELY COUPLED PLASMA-MASS SPECTROMETRY. EPA 821/R-95/033. Washington, D.C., United States Environmental Protection Agency, Office of Water.

USEPA. (2002). Method 1631 Revision E: Mercury in Water by Oxidation, Purge and Trap and Cold Vapor Atomic Fluorescence Spectrometry, EPA-821/R-02/019, Washington, D.C., United States Environmental Protection Agency, Office of Water.

van de Velde, S. J., Hülse, D., Reinhard, C. T., & Ridgwell, A. (2021). Iron and sulfur cycling in the cGENIE. muffin Earth system model (v0. 9.21). *Geoscientific Model Development*, *14*(5), 2713-2745.

Vieira, L. H., Achterberg, E. P., Scholten, J., Beck, A. J., Liebetrau, V., Mills, M. M., & Arrigo, K. R. (2019). Benthic fluxes of trace metals in the Chukchi Sea and their transport into the Arctic Ocean. *Marine Chemistry*, *208*, 43-55.

Wang, J., Zhong, Q., Baskaran, M., & Du, J. (2019). Investigations on the time-series partitioning of 210Pb, 207Bi and 210Po between marine particles and solution under different salinity and pH conditions. *Chemical Geology*, *528*, 119275.

West, D. M., Holler, F. J., Crouch, S. R., & Skoog, D. A. (2014). *Fundamentals of analytical chemistry* (9th ed.). Brooks/Cole Cengage Learning.

Wuttig, K., Townsend, A. T., van Der Merwe, P., Gault-Ringold, M., Holmes, T., Schallenberg, C., Latour, P., Tonnard, M., Rijkenberg, M. J., & Lannuzel, D. (2019). Critical evaluation of a seaFAST system for the analysis of trace metals in marine samples. *Talanta*, *197*, 653-668.

Xu, B., Liu, F., Brookes, P. C., & Xu, J. (2018). The sorption kinetics and isotherms of sulfamethoxazole with polyethylene microplastics. *Marine Pollution Bulletin*, *131*, 191-196.

Yang, W., Guo, L., Chuang, C.-Y., Schumann, D., Ayranov, M., & Santschi, P. H. (2013). Adsorption characteristics of 210Pb, 210Po and 7Be onto micro-particle surfaces and the effects of macromolecular organic compounds. *Geochimica et Cosmochimica Acta*, *107*, 47-64.

Appendices

Appendix A: ICP-MS Results

Appendix B: seaFAST Protocol

Appendix C: Total Hg Calibration Curves

Appendix D: Statistics

Appendix E: Models

Appendix F: Other Results

Appendix A: ICP-MS Results

Table 0.1: Preliminary results of the direct ICP-MS analysis. Concentrations are not blank corrected.

Sample			52 -> 52 Cr [O2]		55 -> 55 Mn [O2]		56 -> 56 Fe [H2]		75 -> 91 As [O2]		208 -> 208 Pb [O2]	
Acq. Date-Time	Sample Name	Comment	Conc [ug/l]	Conc. RSD	Conc [ug/l]	Conc. RSD	Conc [ug/l]	Conc. RSD	Conc [ug/l]	Conc. RSD	Conc [ug/l]	Conc. RSD
02.02.2023 17:33	13	Blank	0,0041	104,2	0,0	N/A	0,0097	108,1	0,00	N/A	0	N/A
02.02.2023 17:36	1	C2-1	0,080	11,6	0,053	10,3	0,53	6,7	0,14	14,1	0,0073	30,8
02.02.2023 17:38	2	Mn50	0,095	0,4	0,32	1,8	0,74	0,9	0,21	21,5	0,0075	50,3
02.02.2023 17:41	3	Fe25	0,068	19,2	0,073	6,2	0,51	3,3	0,19	10,6	0,0049	40,1
02.02.2023 17:43	4	Mn+Fe10	0,072	9,7	0,098	5,1	0,52	2,7	0,18	12,3	0,0057	7,6
02.02.2023 17:46	5	C2-1	0,077	11,8	0,076	5,5	0,69	4,2	0,18	9,7	0,0018	119,4
02.02.2023 17:48	6	Mn50	0,072	5,8	0,33	4,9	0,66	2,1	0,18	9,7	0,0020	76,4
02.02.2023 17:51	7	Fe25	0,078	11,0	0,072	8,6	0,53	4,2	0,18	7,4	0,0024	52,2
02.02.2023 17:53	8	Mn+Fe10	0,083	5,4	0,083	12,0	0,51	2,9	0,17	9,5	0,0027	71,9
02.02.2023 17:56	9	C2-1	0,080	19,2	0,041	13,0	0,52	2,3	0,14	10,9	0	N/A
02.02.2023 17:58	10	Mn50	0,096	3,8	0,26	6,8	0,64	4,3	0,18	22,9	0	N/A
02.02.2023 18:00	11	Fe25	0,076	9,7	0,053	1,8	0,65	3,4	0,18	20,4	0,00099	275,8
02.02.2023 18:03	12	Mn+Fe10	0,081	6,9	0,056	3,4	0,59	5,3	0,18	10,5	0	N/A

Table 0.2: Blank samples in nmol L^{-1}. The limit of detection was calculated from the standard deviation of sample no. 1 to 147. Blank sample number 221 was used to correct the precipitate samples from the centrifugation. The samples are corrected for preconcentration factor.

			55 -> 55 Mn [O2]		56 -> 56 Fe [O2]		208 -> 208 Pb [H2]	
Sample no.	Sample Name	Sample name	Conc. [nM]	RSD	Conc. [nM]	RSD	Conc. [nM]	RSD
1	blank	dTe	0,0500	7,188	1,0560	3,680	0,0151	5,299
22	blank	dTe	0,0374	6,322	0,5326	2,715	0,0235	2,768
43	blank	dTe	0,0496	7,899	0,8819	1,620	0,0127	9,000
64	blank	dTe	0,0294	8,100	0,7245	2,200	0,0057	6,300
85	blank	dTe	0,0499	2,300	0,6934	1,600	0,0057	4,700
106	blank	dTe	0,0542	2,000	0,6878	1,400	0,0196	0,800
127	blank	dTe	0,0278	0,800	0,3966	2,800	0,0040	5,200
146	blank	Wall adsorption	0,0687	2,619	0,9414	0,903	0,0072	6,677
147	blank	Wall adsorption	0,0543	4,396	1,3172	1,557	0,0058	8,479
165	blank	TTe	0,0325	7,328	0,9419	0,503	0,0059	5,726
185	blank	TTe	0,0569	0,845	4,1637	1,706	0,0240	3,647
206	blank	TTe	0,0730	4,255	4,5558	0,190	0,0167	0,562
221	blank	Precipitate	70,8280	1,980	45,9657	0,580	0,0892	2,320

Table 0.3: Measured NASS-7 values. *Data point removed from the calculation in Table 3.6 due to contamination. Values are corrected for blanks and preconcentration factor.

		55 -> 55 Mn [O2]		56 -> 56 Fe [H2]		208 -> 208 Pb [O2]	
Sample no.	Sample name	Conc. [nM]	Conc. RSD	Conc. [nM]	Conc. RSD	Conc. [nM]	Conc. RSD
2	NASS-7	13,42	2,10	5,59	2,81	0,0131	13,21
44	NASS-7	13,23	1,55	5,28	1,49	0,0044	10,52
128	NASS-7	11,39	2,786	4,602	0,701	0,3003*	0,369
148	NASS-7	12,94	2,42	4,97	1,38	0,0437	2,24
207	NASS-7	11,90	3,09	5,61	1,74	0,0050	2,72

Appendix B: seaFAST Usage Protocol

Reagents

- **Buffer: Ammonium Acetate**

To be prepared at least 1 day in advance.
- Prepare the solution in following order:

1. 150mL ultrapure deionized water.
2. 170mL (155 g) 25% Ammonium hydroxide.
3. 140mL (147 g) glacial acetic acid.
4. Dilute to 500mL.
5. If greater quantities are needed, double volume.

Prepare under the hood since this is an exothermic reaction. Add acetic acid slowly to the water and ammonium hydroxide mixture. Let it react and cool down before measuring the pH with a calibrated pH meter. Double check pH. It is likely that more acid needs to be added. If necessary, add dropwise glacial acetic or ammonium hydroxide until pH is between 6.0 and 6.2. Measure pH by pouring a small amount of buffer in a plastic tube. Do NOT put the probe into the buffer solution.

- **Eluent: UP HNO3 (1 M)**

To 465 mL ultrapure DIW, add 35mL (80.03 g) ultrapure 14,4 M HNO3. If greater quantities of eluent are needed, double all volumes. The final sample after preconcentration is 2 ml and 1 M.

Internal standard for eluent: For every 1L eluent, add 1800 µL from a Lutetium (stock 1:10000 ppm or µg/L) spike to reach a final 18 ug/L (103 nM). With another pipette, add 700 µL from a Gallium (stock 1:) spike to a final 6,972 ug/L solution.

- **Rinse solution: UP HNO3 (0.6 M)**

Make 0.6 M HNO3 solution using the rinse solution bottle. Ex: 84 mL of UP HNO3 diluted to 2 L.

- **Carrier: MilliQ-H2O**

Methodology

- **Start – up**

1. Turn on the seaFAST, the autosampler, ventilator, and open the main argon canister valve.
2. Turn the computer and open the ESI software (desktop shortcut)
3. Press "Initialize" under the FAST sub-method to connect the software with the instrument. Look for 2 green labels to ensure proper connection.
4. Under the dropdown menu, choose "Prime SeaFAST no hydride" for priming and press play.
5. Check the SeaFAST log (Excel sheet) to see what has been done the days before. Prime the instrument twice if you or someone else changed the configuration.
6. Observe the probe and the instrument as it is priming to watch for leakages. Check the inside of the autosampler, the syringes, the rotors, and behind the autosampler.
7. Check the gas pressure on the blue valve above the outlet (1 bar ± 0.1).

8. Check the volume levels Milli-Q, Eluent, Buffer, Rinse, and Waste. Remake/empty if needed.

- **Method runs**

1. Choose your rack setup and rack types for the desired racks you will use. (ex: Select Tray, 2x2). Choose rack type (ex: 3x7, LG or MG –will most likely be LG).
2. Place an empty destination tube/vial with the cap off in the destination rack.
3. At the Main Menu, click on Manual.
4. Enter your empty destination tube's position (ex Rack 4, Position 21) and click "Go Here". Recommended to do this for every destination tube to ensure probe will go into each vial.
5. The probe will move to the location and move vertically downward as if dispensing a sample. Adjust the height by pressing the "-10Z" so the probe does not touch the bottom of the vial and will not be touching the final sample volume.
6. Place your samples and destination vials in the appropriate locations on the SeaFast.
7. Go to "Configure" and select *Prep Fast Offline*.
8. Click the button Enable SeaFastpico.
9. Edit and add rows to your sequence. <u>It is recommended to add at least 1 dummy sample at the start of the sequence.</u> DOUBLE CHECK THAT YOUR SEQUENCE IS CORRECT, otherwise you will have wasted sample and possible contamination of other samples.
10. Right click under the method tab. Select *Edit sub-method parameters*. Check and/or change your final sample volume. Check and/or change the # of 10mL loads (ex: 2 10mL loops will aspirate 20mL of initial sample). Check and/or change the final volume elution. Do not change the final elution flow rate.
11. When finished editing the method parameters, click *Save* and then *Close* for each section. Right click on the method tab for the first sample and click *Copy cell contents to all rows below.*
12. Change the name of your sequence/method to your initials and date. Click *Save*. When ready to begin, press *Start prepFAST offline*.
13. It is important to check that your sample caps are OFF and that the racks are aligned PERFECTLY, otherwise you will have errors and spills in your sequence. You must also CHECK EACH DESTINATION VIAL INDIVIDUALLY to ensure that the probe will not hit the side of the tube and deliver the volume where you intend it to.
14. Check pH of effluent line after preconcentration. After each pre-concentration cycle, the thin lines (V3P3 and v1P10). Depending on the sample pH before pre-concentration, sample pH at the effluent will vary. Target pH for optimal recovery on Fe and other elements is ~5.7.

- **Shutdown**

1. Remove your original samples and destination samples from the autosampler.
2. Keep the racks in the autosampler.
3. Check the levels of the MilliQ water, the Eluent, and the buffer, and the rinse.
4. Make sure the instrument has stopped running and completed the full method. IF YOU HAVE INTERRUPTED THE METHOD, YOU MUST CONDITION THE COLUMNS AGAIN BEFORE NEXT USE
5. Close the ESI software by clicking File, Close, OK.
6. Log off and then shut down the computer.
7. Turn off the syringes, autosampler, ventilator, and close the main argon canister valve.

8. Check the waste level. If high, empty waste into the hood while running the water to dilute the waste.
9. Re-insert the waste lines to the waste bottl

Appendix C: THg Calibration Curves

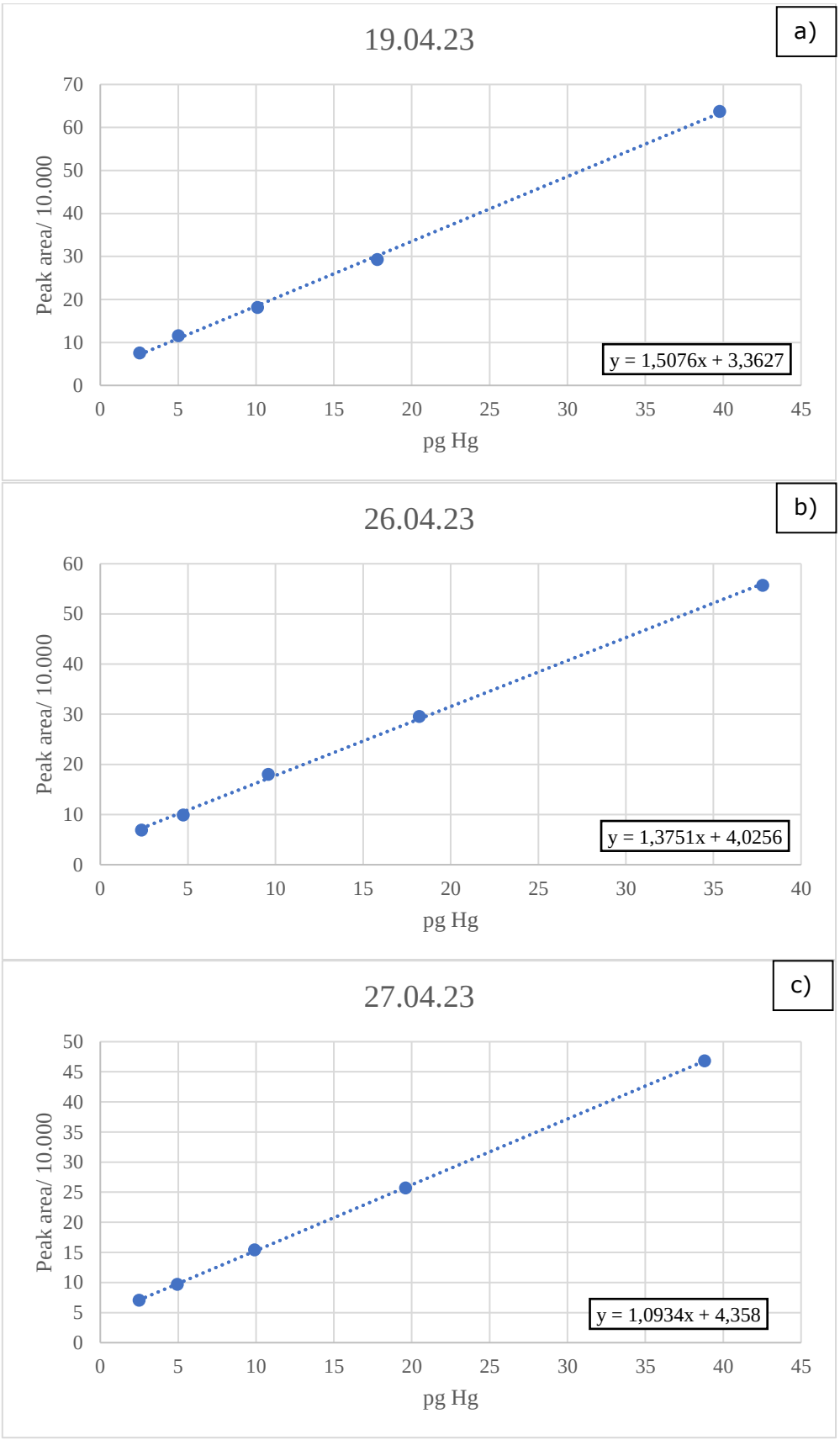

Figure 0.1: Calibration curves for Hg for three sample runs. a) control duplicate samples, b) time zero and 16 hours samples, c) samples collected at 336 hours.

Appendix D: Statistics

Table 0.4: Shapiro-Wilk test to check whether the two controls are normally distributed or not.

Shapiro-Wilk Test at 95 % Confidence Level		
Group	**Control1**	**Control2**
N	8	8
Mean	0.13	0.15
Median	0.12	0.15
Sample std	0.071	0.071
W	0.8557	0.9622
p-value	0.1187	0.9127

```
# Interaction is not significant, so the slope across groups is not different

Analysis of Variance Table

Response: logpb
             Df  Sum Sq Mean Sq  F value    Pr(>F)
hrs           1 0.43807 0.43807 122.2112 6.294e-07 ***
controls      1 0.02946 0.02946   8.2177   0.01676 *
hrs:controls  1 0.00250 0.00250   0.6980   0.42296
Residuals    10 0.03585 0.00358
---
Signif. codes:  0 ‘***’ 0.001 ‘**’ 0.01 ‘*’ 0.05 ‘.’ 0.1 ‘ ’ 1


# The category variable (Controls) is significant, so the intercepts among groups
are different.

Analysis of Variance Table

Response: logpb
           Df  Sum Sq Mean Sq  F value    Pr(>F)
hrs         1 0.43807 0.43807 125.6608 2.335e-07 ***
controls    1 0.02946 0.02946   8.4497   0.01427 *
Residuals 11 0.03835 0.00349
---
Signif. codes:  0 ‘***’ 0.001 ‘**’ 0.01 ‘*’ 0.05 ‘.’ 0.1 ‘ ’ 1
```

Figure 0.2: Test whether the two controls have different TPb concentration different or not.

Table 0.5: Mann-Whitney test to check whether Control 1 had a higher THg concentration than Control 2.

One-Way Mann-Whitney test at 95 % Confidence Level		
Group	**Control1**	**Control2**
N	6	6
Mean	1,03	1,35
Order mean	21	57
Order total	78	78
U	36	0
Critical value	15	

Appendix E: Models

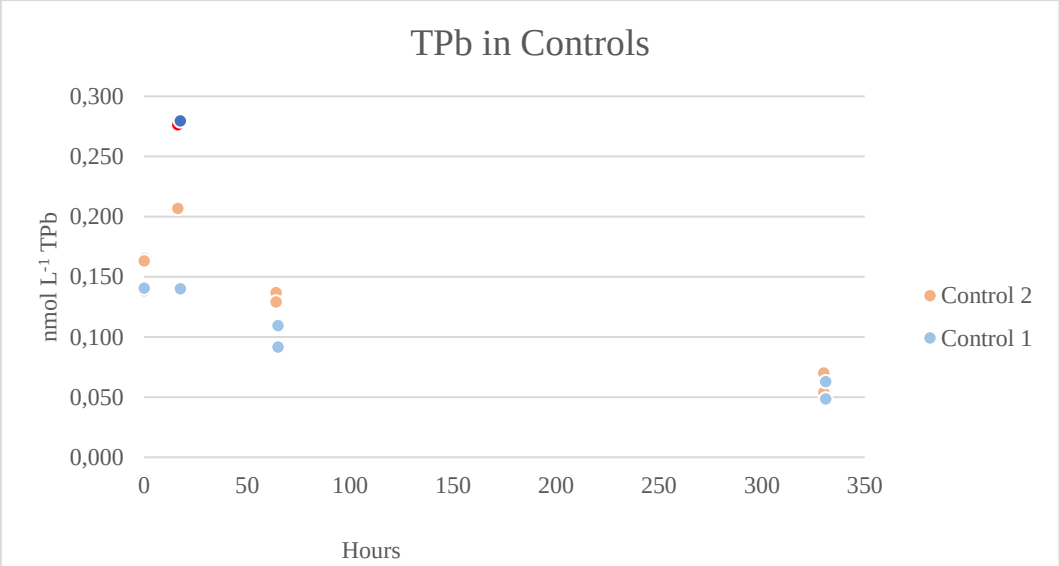

Figure 0.3: TPb as a function of time for all the results. The excluded data points from the TPb model are marked with a brighter color. The values are corrected for blanks and preconcentration factor.

```
Call:
lm(formula = Pbperc_2 ~ hrs + I(hrs^2), data = Control_allPbred)

Residuals:
    Min      1Q  Median      3Q     Max
-13.007  -5.451  -2.159   3.636  27.904

Coefficients:
             Estimate Std. Error t value Pr(>|t|)
(Intercept)  1.055e+02  4.702e+00  22.427 1.56e-10 ***
hrs         -4.645e-01  1.378e-01  -3.372  0.00623 **
I(hrs^2)     7.954e-04  3.922e-04   2.028  0.06749 .
---
Signif. codes:  0 ‘***’ 0.001 ‘**’ 0.01 ‘*’ 0.05 ‘.’ 0.1 ‘ ’ 1

Residual standard error: 10.44 on 11 degrees of freedom
Multiple R-squared:  0.8923,    Adjusted R-squared:  0.8727
F-statistic: 45.57 on 2 and 11 DF,  p-value: 4.756e-06
```

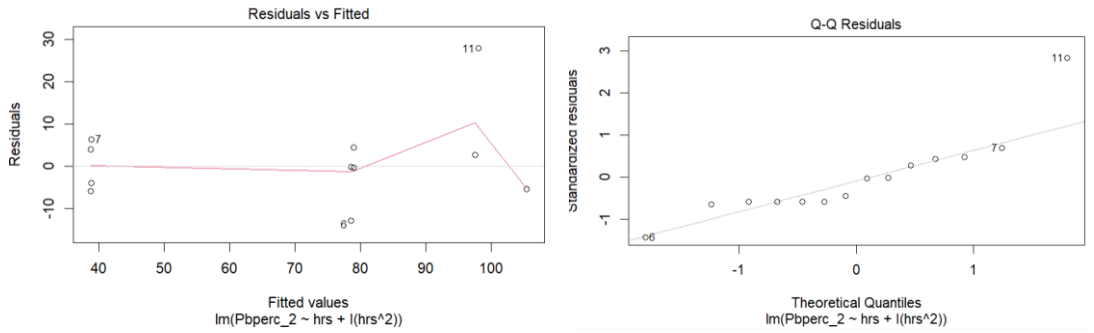

Figure 0.4: Diagnostic plots of the TPb model.

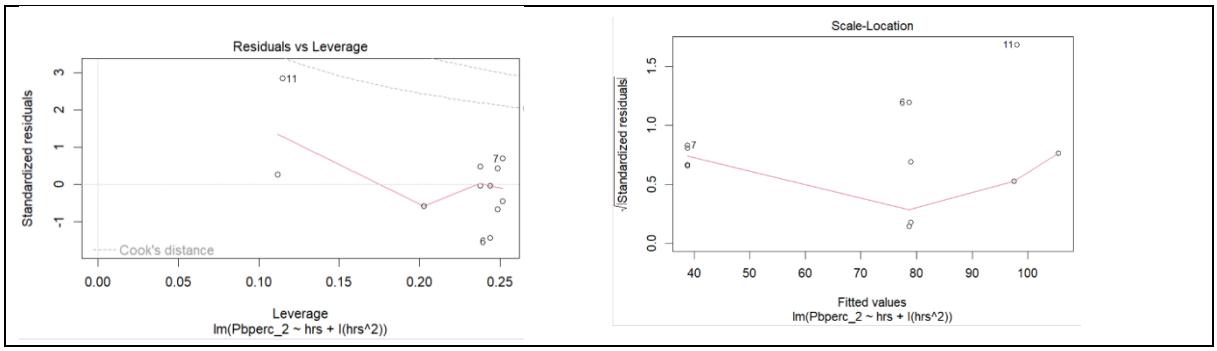

Figure 0.5: Continued

```
Call:
lm(formula = Feperc ~ hrs + I(hrs^2), data = Control_allFered)

Residuals:
   Min     1Q Median     3Q    Max
-6.489 -3.672 -3.109  4.288  9.497

Coefficients:
             Estimate Std. Error t value Pr(>|t|)
(Intercept)  1.035e+02  2.368e+00  43.704 1.71e-15 ***
hrs         -6.552e-01  7.447e-02  -8.798 7.78e-07 ***
I(hrs^2)     1.372e-03  2.129e-04   6.446 2.18e-05 ***
---
Signif. codes:  0 ‘***’ 0.001 ‘**’ 0.01 ‘*’ 0.05 ‘.’ 0.1 ‘ ’ 1

Residual standard error: 5.695 on 13 degrees of freedom
Multiple R-squared:  0.9617,    Adjusted R-squared:  0.9558
F-statistic: 163.4 on 2 and 13 DF,  p-value: 6.142e-10
```

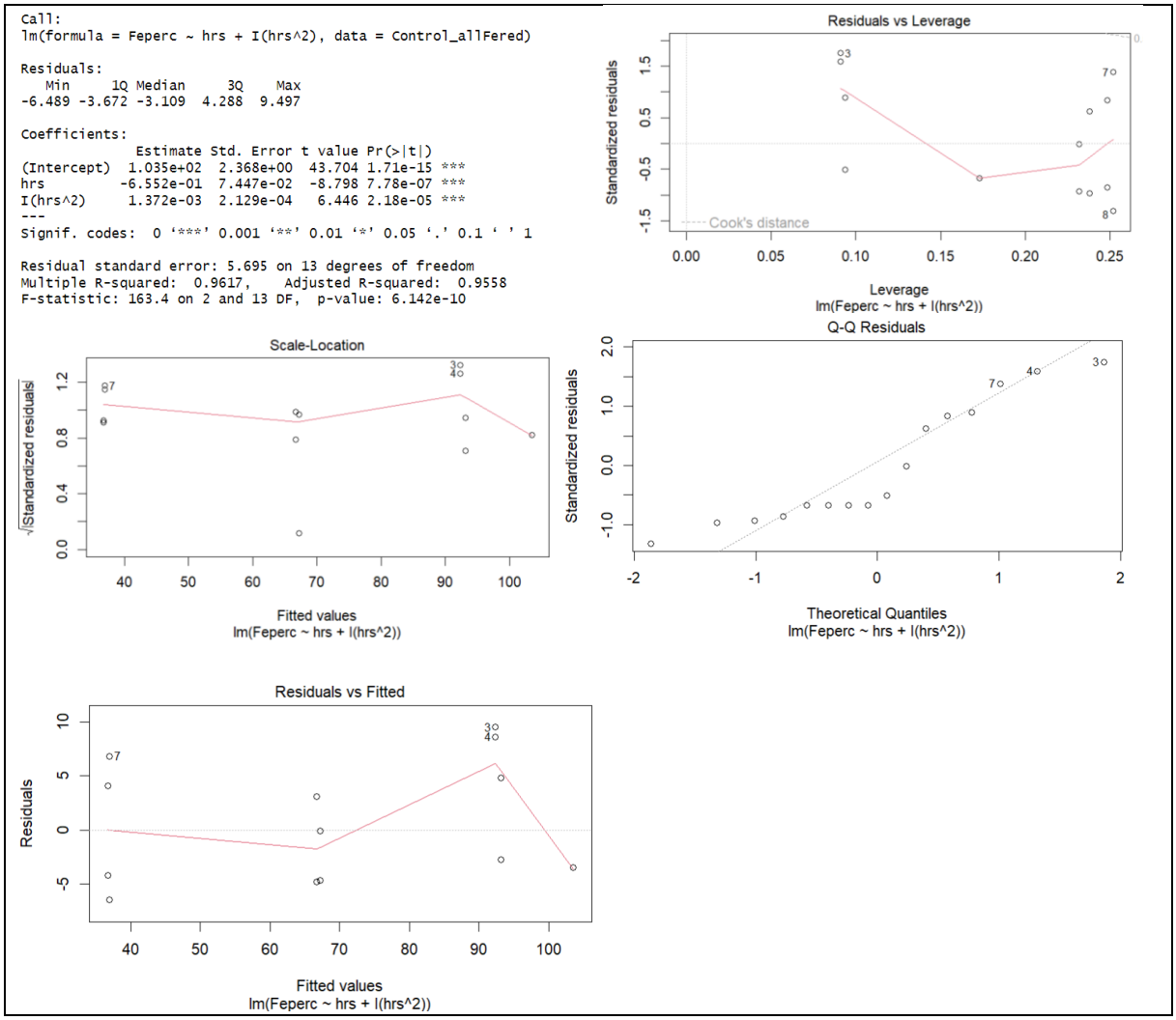

Figure 0.6: Diagnostic plots of TFe model.

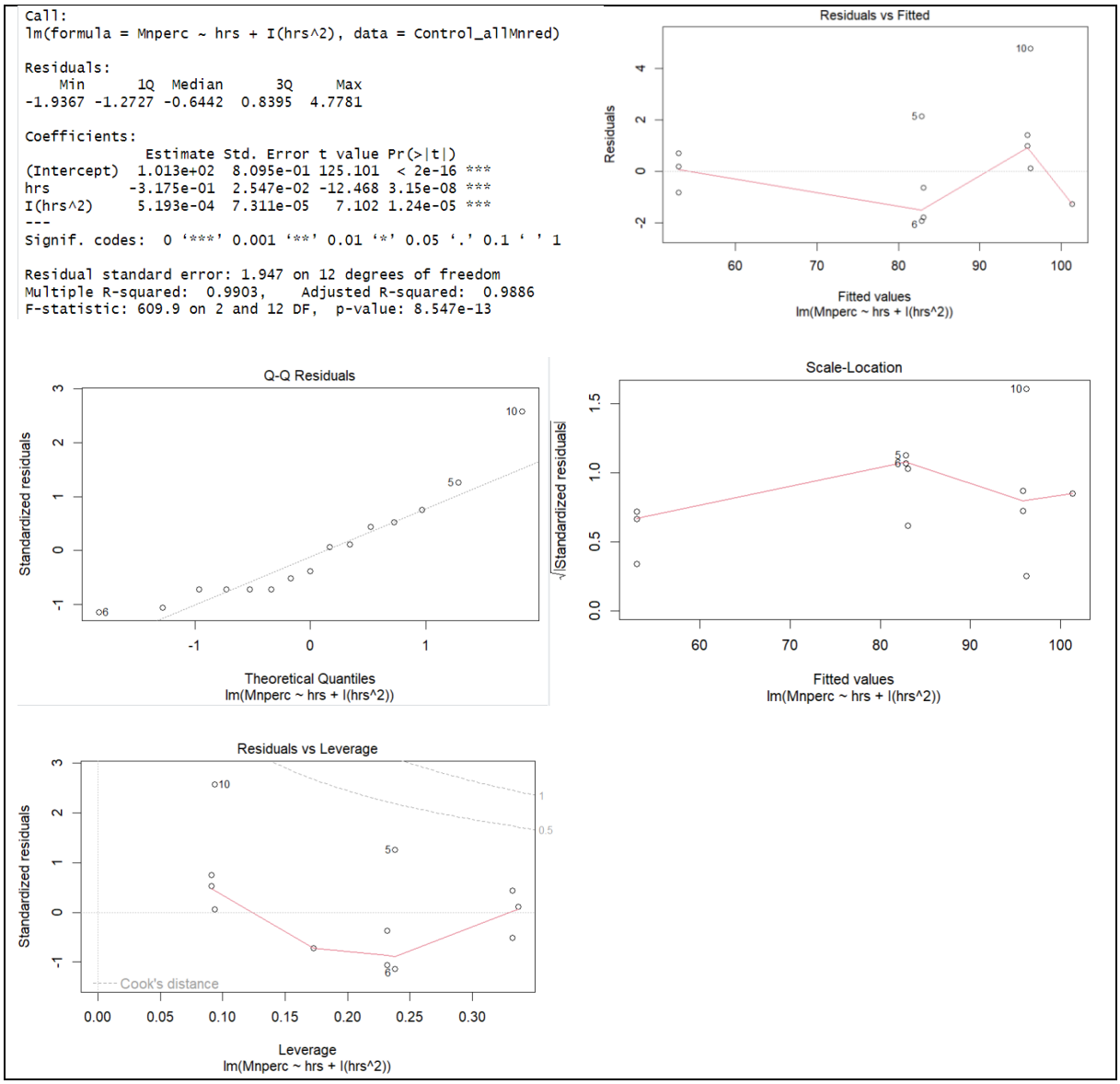

Figure 0.7: Diagnostic plots of TMn model.

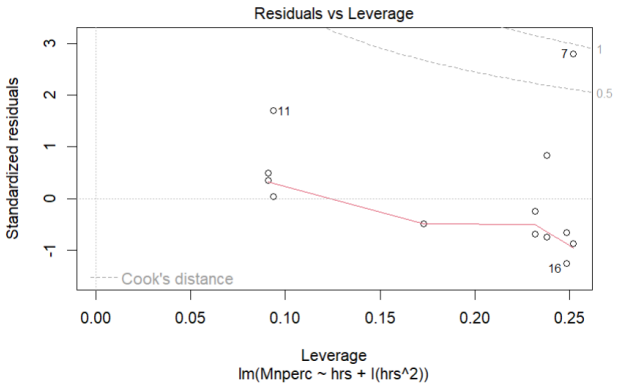

Figure 0.8: Diagnostic plot showing the outlier in the TMn model. The data point was excluded because it was above 0.5 Cook's distance from the standardized residuals.

```
Call:
lm(formula = Pbperc_2 ~ hrs, data = Control_allPbred)

Residuals:
     Min       1Q   Median       3Q      Max
-21.5545  -4.3216   0.6029   3.2779  29.6470

Coefficients:
            Estimate Std. Error t value Pr(>|t|)
(Intercept) 99.39707    4.07664  24.382 1.37e-11 ***
hrs         -0.18815    0.02263  -8.313 2.53e-06 ***
---
Signif. codes:  0 ‘***’ 0.001 ‘**’ 0.01 ‘*’ 0.05 ‘.’ 0.1 ‘ ’ 1

Residual standard error: 11.72 on 12 degrees of freedom
Multiple R-squared:  0.852,     Adjusted R-squared:  0.8397
F-statistic:  69.1 on 1 and 12 DF,  p-value: 2.534e-06
```

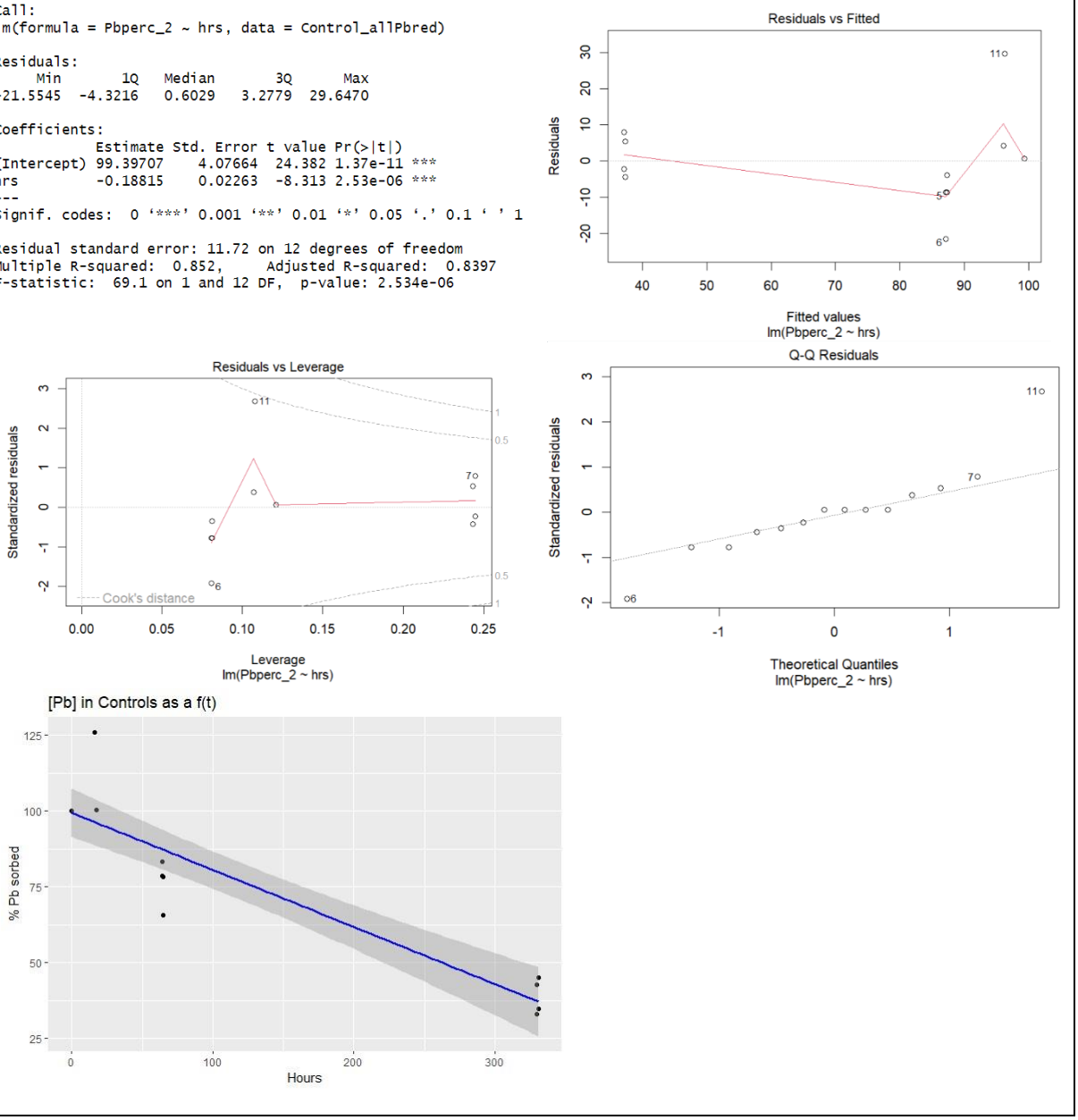

Figure 0.9: Linear Model of the TPb as a function of time.

Appendix F: Other Results

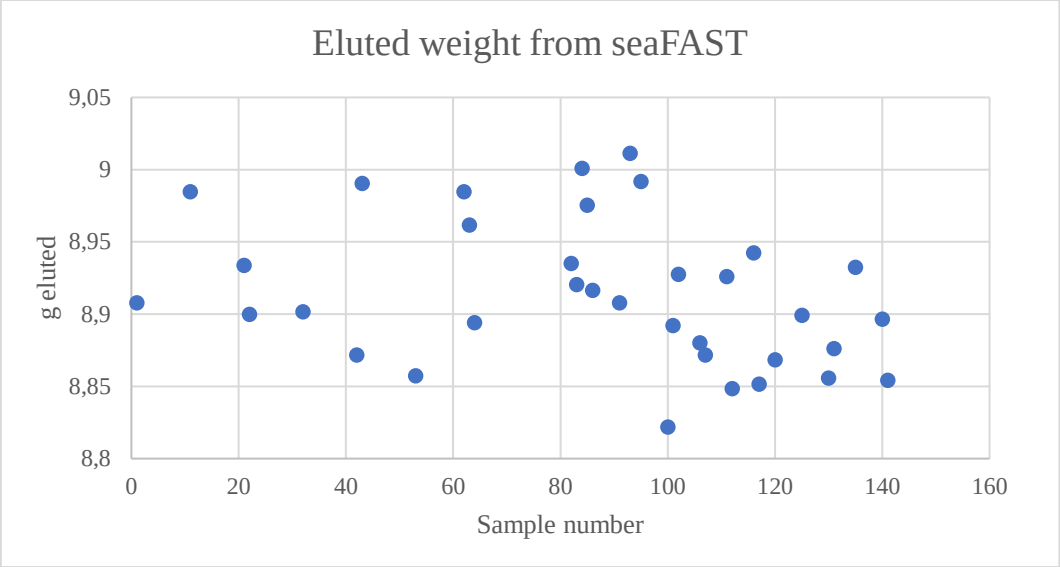

Figure 0.10: Elution weights + vial weight as a function of sample number.

Table 0.6: Test to check if the weighted eluent were the same as the theoretical value. Theoretical value (g) = empty falcon tube (g) + 2 g. Measured value (g) = empty falcon tube (g) + eluent (g).

Paired Two-Way t-Test at 95 % Confidence Level		
Variable	**Theoretical**	**Measured**
Mean	8.8912	8.9140
Standard dev.	0.04729	0.04977
N	35	35
df	68	
t stat	1,962	
Critical t-value	1.671	
p-value	0,054	

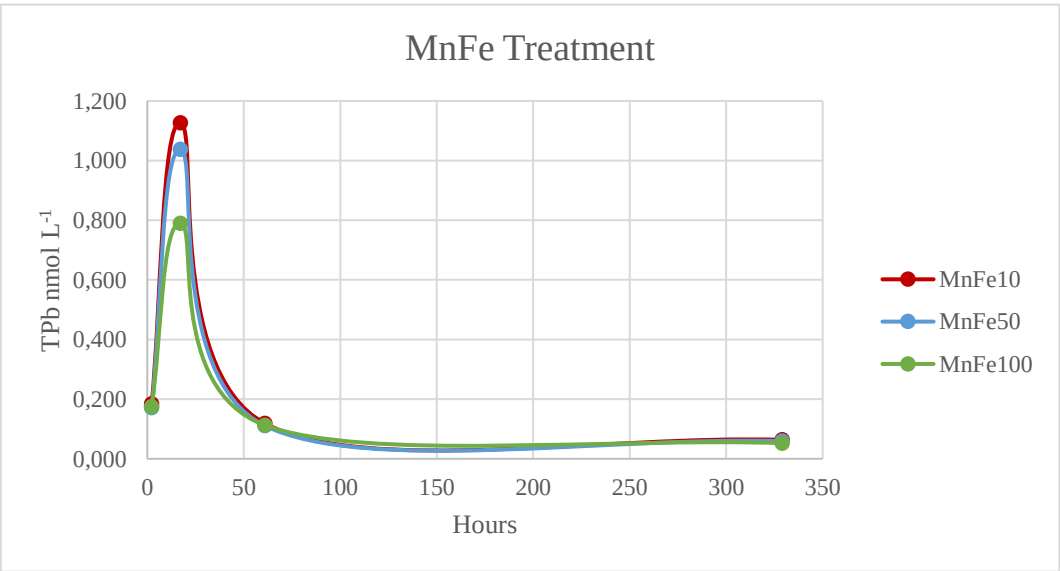

Figure 0.11: TPb as a function of time. Values are blank and preconcentration corrected

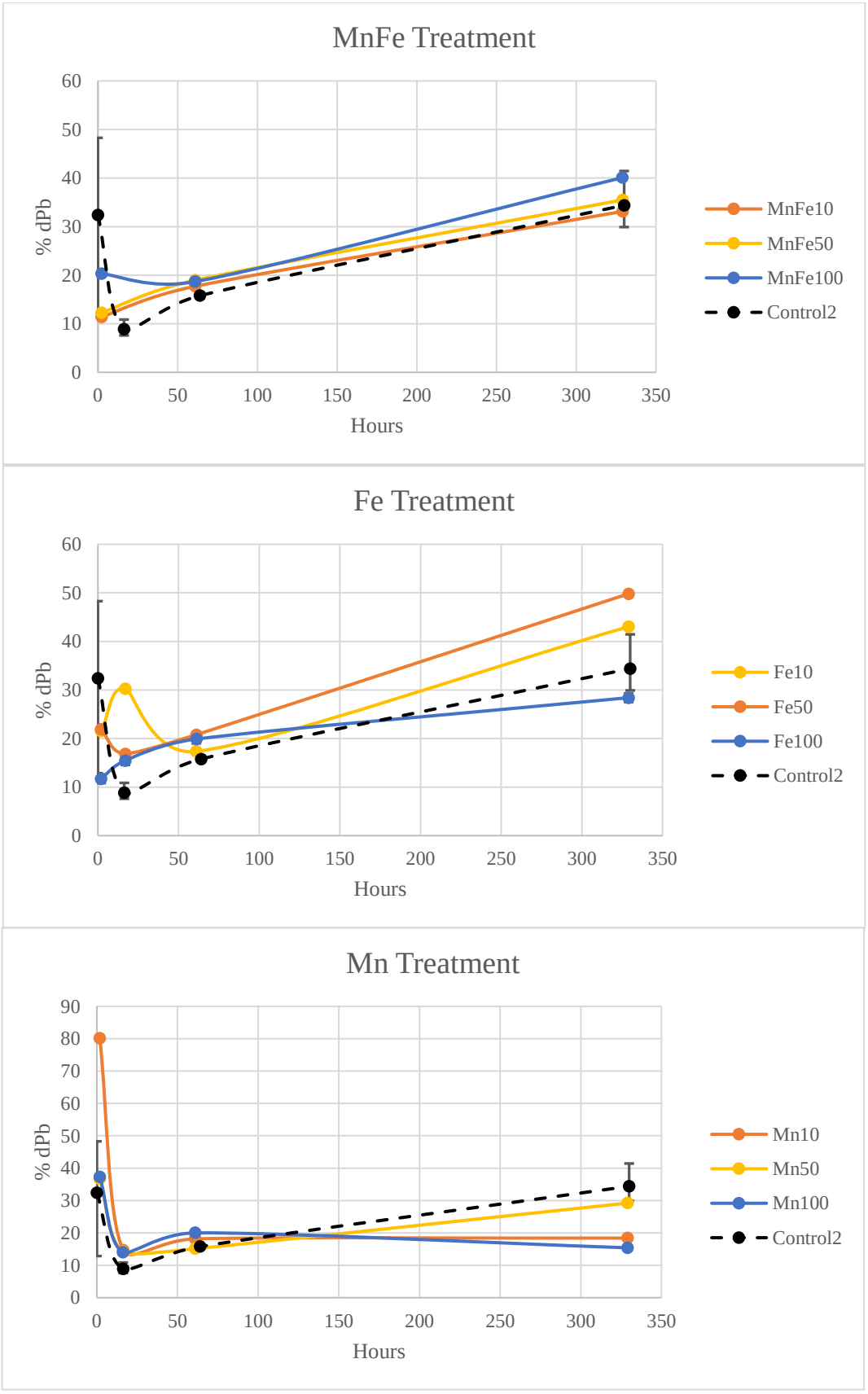

Figure 0.12: In the figure, the dashed line represents the average of the spiked seawater controls. The flat end of the error bars indicates the duplicate control concentrations.

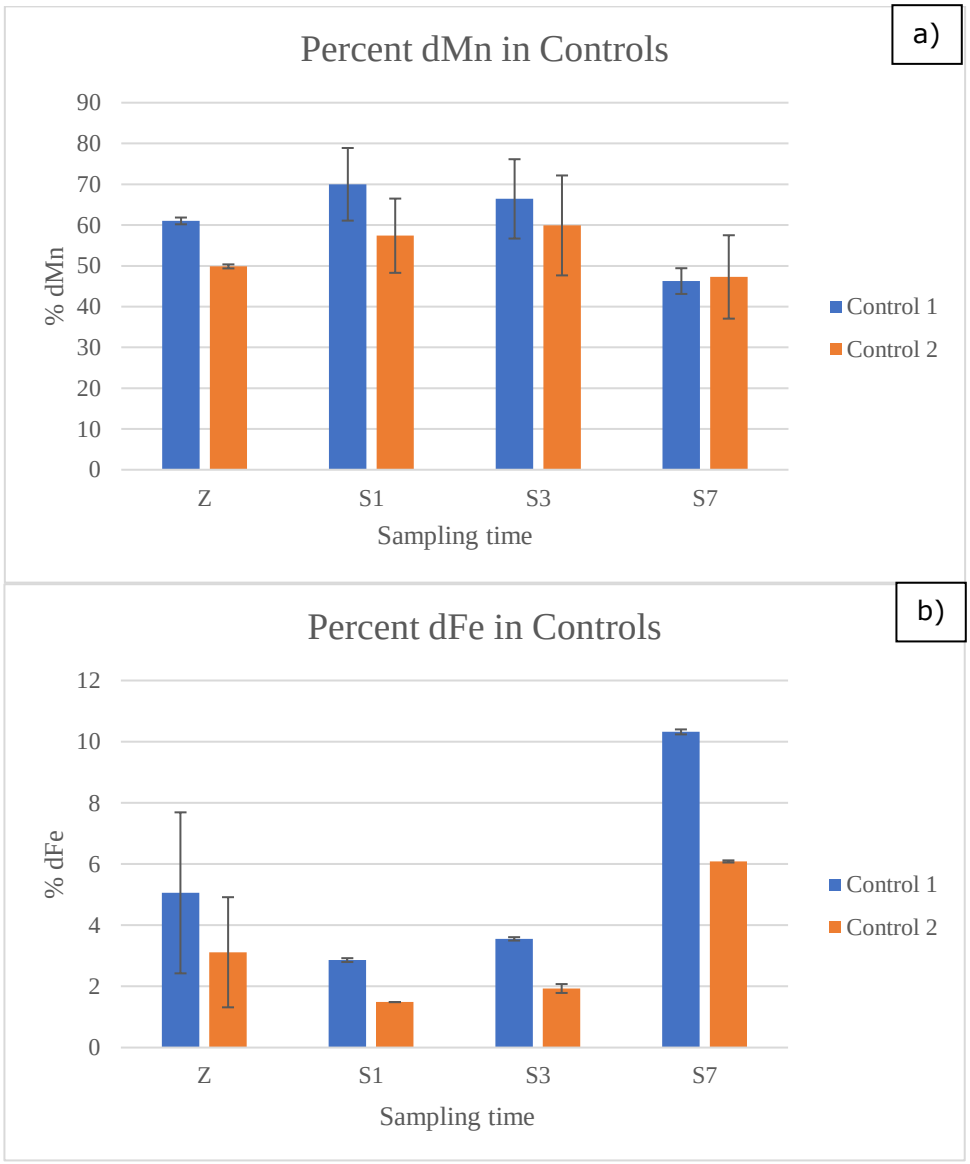

Figure 0.13: % dFe and % dMn over time. Z= time zero, S1 = 16 hours, S3 = 64 hours, S7 = 336 hours

Table 0.7: Centrifugation of TMn. Samples are corrected for blanks and preconcentration factor.

	Samples		Centrifugation	
	nM dMn n=3	**nM TMn n=2**	**nM Mn Supernatant n=7**	**nM Mn Precipitate n=6**
average	50,89	63,18	62,2	-90,9
std	21,84	25,49	20,2	9,0
RSD	42,92	40,35	32,5	-9,9

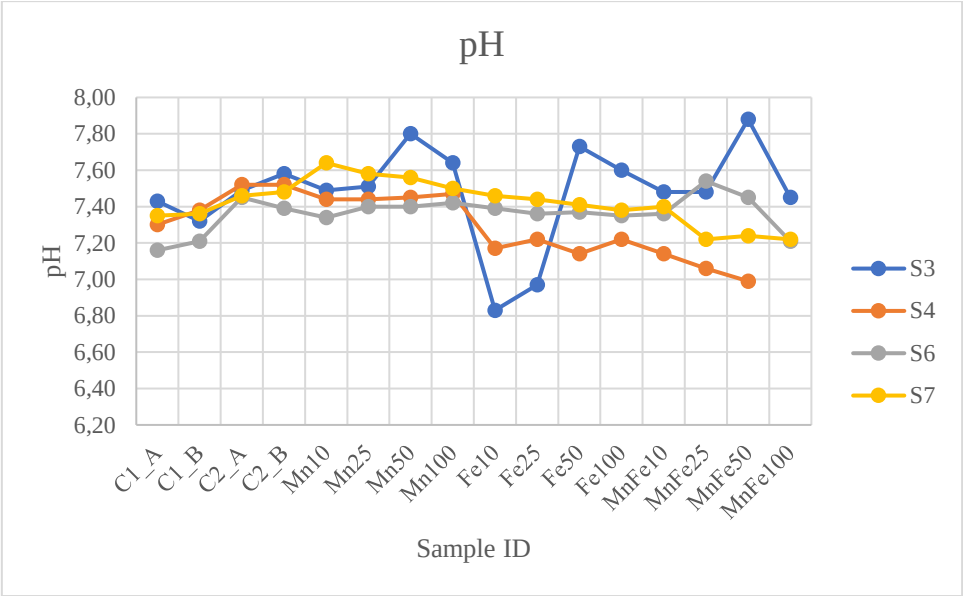

Figure 0.14: pH in experimental bottles at four sampling times: S3 = 64 hours, S4 = 6 days, S6 = 10 days, S7 = 14 days.

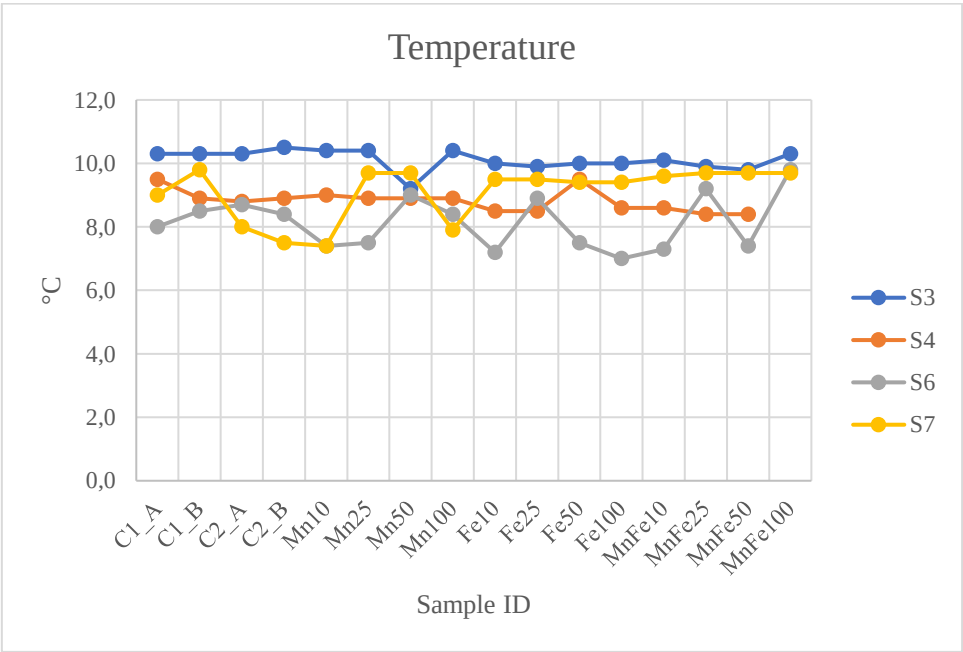

Figure 0.15: Temperature in experimental bottles at four sampling times: S3 = 64 hours, S4 = 6 days, S6 = 10 days, S7 = 14 days.

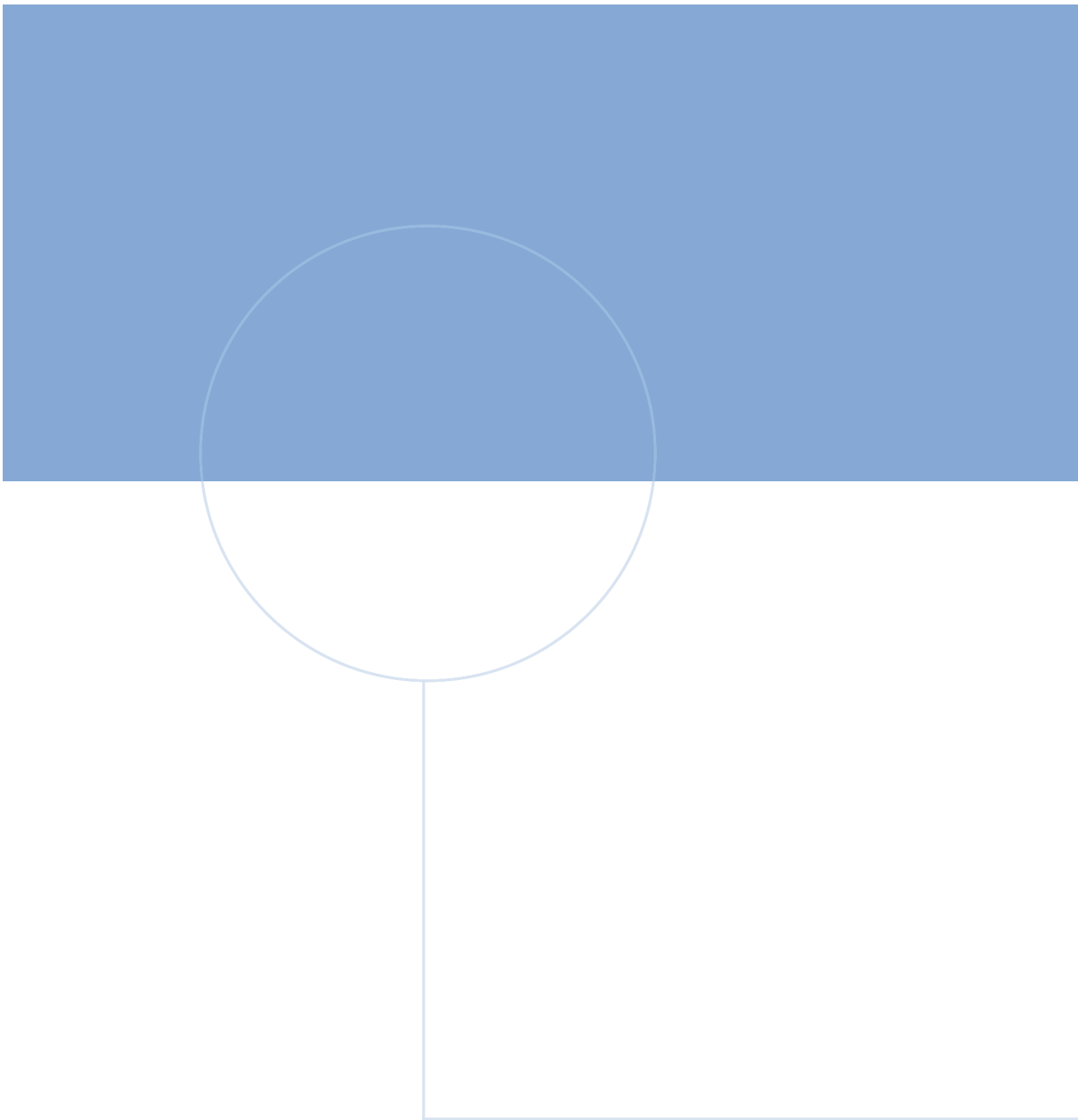

NTNU

Norwegian University of
Science and Technology